RSS

RUSSIAN SPACE SYSTEMS

Scientific and technical journal

ROCKET-SPACE DEVICE ENGINEERING AND INFORMATION SYSTEMS

Volume 5. Issue 2. 2018

Scientific and technical journal

“Rocket-Space Device Engineering and Information Systems”

Vol. 5. No. 2. 2018

Founder:
Joint Stock Company “Russian Space Systems”

The publication frequency is four issues per year.
The journal is included into the Russian Science Citation Index.
The journal is included into the List of peer-reviewed scientific publications approved by the Higher Attestation Commission (VAK RF).
The opinions expressed by authors of the papers do not necessarily those of the editors.
ISSN 2409-0239
DOI 10.30894/issn2409-0239.2018.5.2
The subscription number of the journal in the united catalogue “The Russian Press” is 94086.

Joint Stock Company “Russian Space Systems”,
ul. Aviamotornaya 53, Moscow, 111250 Russia
Tel. +7 (495) 673-96-29, www.russianspacesystems.ru
e-mail: journal@spacecorp.ru

Moscow
FIZMATLIT ®
2018

Contents

Vol. 5, Iss. 2, 2018

Space Navigation Systems and Devices. Radiolocation and Radio Navigation

Aerospace Methods for Earth Remote Sensing

Radio Engineering and Space Communication

Systems Analysis, Spacecraft Control, Data Processing, and Telemetry Systems

Solid-State Electronics, Radio Electronic Components, Micro- and Nanoelectronics, Quantum Effect Devices

ROCKET-SPACE DEVICE ENGINEERING AND INFORMATION SYSTEMS
Vol. 5, Iss. 2, 2018, pp. 2–9

Estimation of Root-Mean-Square Errors in Measurements of Radio Navigation Parameters

A.V. Molokanov, *contact@spacecorp.ru*
Joint Stock Company "Russian Space Systems", Moscow, Russian Federation
V.E. Vovasov, *Cand. Sci. (Engineering), contact@spacecorp.ru*
Joint Stock Company "Russian Space Systems", Moscow, Russian Federation

Abstract. It is often necessary to evaluate the performance of the user navigation equipment or its compliance with the requirements of the technical task by its measurements. One of the indicators of the quality of the user navigation equipment is the root-mean-square error of the radio navigation parameters.
The article presents a methodology for estimating root-mean-square errors in the measurements of radio navigation parameters obtained by the user navigation equipment installed on spacecraft. The issues of a representative sampling of the number of measurements for determining the root-mean-square errors of measurements eliminating the mutual dynamics of the navigation satellite and user navigation equipment, the dynamics of the receiver time scale shift, as well as the ionospheric component of the measurements are considered. The method includes an estimate of the instability of the receiver reference oscillator.
Based on the technique, the experimental estimates of the root-mean-square errors in pseudorange measurements by code and the carrier phase are made. Application of the developed technique allows evaluating the quality of the user navigation equipment and the correspondence of its characteristics to the specified criteria.

Keywords: GLONASS, GPS, radio navigation parameter, root-mean-square error

Introduction

Rather often, based on the measurements of the user navigation equipment (UNE), it is necessary to estimate the quality of its operation or meeting the requirements of Statement of Work (SOW). One of the indicators of the UNE performance quality is the root-mean-square error (RMS) of radio navigation parameters (RNP). RNP is understood as pseudoranges by the code and pseudoranges by the phase of carrier frequencies. If necessary, it is possible to determine an RMS error and other navigation parameters using the approach described in this article.

Defining the sampling value of measurements

To receive an RMS error, it is necessary to plan an experiment correctly. Firstly, the received measurements are divided into groups. In compliance with [6], the minimum quantity of measurements to define an RMS error, in each group should have not less than 30. In this case the received an RMS error value (x_i) can be considered distributed under the normal law. The number of sessions for receiving the statistics of an RMS error with the set number of reading has to be not less n=10-20 .

At first, we should find an estimate $\tilde{m}$ for the expectation value of an RMS error:

$$\tilde{m} = \frac{1}{n} \cdot \sum_{i=1}^{n} x_i \tag{1}$$

An RMS error dispersion will be equal to:

$$\tilde{D} = \frac{\sum_{i=1}^{n} (x_i - \tilde{m})^2}{n-1} \tag{2}$$

A root-mean-square deviation (RMSD) of an RMS error is defined as:

$$\sigma_{\tilde{m}} = \sqrt{\frac{\tilde{D}}{n}} \tag{3}$$

Hence, a confidential interval is as follows:

$$I_\beta = (\tilde{m} - t_\beta \cdot \sigma_{\tilde{m}} ; \tilde{m} + t_\beta \cdot \sigma_{\tilde{m}}) \tag{4}$$

where the value t_β is defined for the normal law as a number of RMSDs which needs to be postponed from the center of dispersion to the right and to the left in order that the probability of getting to the received site was equal to β .

The value t_β is defined by the formula:

$$t_\beta = \sqrt{2} \cdot \Phi^{-1}(\beta) \tag{5}$$

where $\Phi^{-1}(\beta)$ is the function inverse to the Laplace's function. Usually, to ease calculations to obtain t_β, a special Table (14.3.1) [6] is employed. For instance, at the set value $\beta = 0.997$, the value $t_\beta = 3$.

Method to determine an RMS error

The problem of defining the dispersion of an RMS error of the specified parameters is that their mathematical expectation $\tilde{m}$ is not a constant value in the course of measurements, so application of the traditional expression for dispersion (2) is almost impossible. In this regard, it is offered to make differentiation of the values of the parameters until $\tilde{m}$ of the received derivatives becomes either a constant or equal to zero. The received RMS error of this derivative is easily recalculated into the RMS error of the initial parameter, since differentiation is a linear operation.

We will bring for an example, the known mathematical expressions for pseudoranges by a high precision (HP) code for the navigation receiver installed on the satellite with the altitude of an orbit of 1000 km in the L1 band for GLONASS [1–3].

$$D^{L1}_{j,HP}(t_i) = R_j(t_i) + c \cdot \Delta T - c \cdot (\Delta T^j) + \\ + c\left(T^j_{ion,L1} + \tau_{j,L1,H}\right) - \xi^j_{L1,H} \quad , j = \overline{1, J} \tag{6}$$

by the HP code in the L2 band for GLONASS

$$D^{L2}_{j,HP}(t_i) = R_j(t_i) + c \cdot \Delta T - c \cdot (\Delta T^j + \Delta \tau^j_n) + \\ + c\left(T^j_{ion,L2} + \tau_{j,L2,H}\right) - \xi^j_{L2,H} \quad , j = \overline{1, J} \tag{7}$$

where

J is the number of visible GLONASS satellites;

t_i is the moment of measurement formation;

R_j is the path of signal propagation from the phase center of the antenna of the j-th satellite to the phase center of the receiver's antenna equal to

$$R_j(t_i) = \\ \sqrt{\left(x^j - x(t_i)\right)^2 + \left(y^j - y(t_i)\right)^2 + \left(z^j - z(t_i)\right)^2} \tag{8}$$

This is the distance between the points which were occupied by the j-th satellite at the moment of precedence and the receiver at the time of measurement formation.

A measurement formation is understood as a time point, which precedes the moment of measurement formation for the period of signal propagation;

x^j, y^j, z^j are the coordinates of the *j*-th satellite at the moment of precedence recalculated in that position of the Greenwich system of coordinates which it occupies at the time of measurement of pseudorange;

$x(t_i), y(t_i), z(t_i)$ are the receiver's coordinates at the time of measurement formation;

$T^j_{ion,L1}, T^j_{ion,L2}$ is the delay of a code signal of the L1 and L2 bands of the *j*-th satellite in the ionosphere;

ΔT is the shift of a time scale of the receiver relative to the system time scale of GLONASS;

ΔT^j is the time scale shift of the *j*-th GLONASS satellite which coincides with the time scale of the L1BT signal relative to the system time scale of GLONASS;

$\tau_{j,L1,HP}$, $\tau_{j,L2,HP}$ is the delay of the code HP signal of the L1 and L2 bands of the *j*-th GLONASS satellite in the radio frequency part of the receiver;

$\Delta\tau^j_n$ is the shift of the time scale of the L2BT signal relative to the L1BT signal.

$\xi^j_{L1,HP}, \xi^j_{L2,HP}$ is the noise component of measurement of pseudoranges by the receiver based on the signal of the L1 and L2 ranges of the HP code of the *j*-th GLONASS satellite.

Considering the known formulae [1]

$$T^j_{ion,L2} = \gamma \cdot T^j_{ion,L1} \tag{9}$$

where

$$\gamma = \left(\frac{f^j_{L1}}{f^j_{L2}}\right)^2 \tag{10}$$

f^j_{L1} is the frequency of the carrier of the signal of the *j*-th satellite in the L1 band;

f^j_{L2} is the frequency of the carrier of the signal of the *j*-th satellite in the L2 band.

The value $\gamma = \left(\frac{9}{7}\right)^2$ is for GLONASS.

Considering [5]

$$c \cdot T^j_{ion,L1} = I^j_g \cdot \frac{f^2}{f^2_{j,L1}} \cdot \frac{\alpha}{\sqrt{1 - \left[\frac{R_3}{R_3 + h}\cos\{\eta_j(t_i)\}\right]^2}} \tag{11}$$

we will obtain the pseudorange shift of the *j*-th signal in the L1 band caused by the ionosphere.

Here I^j_g is the ionosphere vertical delay of the GLONASS signal at the frequency L1;

R_3 is the radius of the Earth;

$h = 432.5 \cdot 10^3$ m is the altitude of the ionosphere layer where an integral concentration of electrons in the vertical column reaches 50%;

f is the carrier frequency where the estimation I^j_g is received (in the paper it is L1);

$\eta_j(t_i)$ is the elevation of the *j*-th navigation satellite relative to the receiver;

α is the coefficient taking into account the decrease in the sum concentration of electrons in the ionosphere column due to the object is located not on the Earth surface.

Allowing for (11), we will rewrite (6) and (7) as following:

$$D^{\mathrm{L1}}_{j,\mathrm{BT}}(t_i) = R_j(t_i) + c \cdot \Delta T - c \cdot (\Delta T^j) + \\ + I^j_g \cdot \frac{\alpha}{\sqrt{1 - \left[\frac{R_3}{R_3 + h}\cos\{\eta_j(t_i)\}\right]^2}} + \\ + c \cdot \tau_{j,\mathrm{L1,BT}} - \xi^j_{\mathrm{L1,BT}} \tag{12}$$

$$D^{\mathrm{L2}}_{j,\mathrm{BT}}(t_i) = R_j(t_i) + c \cdot \Delta T - c \cdot (\Delta T^j + \Delta\tau^j_n) + \\ + I^j_g \cdot \gamma \cdot \frac{\alpha}{\sqrt{1 - \left[\frac{R_3}{R_3 + h}\cos\{\eta_j(t_i)\}\right]^2}} + \\ + c \cdot \tau_{j,\mathrm{L2,BT}} - \xi^j_{\mathrm{L2,BT}} \tag{13}$$

It is obvious that on the interval corresponding to the group of changes such parameters as ΔT^j, $\Delta\tau^j_n$, $\tau_{j,\mathrm{L2,BT}}$, $\tau_{j,\mathrm{L1,BT}}$, $\eta_j(t_i)$, can be considered constants while the values $R_j(t_i), \Delta T, \alpha \cdot I^j_g$ have a significant dynamics.

The known mathematical expressions for pseudorange at the phase of the carrier for the navigation receiver installed on the satellite with the orbit altitude 1000 km [1, 3] should be given.

$$G^{L1}_j(t_i) = -c \cdot (\Delta T^j + \Delta\tau^j_{L1}) + c \cdot \Delta T + \\ + R_j(t_i) + \lambda^j_{L1}\left(\varphi_{0,L1} + \varphi^j_{0,L1} + \varsigma^{L1}_{\psi_j}\right) - \\ - c\left(T^j_{ion,L1}\right) - \lambda^j_{L1}\left(\varphi^j_{h,L1}\right) - M^{L1}_j \cdot \lambda^j_{L1} \tag{14}$$

$$G^{L2}_j(t_i) = -c \cdot (\Delta T^j + \Delta\tau^j_n + \Delta\tau^j_{L2}) + \\ + c \cdot \Delta T + R_j(t_i) + \lambda^j_{L2}\left(\varphi_{0,L2} + \varphi^j_{0,L2} + \varsigma^{L2}_{\psi_i}\right) - \\ - c\left(T^j_{ion,L2}\right) - \lambda^j_{L2}\left(\varphi^j_{h,L2}\right) - M^{L2}_j \cdot \lambda^j_{L2} \tag{15}$$

where λ^j_{L1}, λ^j_{L2} is the wavelength of the carrier of the *j*-th satellite in the L1 and L2 bands;

$\varphi_{0,L1}$, $\varphi_{0,L2}$ is the initial phase of the receiver in the L1 and L2 bands;

$\varphi^j_{0,L1}$, $\varphi^j_{0,L2}$ is the indefinite initial radiation phase of the *j*-th satellite in the L1 and L2 bands;

$\Delta\tau^j_{L1}=(\tau^j_{L1,CT} - \tau^j_{L1,BT})$ is the delay of the average precision (AP) code relative to HP in the L1 range in the equipment of the GLONASS satellite;

$\Delta\tau^j_{L2}=(\tau^j_{L2,CT} - \tau^j_{L2,BT})$ is the delay of the AP code relative to HP in the L2 range in the equipment of the GLONASS satellite;

$\varphi^j_{h,L1}$, $\varphi^j_{h,L2}$ is the phase aperture signal distortions of the *j*-th satellite in the receiver in the L1 and L2 bands;

M^{L1}_j, M^{L2}_j is the indefinite integer being nonuniqueness of phase measurements of the signal of the *j*-th satellite in the receiver in the L1 and L2 bands;

$\varsigma^{L1}_{\psi_j}$, $\varsigma^{L2}_{\psi_j}$ is the noise term of the measurement of the signal pseudopahse of the *j*-th satellite in the receiver in the L1 and L2 ranges.

Considering (11), we will rewrite (14) and (15) as following:

$$G^{L1}_j(t_i) = -c\cdot(\Delta T^j + \Delta\tau^j_{L1}) + c\cdot\Delta T + R_j(t_i) + \lambda^j_{L1}\left(\varphi_{0,L1} + \varphi^j_{0,L1} + \varsigma^{L1}_{\psi_j}\right) - I^j_g\cdot\frac{\alpha}{\sqrt{1-\left[\frac{R_3}{R_3+h}\cos\{\eta_j(t_i)\}\right]^2}} - \lambda^j_{L1}\left(\varphi^j_{h,L1}\right) - M^{L1}_j\cdot\lambda^j_{L1} \quad (16)$$

$$G^{L2}_j(t_i) = -c\cdot(\Delta T^j + \Delta\tau^j_n + \Delta\tau^j_{L2}) + c\cdot\Delta T + R_j(t_i) + \lambda^j_{L2}\left(\varphi_{0,L2} + \varphi^j_{0,L2} + \varsigma^{L2}_{\psi_j}\right) - I^j_g\cdot\gamma\cdot\frac{\alpha}{\sqrt{1-\left[\frac{R_3}{R_3+h}\cos\{\eta_j(t_i)\}\right]^2}} - \lambda^j_{L2}\left(\varphi^j_{h,L2}\right) - M^{L2}_j\cdot\lambda^j_{L2} \quad (17)$$

It is obvious that on the interval corresponding to the measurements such parameters as ΔT^j, $\Delta\tau^j_n$, $\eta_j(t_i)$, $\Delta\tau^j_{L1}$, $\lambda^j_{L1}\cdot(\varphi_{0,L1}+\varphi^j_{0,L1})$, $\lambda^j_{L1}\cdot(\varphi^j_{h,L1})$, $M^{L1}_j\cdot\lambda^j_{L1}$ can be considered constants while the values $R_j(t_i)$, ΔT, $\alpha\cdot I^j_g$ have a significant dynamics. As it was already specified, we will make differentiation of the received measurements for decrease in dynamics. Derivatives are needed to be taken until the dynamic error does not turn out to be less than noise. Since measurements of pseudorange based on the carrier phase are the most accurate, they will demand the highest derivative. Elimination of the dynamics of navigation spacecraft and the satellite with the height of an orbit of 1000 km, dynamics of the drift of the time scale of the receiver and also an ionospheric component of the expressions of pseudoranges, as the experiment has shown, requires receiving the sixth derivative of the measured pseudorange on the carrier phase. To sum up the results, we will use the sixth derivative at measurements of pseudorange by the code. In this case the values of the measurements $D^{L1}{}_{j,HP}(t_i)$, $D^{L2}{}_{j,HP}(t_i)$, $G^{L1}_j(t_i)$ and $G^{L2}_j(t_i)$ will be written as $G_j(t_i)$. An approximate value of the six derivative can be estimated with the following polynominal:

$$\Delta G_j(t_i) = G_j(t_{i+6}) - 6\cdot G_j(t_{i+5}) + 15\cdot G_j(t_{i+4}) - 20\cdot G_j(t_{i+3}) + 15\cdot G_j(t_{i+2}) - 6\cdot G_j(t_{i+1}) + G_j(t_i) \quad (18)$$

The dispersion of differences $\sigma^2_{\Delta G_j}$ will be equal to

$$\sigma^2_{\Delta G_j} = \frac{1}{N}\sum_{i=1}^{N}[\Delta G_j(t_i)]^2 = 924\cdot\sigma^2_{G_j} \quad (19)$$

Hence, an RMS error of measurements $G_j(t_i)$ will be equal to

$$\sigma_{G_j} = \sqrt{\sigma^2_{\Delta G_j}/924} \quad (20)$$

As an example of the use of the expression (18), Fig. 1 gives the graph of the change of the calculated σ_{G_j} pseudorange GLONASS of the L1 band by the code (**a**) and phase (b) of the carrier applying the six derivative. The Figure shows the relative time as a quantity of 10 second readings during a navigation session. A dashed graph is stipulated by the conditions of the navigation spacecraft by the antenna system UNE located on the satellite with the orbit about 1000 km.

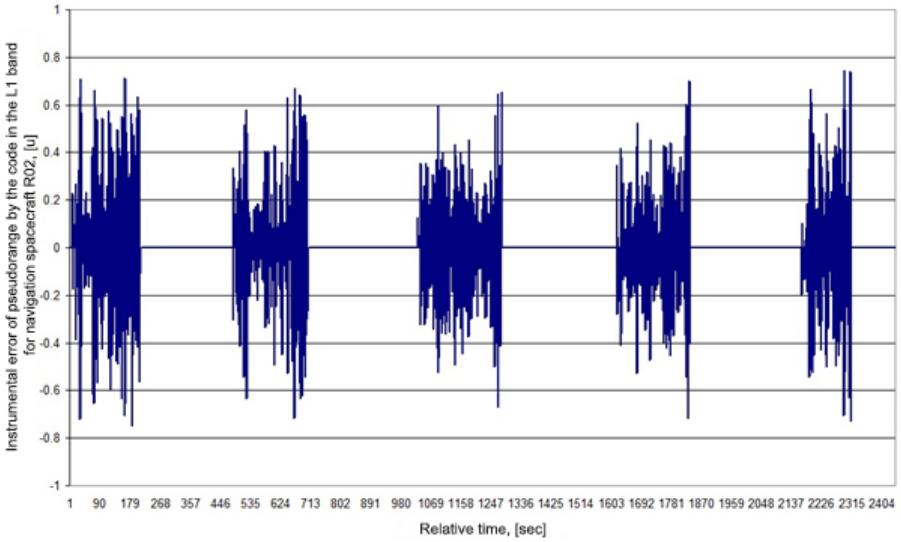

(a)

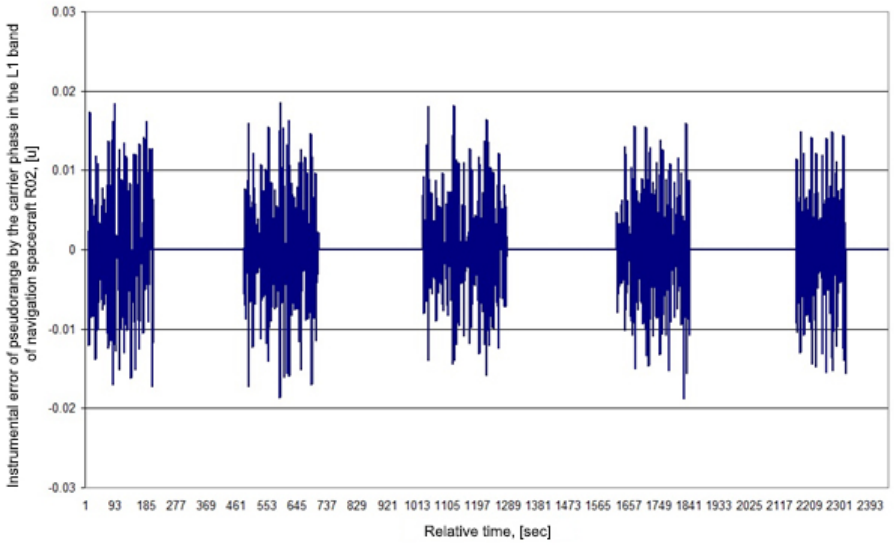

(b)

Fig. 1. An instrumental RMS error of measurement of pseudorange GLONASS of the L1 band by the code (a) and by the phase (b) of the carrier frequency.

Method to determine an RMS error regardless the noises of the reference generator

For the UNE developer, it is very important to be convinced of correctness of operation of the receiver. Usually at creation of UNE, a reference generator which noises are much lower than thermal noise of the receiver is chosen. However because of different errors of creation of the receiver it is important to know a contribution of noise of the reference generator to an error of measurements of pseudorange by the phase carrier. Definition of RMS errors of measurements of pseudoranges by the phase carrier regardless of the noises of the master oscillator is used for this purpose.

As it is necessary to determine RMS errors of measurements of pseudoranges by the carrier phase without the noises of the master oscillator, one should receive the expression where there is no value ΔT . To do this, using the difference of the expressions (16) and (17), we will receive

$$\Delta G_j(t_i) = G_j^{L2}(t_i) - G_j^{L1}(t_i) =$$

$$= -c \cdot (\Delta\tau_n^j + \Delta\tau_{L2}^j - \Delta\tau_{L1}^j) +$$

$$+ (\gamma - 1) \cdot I_g \cdot \frac{\alpha}{\sqrt{1 - \left[\frac{R_3}{R_3 + h}\cos\{\eta_j(t_i)\}\right]^2}} +$$

$$+ \lambda_{L2}^j\left(\varphi_{0,L2} + \varphi_{0,L2}^j - \varphi_{h,L2}^j + \varsigma_{\psi_j}^{L2}\right) -$$

$$- \lambda_{L1}^j\left(\varphi_{0,L1} + \varphi_{0,L1}^j - \varphi_{h,L1}^j + \varsigma_{\psi_j}^{L1}\right) +$$

$$+ M_j^{L1} \cdot \lambda_{L1}^j - M_j^{L2} \cdot \lambda_{L2}^j \qquad (21)$$

It is experimentally determined that for the navigation receiver installed on the satellite with the altitude of an orbit of 1000 km, the second derivative of the difference of pseudoranges by the carrier phase is almost equal to zero. The approximate value of the second derivative can be received by means of the following polynomial.

$$\Delta\Delta G_j(t_i) = \Delta G_j(t_{i+1}) -$$

$$- 2 \cdot \Delta G_j(t_i) + \Delta G_j(t_{i-1})$$

We should determine the pseudorange dispersion by the carrier phase in the L1 band as $\sigma^2_{G_j^{L1}} = [\lambda_{L1}^j]^2 \cdot \sigma^2_{\varsigma_{\psi_j}^{L1}}$ and in the L2 band as $\sigma^2_{G_j^{L2}} = [\lambda_{L2}^j]^2 \cdot \sigma^2_{\varsigma_{\psi_j}^{L2}}$.

The dispersion of the $\sigma^2_{\Delta\Delta G_j(t_i)}$ value will be equal to

$$\sigma^2_{\Delta\Delta G_j(t_i)} = \frac{1}{N}\sum_{i=1}^{N}[\Delta\Delta G_j(t_i)]^2 =$$

$$= \frac{1}{N}\sum_{i=1}^{N}\left[\Delta G_j(t_{i+1}) - 2 \cdot \Delta G_j(t_i) + \Delta G_j(t_{i-1})\right] \times$$

$$\times \left[\Delta G_j(t_{i+1}) - 2 \cdot \Delta G_j(t_i) + \Delta G_j(t_{i-1})\right] =$$

$$= \frac{1}{N}\sum_{i=1}^{N}[\Delta G_j(t_{i+1})]^2 + \frac{4}{N}\sum_{i=1}^{N}[\Delta G_j(t_i)]^2 +$$

$$+ \frac{1}{N}\sum_{i=1}^{N}[\Delta G_j(t_{i-1})]^2 = \frac{6}{N}\sum_{i=1}^{N}[\Delta G_j(t_i)]^2 =$$

$$= 6 \cdot \sigma^2_{\Delta G_j(t_i)} \qquad (22)$$

Here a statistical independency of readings of pseudoranges by the carrier phase is considered as well as their similar dispersion during the session.

The dispersion of differences $\Delta G_j(t_i)$ is to be determined:

$$\sigma^2_{\Delta G_j(t_i)} = \frac{1}{N}\sum_{i=1}^{N}[\Delta G_j(t_i)]^2 =$$

$$= \frac{1}{N}\sum_{i=1}^{N}[\Delta G_j(t_i)]^2 = \frac{1}{N}\sum_{i=1}^{N}[G_j^{L2}(t_i) - G_j^{L1}(t_i)]^2 =$$

$$= \frac{1}{N}\sum_{i=1}^{N}[G_j^{L2}(t_i)]^2 + \frac{1}{N}\sum_{i=1}^{N}[G_j^{L1}(t_i)]^2 = \sigma^2_{G_j^{L2}} + \sigma^2_{G_j^{L1}} \qquad (23)$$

Hence,

$$\sigma^2_{\Delta\, G_j(t_i)} = 6 \cdot \sigma^2_{G_j^{L2}} + 6 \cdot \sigma^2_{G_j^{L1}} \qquad (24)$$

The dispersions of pseudophases in the L_1 and L_2 bands caused by the noises of the equipment, which in case are determined by the expressions [1,4]:

$$\sigma^2_{G_j^{L1}} = [\lambda_{L1}^j]^2 \cdot \left[\frac{\Delta f_{C\ \hat{O}}\left(1 + \frac{1}{2 \cdot k \cdot q_{c/n_0,L1} \cdot T'}\right)}{k \cdot q_{c/n_0,L1}}\right] \qquad (25)$$

$$\sigma^2_{G_j^{L2}} = [\lambda_{L2}^j]^2 \cdot \left[\frac{\Delta f_{C\ \hat{O}}\left(1 + \frac{1}{2 \cdot k \cdot q_{c/n_0,L2} \cdot T'}\right)}{k \cdot q_{c/n_0,L2}}\right] \qquad (26)$$

where

$\Delta f_{\text{ССФ}} = 25$ Hz, the noise band of PLL;

k is the reserve coefficient;

$q_{c/n_0,L1}$, $q_{c/n_0,L2}$ is the energy potential of the radio link in the L_1 and L_2 bands;

$T' = 1$ sec is the time for accumulation of information parameters of the digital receiver.

Taking into account the dependences $q_{c/n_0,L1} = \beta \cdot q_{c/n_0,L2}$ will be written as

$$\sigma^2_{\Delta\Delta G_j(t_i)} \approx 6 \cdot [\lambda^j_{\mathrm{L1}}]^2 \times$$
$$\times \left[\frac{\Delta f_{\mathrm{CC\Phi}} \left(1 + \frac{1}{2 \cdot k \cdot q_{c/n_0,\mathrm{L1}} \cdot T'} \right)}{k \cdot q_{c/n_0,\mathrm{L1}}} \right] \cdot (1 + \gamma \cdot \beta) \approx$$
$$\approx 6 \cdot [\lambda^j_{\mathrm{L2}}]^2 \cdot \left[\frac{\Delta f_{\mathrm{CC\Phi}} \left(1 \right) \frac{1}{2 \cdot k \cdot q_{c/n_0,\mathrm{L2}} \cdot T'} \right)}{k \cdot q_{c/n_0,\mathrm{L2}}} \right] \times$$
$$\times \left(1 + \frac{1}{\gamma \cdot \beta} \right) \quad (27)$$

Hence, we receive the values of RMS error pseudoranges by the carrier phase in the L_1 and L_2 bands.

$$\sigma_{G^{\mathrm{L1}}_j} \approx \left[\frac{\sigma^2_{\Delta\Delta G_j(t_i)}}{6 \cdot (1 + \gamma \cdot \beta)} \right]^{0,5} \quad (28)$$

$$\sigma_{G^{\mathrm{L2}}_j} \approx \left[\frac{\sigma^2_{\Delta\Delta G_j(t_i)}}{6 \cdot (1 + \gamma \cdot \beta)} \cdot \gamma \cdot \beta \right]^{0,5} \quad (29)$$

As an example of using the expression (28) in the Fig. 2, the graph of the change of the calculated σ_{G_j} pseudorange GLONASS of the L1 band by the carrier phase regardless the noises of the reference oscillator is given. In the Figure, the relative time is a number of 10-second readings during navigation session. A dashed graph is explained by the conditions of the visibility zone of the navigation spacecraft by the antenna system of UNE located on the satellite with the orbit of about 1000 km.

Assessment of instability of the reference generator

In case of obtaining an essential difference in RMS errors of pseudoranges by the carrier phase in the corresponding range taking into account noises of the reference generator and without the noises, it is possible to approximately estimate instability of the reference generator under operation.

The known formula of Doppler frequency

$$F_{\mathrm{D}} = -F_0 \cdot \frac{V}{c}$$

where

F_0 is the carrier frequency, V is the radial velocity, c is the light speed.

Hence, frequency errors are connected with speed errors as follows:

$$\Delta F_{\mathrm{D}} = -F_0 \cdot \frac{\Delta V}{c}$$

Hence,

$$\frac{\Delta F}{F_0} = \frac{|\Delta F_{\mathrm{D}}|}{F_0} = \frac{|\Delta V|}{c}$$

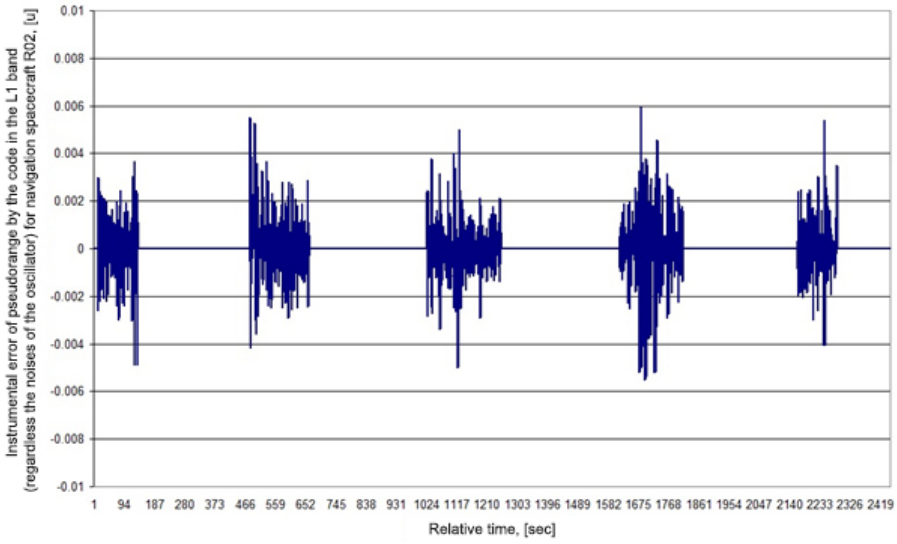

Fig. 2. Instrumental RMS error of measurement of pseudorange GLONASS of the L1 band by the carrier phase (regardless the noises of the reference oscillator)

Here $\frac{\Delta F}{F_0}$ is a short-term instability of the reference generator.

The speed in the moment of time *i* is connected with the range by the following ratio: $V_i = \dot{D}_i = \frac{D_{i+1} - D_{i-1}}{2 \cdot \Delta t}$

Here D_{i+1}, D_{i-1} are the readings of pseudorange by the phase in $i + 1$ and $i - 1$ moments of time,

Δt is the time interval between the readings (this interval is equal to 1 second in the receiver).

In this case, the error of the speed will be determined through the RMS error of pseudorange (σ_D) obtained regardless the noises of the reference generator and the RMS error of pseudorange (σ_{D+}) obtained taking into account the noises of the reference generator in the form:

$$\Delta V = \frac{\sqrt{\sigma_{D+}^2 - \sigma_D^2}}{\sqrt{2} \cdot \Delta t}$$

Hence,

$$\frac{\Delta F}{F_0} = \frac{|\Delta V|}{c} = \frac{\sqrt{\sigma_{D+}^2 - \sigma_D^2}}{\sqrt{2} \cdot c \cdot \Delta t} \quad (30)$$

One should take a right border of the confidence limit as the values of the RMS error of pseudoranges. This approach is valid when $\sigma_{D+}^2 > \sigma_D^2$.

Conclusion

The technique is developed to determine RMS errors of measurements of radio navigation parameters determined by the UNE. In the developed technique the selection of the number of measurements of radio navigation equipment sufficient for evaluation of a RMS error, definition of an RMS error of measurements of radio navigation equipment taking into account and without instability of the reference generator of the receiver is performed, and assessment of instability of the reference generator is given. The assessment of operation quality of the UNE and compliance of its characteristics to the set criteria is the result of application of this technique.

The carried out experimental estimates by the offered technique of definition of RMS errors clearly demonstrate the influence of instability of the reference generator on characteristics of UNE.

References

1. *GLONASS. Printsipy postroeniya i funktsionirovaniya* [GLONASS. Principles of construction and operation]. Moscow, Radiotekhnika, 2010, 800 p. Eds. Perov A.I., Kharisov V.N. 4th ed. rev. (in Russian)
2. Povalyaev A.A. *Sputnikovye radionavigatsionnye sistemy: vremya, pokazaniya chasov, formirovanie izmereniy i opredelenie otnositel'nykh koordinat* [Satellite radio navigation systems: time, clock readings, formation of measurements and determination of relative coordinates]. Moscow, Radiotekhnika, 2008, 328 p. (in Russian)
3. Povalyaev A.A., Veytsel' V.A., Mazepa R.B. *Global'nye sputnikovye sistemy sinkhronizatsii i upravleniya v okolozemnom prostranstve: ucheb. posobie* [Global satellite systems for synchronization and control in near-Earth space: Textbook]. Moscow, Vuzovskaya kniga, 2012, 188 p. Ed. Povalyaev A.A. (in Russian)
4. *Statisticheskaya teoriya radiotekhnicheskikh sistem. Uchebnoe posobie dlya vuzov.* [Statistical theory of radio engineering systems. Textbook for universities]. Moscow, Radiotekhnika, 2003, 400 p. (in Russian)
5. Vovasov V.E., Ipkaev N.B. Metodika opredeleniya apparaturnykh zaderzhek signala dlya dvukhchastotnogo priemnika SRNS GLONASS [Technique of Definition of Hardware Delays of a Signal for Two-Frequency Receiver SRNS GLONASS]. *Raketno-kosmicheskoe priborostroenie i informatsionnye sistemy* [Rocket-Space Device Engineering and Information Systems]. 2014, Vol. 1, No. 2, pp. 25–32. (in Russian)
6. Venttsel' E.S. *Teoriya veroyatnostey* [Probability theory]. Moscow, Nauka, 1968, 576 p. (in Russian)

ROCKET-SPACE DEVICE ENGINEERING AND INFORMATION SYSTEMS
Vol. 5, Iss. 2, 2018, pp. 10–17

Variant of Technical Realization of Non-Linear Multiplexing GLONASS FDMA and CDMA Navigation Signals

A.A. Biryukov, *povalyaev_aa@spacecorp.ru,*
Joint Stock Company "Russian Space Systems", Moscow, Russian Federation

Abstract. Due to modernization of the GLONASS system, a problem of non-linear multiplexing of GLONASS FDMA and CDMA navigation signals has become of interest. The multiplexing allows transmitting these signals through a common space vehicle (SV) antenna. Development of an apparatus for generating composite (group) L1 and L2 signals each formed by non-linear multiplexing of GLONASS FDMA and CDMA navigation signals may reduce mass-dimensional characteristics of SV with a simultaneous improvement of accuracy characteristics of the signals. However, the difficulty of such multiplexing is that clock frequencies and central frequencies of the multiplexed GLONASS navigation signals have an unacceptably great value of lowest common multiple, as opposed to the value for known methods of non-linear multiplexing, such as AltBOC modulation.
The article proposes an algorithm for computing model values of a composite signal. The algorithm considerably simplifies technical realization of the non-linear multiplexer (NMUX) to form GLONASS signals. A method of computing energy loss is proposed. Spectrum of a composite signal in radio astronomy band is estimated.

Keywords: global navigation satellite system (GNSS), GLONASS, non-linear multiplexing, energy loss, AltBOC

Introduction

In the course of modernization of the GLONASS system, in addition to frequency signals (signals with frequency division), code signals are introduced (signals with code division). Spectra of frequency and code signals are blocked in the radio-frequency ranges L1 and L2 GLONASS. In this regard, the problem of consolidation (multiplexing) of these signals for their radiation via the general antenna is of interest.

The structure of the mentioned GLONASS signals is such that the problem of their consolidation in each of the ranges L1 and L2 comes down to consolidation of two quadrature pairs of signals. In the world practice, AltBOC modulation [1], which belongs to nonlinear methods of consolidation, is applied to solve a similar task. However, AltBOC modulation is developed provided that clock frequencies of the modulating sequences of the condensed signals and the central frequencies of their ranges are a multiple of the frequency of 1.023 MHz. In case of GLONASS signals, this condition it is not satisfied and leads to the fact that the clock frequency of the nonlinear consolidation device (NCD) within these methods has to be unacceptably high. For example, if in the range of L1 code GLONASS signals (the central frequency of the spectrum is 1600.995 MHz) and GLONASS frequency signals at a frequency with the number k = 6 are condensed, i.e., at the frequency (1600.995 + 4.38) MHz, then in case of application of AltBOC –type modulation, the clock frequency of NCD will be equal 41820.24 MHz. This value is equal to a least common multiple of the following frequencies (in megahertz): 1.023; 2.046; 10.23; 0.511; 5.11; 4.38×4.

In [2] and [3] it is shown that in the mathematical model of a compound AltBOC signal, a method of linear summation of components (condensed signals) with the subsequent restriction of an amplitude is used and that this method is optimum by the minimum criterion of power losses from alignment. In [2] and [3] it is also shown that the simulating sequence of a compound AltBOC signal is formed by calculation of model values of this sequence in discrete moments of time.

In the paper, the algorithm of calculation of model values of GLONASS compound signals, which allows one to simplify technical implementation of the shaper of these signals is offered. This algorithm is applicable for consolidation of two quadrature couples of any signals.

Structure of the multiplexed GLONASS signals

Initially in the GLONASS system, frequency navigation signals were used. Each navigation spacecraft of the GLONASS system has two carrier frequencies, one in the radio-frequency range L1, another is in L2 range. These carrier frequencies are determined by the formulas:

$$f_{k1}=f_{01}+k \cdot \Delta f_1,$$

$$f_{k2}=f_{02}+k \cdot \Delta f_2$$

where k is the number of the carrier frequency that takes the values from -7 to +6;

$f_{01}=1602$ *MHz*, $\Delta f_1=562.5$ *kHz* are the parameters for the L1 band;

$f_{02}=1246$ *MHz*, $\Delta f_2=437.5$ *kHz* are the parameters for the L2 band.

On each of the carrier frequencies f_{k1} and f_{k2}, the navigation spacecraft radiated two signals of an equal power called by average precision (AP) and high precision (HP). Thus, each navigation spacecraft radiated four navigation signals: L1 AP, L1 HP, L2 AP, and L2 HP. These signals are also known as L1OF, L1SF, L2OF, L2SF, respectively. At first, these signals were multiplexed with a quadrature method in each of the L1 and L2 ranges, and then the received quadrature couples were multiplexed by a diplexer. Range codes for AP and HP signals have clock frequencies of 0.511 and 5.11 MHz, respectively.

In the course of modernization of the GLONASS system, new code navigation signals were introduced into it. Each navigation spacecraft of the GLONASS system were given three carrier frequencies in the L1, L2, L3 radio-frequency ranges:

$$f_{L1}=1565 \cdot 1.023=1600.995 \text{ MHz},$$

$$f_{L2}=1220 \cdot 1.023=1248.06 \text{ MHz},$$

$$f_{L3}=1175 \cdot 1.023=1202.025 \text{ MHz}.$$

On these carrier frequencies, it is planned to radiate L1OC, L1SC, L2OCp, L2 KSI, L2SC, and L3OC code signals.

Vector charts of the specified GLONASS navigation signals are given in Fig. 1 (a HP signal lags behind in phase from an AP signal by 90 °). The powers of quadrature couples of signals in the L1 and L2 ranges for GLONASS code signals are twice higher, than for GLONASS frequency signals.

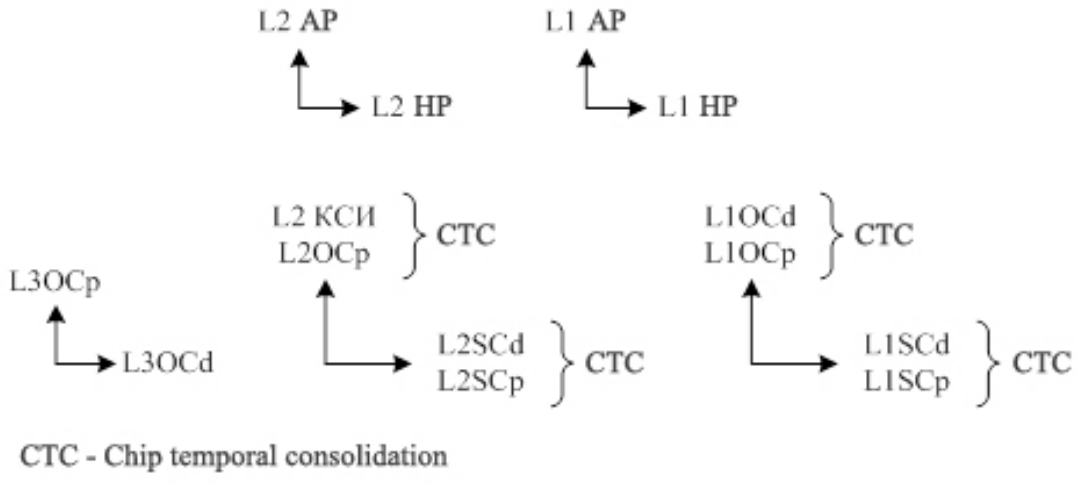

Fig. 1. Vector diagrams of GLONASS navigation signals

The offered scheme of creation of NCD signals of L1 GLONASS

In terms of NCD, L1 and L2 GLONASS signals differ only by carrier frequencies therefore consolidation only in the L1 band will be considered further. As a mathematical model of a compound signal the following complex function is offered:

$$s(t)=\text{sign}[s_{L1SC}(t)+s_{L1OC}(t)+ +s_{HP}(t)+s_{AP}(t)] \cdot \exp(j2\pi f_0 t) \quad (1)$$

where f_0 is the carrier frequency of a compound signal equal to 1600.995 MHz for simplification of NCD;

sign (z) is the operation of amplitude restriction, equates the module of the complex number z to one unit, and leaves the argument in variable according to the formula $\text{sign}(z) = z/|z| = [\text{Re}(z) + j \cdot \text{Im}(z)]/\sqrt{\text{Re}(z)^2 + \text{Im}(z)^2}$;

$s_{L1SC}(t)$, $s_{L1OC}(t)$, $s_{HP}(t)$, $s_{AP}(t)$ are the complex signals determined by the formulas:

$$s_{L1SC}(t)=\text{PRS}_{L1SC}(t),$$

$$s_{L1OC}(t)=j \cdot \text{PRS}_{L1OC}(t),$$

$$s_{HP}(t)=\text{PRS}_{HP}(t) \cdot a \cdot \exp[j2\pi f_1 t]= =\text{PRS}_{HP}(t) \cdot a \cdot [\cos(2\pi f_1 t)+j \cdot \sin(2\pi f_1 t)],$$

$$s_{AP}(t)=\text{PRS}_{AP}(t) \cdot a \cdot \exp[j(2\pi f_1 t+\pi/2)]= =\text{PRS}_{AP}(t) \cdot a \cdot [\cos(2\pi f_1 t+\pi/2)+j \cdot \sin(2\pi f_1 t+\pi/2)]= =\text{PRS}_{AP}(t) \cdot a \cdot [-\sin(2\pi f_1 t)+j \cdot \cos(2\pi f_1 t)];$$

$\text{PRS}_{L1SC}(t)$, $\text{PRS}_{L1OC}(t)$, $\text{PRS}_{HP}(t)$, $\text{PRS}_{AP}(t)$ are the modulating sequences of navigation signals L1SC, L1OC, L1 VT, and L1 ST taking the valuesvalues {1; −1};

a is the amplitude coefficient equal to 0.903585 that in the compound signal the power of HP and AP signals was twice less than the power of L1SC and L1OC signals according to the calculation procedure given in the section "Calculation of characteristics of nonlinear consolidation";

$f_1=(1.005+k \cdot 0.5625)$ is the difference (in megahertz) between the carrier frequency of HP and AP signals and the carrier frequency of L1SC and L1OC signals.

The Formula (1) is the foundation of the NCD building. The equalized signal $\text{sign}[s_{L1SC}(t)+s_{L1OC}(t)+s_{HP}(t)+s_{AP}(t)]$ is a signal for modulation. Its real part is fed onto an inphase (I) input of the quadrature modulator, and an imaginary part is fed onto a quadrature (Q) input (in the present article it is accepted that a quadrature component of the carrier advances in phase the inphase component by 90 °). The multiplier $\exp(j2\pi f_0 t)$ describes transfer of the modulating signal to the carrier frequency f_0.

In the sum signal $[s_{L1SC}(t)+s_{L1OC}(t)+s_{HP}(t)+s_{AP}(t)]$,one can it is possible to allocate the real $x(t)$ and the imaginary $y(t)$ part:

$$x(t)=\text{PRS}_{L1SC}(t)+\text{PRS}_{HP}(t) \cdot a \cdot \cos(2\pi f_1 t) - - \text{PRS}_{AP}(t) \cdot a \cdot \sin(2\pi f_1 t),$$

$$y(t)=\text{PRS}_{L1OC}(t)+\text{PRS}_{HP}(t) \cdot a \cdot \sin(2\pi f_1 t) - - \text{PRS}_{AP}(t) \cdot a \cdot \cos(2\pi f_1 t). \quad (2)$$

Hence, we receive the formula defining input signals of the quadrature modulator:

$$I(t) = x(t)/\sqrt{x^2(t) + y^2(t)},$$

$$Q(t) = y(t)/\sqrt{x^2(t) + y^2(t)}. \quad (3)$$

The compound signal created on the formulas (1)–(3) has power losses of 17.17% according to the calculation procedure which will be given later.

The $I(t)$ and $Q(t)$ signals are calculated using the functions sin, cos, $f(x,y)=1/\left|\sqrt{x^2+y^2}\right|$. These three functions in the real wave shaper can be realized only in the tabular way. To ease NCD, it is offered instead of employing the tables for the above-stated functions sin, cos and $f(x,y)$, to calculate $I(t)$ and $Q(t)$ directly as a tabular function of phases of components. Further, the basic principles of realization of this tabular function are described.

Let us consider the Formula (1). The constellation (phase chart) of the signal $[s_{L1SC}(t)+s_{L1OC}(t)]$ is made of four phases, evenly distributed on a circle and numbered from 0 to 3 (Fig. 2, *a*). The constellation of the signal $[s_{HP}(t)+s_{AP}(t)]$ are created of an infinite set of phases of this signal by the choice of the final amount of the phase values n which are evenly distributed around the circle (Fig. 2, *b*). At the same time it is important that phases with the number 0 in these two constellations differed by $(\pi/n)rad$. It excludes a possibility of a zero value of the sign (z) function in the Formula (1) and also minimizes power losses for the set n.

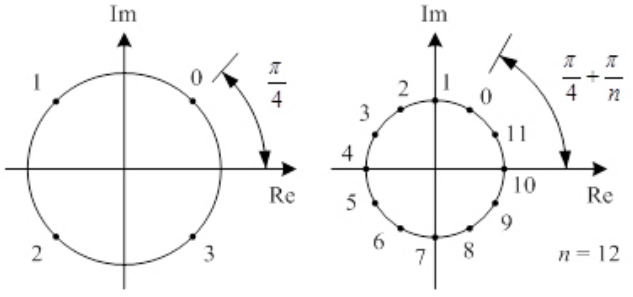

a - Signal constellation $[s_{L1SC}(t)+s_{L1OC}(t)]$

b - Signal constellation $[s_{HP}(t)+s_{AP}(t)]$

Fig. 2. Phase diagams of GLONASS signals being consolidated

It is obvious that each combination of numbers of phases of two constellations (Fig. 2) can be given the value of signals $I(t)$ and $Q(t)$ as compliance. These values can be calculated and kept in memory in advance. The parameter n and also clock frequency NCD f_s and bit depth C of the representation of each of the signals $I(t)$ and $Q(t)$ are determined based on the requirements to the precision characteristics if the signals being formed.

Thus, the scheme of NCD creation is offered to be realized in the form of the program which in discrete time points calculates the numbers of phases for two constellations (Fig. 2), and further, depending on these numbers, it takes from the memory the values $I(t)$ and $Q(t)$, which move further to the inputs of the quadrature modulator. Below the main ratios based on which it is possible to construct this program are described. The value of the phase in the constellation of the signal $[s_{L1SC}(t)+s_{L1OC}(t)]$ (Fig. 2, a) are calculated by the formula

$$p_1=\pi/4+n_1\cdot\pi/4, \quad (4)$$

where $n_1=\overline{0,3}$ is the number of the phase, which is determined depending on the values of $PRS_{L1SC}(t)$ and $PRS_{L1OC}(t)$ according to the Table 1.

Table 1. A rule for calculating the phase number n_1 in the constellation $[s_{L1SC}(t)+s_{L1OC}(t)]$

$PRS_{L1SC}(t)$	$PRS_{L1OC}(t)$	n_1	p_1, *rad*
1	1	0	π/4
-1	1	1	3π/4
-1	-1	2	-3π/4
1	-1	3	-π/4

The phase value in the constellation of the signal $[s_{HP}(t)+s_{AP}(t)]$ (Fig. 2, *b*) is calculated by the formula

$$p_2=\pi/4+\pi/n+n_2\cdot 2\pi/n \quad (5)$$

where $n_2=\overline{0,n-1}$ is the phase number determined by the formula n_2=modn[phase2num$(p)+n_0\cdot n/4$];

p is the phase (in cycles) of the complex harmonica $\exp(j2\pi f_1 t)$

phase2num(p) is the operation операция, which carries out the choice of one of the numbers of the phases given in Fig. 2, the one that the value of the phase corresponding to it differed from p by minimum;

$n_1=\overline{0,3}$ is determined depended on the values of значений $PRS_{HP}(t)$ and $PRS_{AP}(t)$ в according to the Table 2;

$$\mathrm{modn}(x)=\begin{cases} x,\ 0\le x\le n-1,\\ x-n,\ x\ge n,\\ x+n,\ x<0. \end{cases}$$

Table 2. A rule for calculating n_0

$PRS_{HP}(t)$	$PRS_{AP}(t)$	n_0
1	1	0
-1	1	1
-1	-1	2
1	-1	3

The calculation of p is realized recursively by the formula

$$p = \mathrm{mod1}(p+\Delta p)$$

where $\Delta p=f_1/f_s$ is the increment p per one step of NCD;

$$\mathrm{mod1}(x)=\begin{cases} x, 0 \le x < 1, \\ x-1, x \ge 1, \\ x+1, x < 0. \end{cases}$$

Using the formulae (4) and (5), for each pair of the numbers n_1 and n_2, it is possible to calculate the values $I(t)$ and $Q(t)$ write them down into the files. However, if n is a multiple of four thus, using reduction formulae from trigonometry, one can store data only for n_1=0. If the values $I(t)$ and $Q(t)$ are written for n_1=0 in to the one-dimensional files A and B indexed from 0 to (n-1), these files can be employed to obtain the values $I(t)$ and $Q(t)$ for all n_1 and n_2 c using the following algorithm.

A case n_1=0, then

$$I(t)=A(n_2),\ Q(t)=B(n_2).$$

A case n_1=1, then

$$I(t)=-B(\mathrm{modn}(n_2-n/4),$$

$$Q(t)=A(\mathrm{modn}(n_2-n/4).$$

A case n_1=2, then

$$I(t)=-A(\mathrm{modn}(n_2-2\cdot n/4),$$

$$Q(t)=-B(\mathrm{modn}(n_2-2\cdot n/4).$$

A case n_1=3, then

$$I(t)=B(\mathrm{modn}(n_2-3\cdot n/4),$$

$$Q(t)=-A(\mathrm{modn}(n_2-3\cdot n/4).$$

It is obvious that in the given algorithm the index of the element of the files A and B for each of the stated four cases can be calculated by the formula

$$index=\mathrm{modn}(n_2-n_1\cdot m)$$

where $m=n/4$.

The scheme for NCD building given in Fig. 3, where the parameters f_s=102.3 MHz and $n=2^{12}=4096$ were given as an example, corresponds to the stated mathematical ratios.

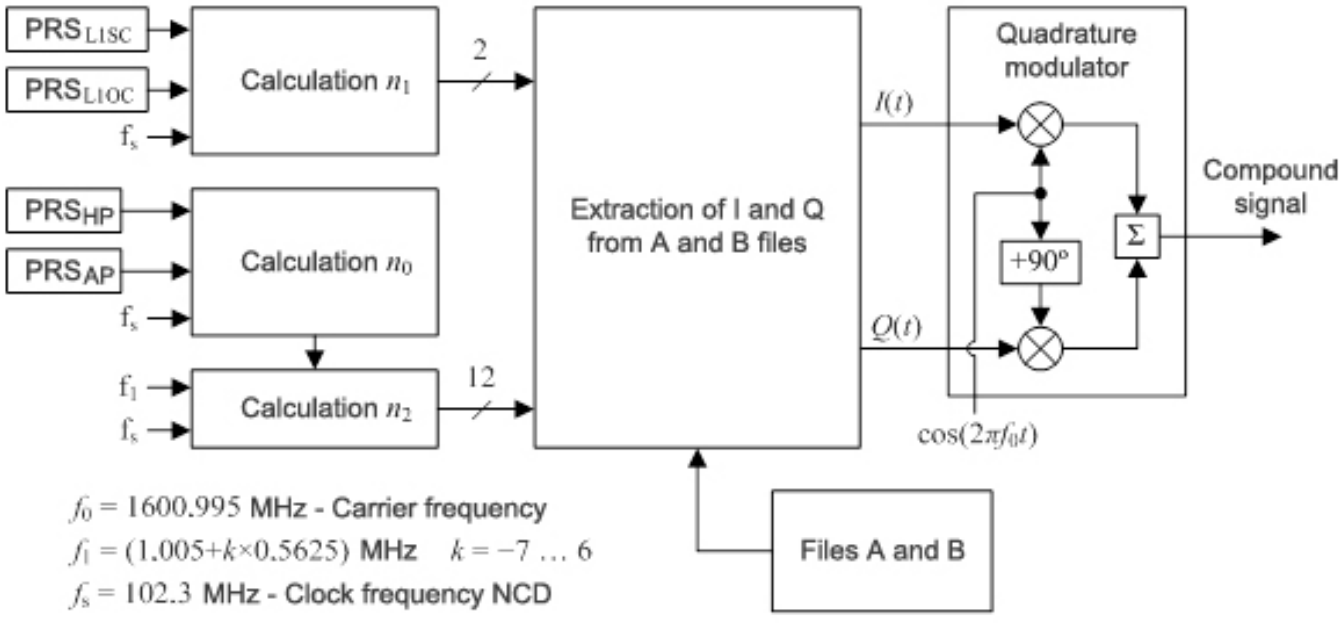

Fig. 3. The offered scheme for NCD building of L1 GLONASS signals

Calculation of nonlinear consolidation characteristics

The main characteristics of nonlinear consolidation are energy losses and distribution of the power of the components. There are no analytical expressions to calculate these characteristics in general case; hence, it is necessary to use numerical methods. One should calculate a spectral density of power flow (SDPF) in the radioastronomical range (RAR) (1610.6–1613.8) MHz for a compound GLONASS signal in the L1 range.

The present article calls energy losses as a share of power of a compound signal, which cannot be used in user navigation equipment (UNE). The most simple and vivid but not always precise accurate way to calculate energy losses is the following: a sum signal is formed (a linear sum of components) as well as compound (the same linear sum of components, but with the following amplitude limitation) in the complex form. These signals are being normed, thus their energies are equal. Later, two scalar products are calculated:

- a_{sign} is the scalar product of the reference signal of the reference and compound signals;
- a_{Σ} is the scalar product of the reference and compound signals.

These scalar products modulate the response of the correlator, respectively, onto the compound signal and sum signal. The squared ratio of these scalar products equals the ratio of signal powers when there is an amplitude limitation and the absence of such (squaring is needed because the response of the correlator is proportional to the amplitude but not to the power of the received signal). Energy losses are calculated by the formula

$$L = \overline{1-(a_{sign}/a_{\Sigma})^2} \qquad (6)$$

where the horizontal line is a statistical averaging.

A separate component and sum of several or all components can be chosen as a reference signal, i.e., energy losses can be calculated for both separate components and sum of components. The simulation has shown that in case when the amplitudes of the signals $s_{L1SC}(t)$, $s_{L1OC}(t)$, $s_{HP}(t)$, $s_{AP}(t)$ differ in the Formula (1), thus losses for separate components calculated by the formula (6) turn out to be different. That means that at the amplitude limitation, redistribution of the power of components takes place. Under such conditions, the components with a bigger amplitude strengthen and the components with a less amplitude weaken.

If the amplitudes of the signals $s_{L1SC}(t)$, $s_{L1OC}(t)$, $s_{HP}(t)$, $s_{AP}(t)$ are designated as a_1, a_2, a_3, a_4, and the corresponding losses calculated by the Formula (6) are designated as L_1, L_2, L_3, L_4, so the power of separate components of a compound signal are determined by the formulae:

$$P_1 = a_1^2 \cdot (1-L_1),\ P_2 = a_2^2 \cdot (1-L_2),$$

$$P_3 = a_3^2 \cdot (1-L_3),\ P_4 = a_4^2 \cdot (1-L_4) \qquad (7)$$

And the power of a compound signal (the one based on the stipulation above equals to the power of a sum signal) is determined by the formula

$$P_{\Sigma} = a_1^2 + a_2^2 + a_3^2 + a_4^2. \qquad (8)$$

Based on the formulae (7) and (8), it is possible to determine the shares of the power of the components in the compound signal (they are equal to P_1/P_{Σ}, P_2/P_{Σ}, and so on) and the ratio of the power of the components (P_1/P_2, P_1/P_3 and so on).

Since energy losses can be determined as a share of the power of a compound signal, which does not account for useful components, we receive one more formula to determine energy losses:

$$L_{\Sigma} = 1-(P_1+P_2+P_3+P_4)/P_{\Sigma}. \qquad (9)$$

The difference between the formulae (6) and (9) is the following: the Formula (9) defines losses when all components are taken independently, i.e., for reception of each component one of the reference signals $s_{L1SC}(t)$, $s_{L1OC}(t)$, $s_{HP}(t)$, $s_{AP}(t)$ is used. The Formula (6) defines losses when a reference signal is equal to the linear sum of two or more components.

The simulation has shown that in general case the formulae (6) and (9) give a different result. For example, if GLONASS signals are consolidated by the formula (1), thus L=0.1835 and L_{Σ}=0.1717. Hence, when receiving the components separately, the sum accumulated energy is bigger than when joint reception of the components. It can be concluded that a sum signal is not considered to be an optimum reference signal, and the formula (6) gives an overestimated value of energy losses. Thus, the present paper determines energy losses by the formula (9).

Table 3 gives the findings of the calculation of energy L_{Σ} and amplitude coefficient a for different values of the P_3/P_1 ratio of the output power of one quadrature pair of equal power signals to another one. The calculation if carried out for the case of using the n = 4096 parameter.

Table 3. The calculation of nonlinear consolidation of two quadrature signal pairs

P_3/P_1	L_Σ, %	a	P_3/P_1	L_Σ, %	a	P_3/P_1	L_Σ, %	a	P_3/P_1	L_Σ, %	a
0.01	0.97	0.197073	0.26	13.36	0.769662	0.51	17.26	0.907173	0.76	18.64	0.970622
0.02	1.87	0.274757	0.27	13.61	0.777985	0.52	17.35	0.910657	0.77	18.66	0.972364
0.03	2.71	0.331894	0.28	13.84	0.785960	0.53	17.44	0.914040	0.78	18.69	0.974058
0.04	3.51	0.378142	0.29	14.07	0.793608	0.54	17.52	0.917326	0.79	18.71	0.975705
0.05	4.25	0.417317	0.30	14.28	0.800949	0.55	17.60	0.920518	0.80	18.74	0.977306
0.06	4.95	0.451412	0.31	14.49	0.808002	0.56	17.67	0.923621	0.81	18.76	0.978862
0.07	5.61	0.481629	0.32	14.69	0.814785	0.57	17.74	0.926636	0.82	18.78	0.980373
0.08	6.24	0.508763	0.33	14.88	0.821311	0.58	17.81	0.929568	0.83	18.80	0.981841
0.09	6.83	0.533374	0.34	15.06	0.827596	0.59	17.88	0.932419	0.84	18.82	0.983265
0.10	7.39	0.555873	0.35	15.24	0.833652	0.60	17.94	0.935191	0.85	18.83	0.984647
0.11	7.91	0.576574	0.36	15.41	0.839492	0.61	18.00	0.937887	0.86	18.85	0.985986
0.12	8.41	0.595724	0.37	15.57	0.845127	0.62	18.06	0.940510	0.87	18.86	0.987283
0.13	8.89	0.613519	0.38	15.73	0.850567	0.63	18.11	0.943062	0.88	18.87	0.988539
0.14	9.34	0.630121	0.39	15.87	0.855822	0.64	18.16	0.945545	0.89	18.89	0.989753
0.15	9.77	0.645662	0.40	16.02	0.860900	0.65	18.22	0.947961	0.90	18.90	0.990925
0.16	10.18	0.660254	0.41	16.16	0.865811	0.66	18.26	0.950312	0.91	18.90	0.992056
0.17	10.57	0.673992	0.42	16.29	0.870561	0.67	18.31	0.952600	0.92	18.91	0.993144
0.18	10.94	0.686957	0.43	16.41	0.875159	0.68	18.35	0.954827	0.93	18.92	0.994188
0.19	11.29	0.699218	0.44	16.54	0.879611	0.69	18.40	0.956994	0.94	18.93	0.995188
0.20	11.63	0.710837	0.45	16.65	0.883923	0.70	18.44	0.959104	0.95	18.93	0.996143
0.21	11.95	0.721868	0.46	16.77	0.888101	0.71	18.47	0.961156	0.96	18.94	0.997048
0.22	12.26	0.732356	0.47	16.87	0.892151	0.72	18.51	0.963154	0.97	18.94	0.997900
0.23	12.55	0.742345	0.48	16.98	0.896079	0.73	18.54	0.965099	0.98	18.94	0.998693
0.24	12.83	0.751870	0.49	17.08	0.899889	0.74	18.58	0.966990	0.99	18.94	0.999422
0.25	13.10	0.760966	0.50	17.17	0,903585	0.75	18.61	0.968831	1.00	18.94	1.000000

As for power spectrum of the composed signal, its form is strongly depended on the number of the k frequency. Fig. 4 depicts the case $k = 6$, for which the excess of the admitted radiation level in rad. is maximum and equals 26 dB (this is about by 3 dB more than for the case of linear summation of signals). However, for the other k the situation is different. For instance, for $k = -3$ and $k = 0$, an admitted radiation level in rad. is exceeded insignificantly, and for $k = -1$ and $k = -2$ is not exceeded.

Conclusion

The present article based on the example of frequency and code GLONASS navigation signals, the calculation algorithm of model values of the compound signal formed by nonlinear consolidation of two quadrature pairs of signals having any central frequencies of ranges and any clock frequencies of the modulating sequences is offered. This algorithm allows one to significantly simplify technical implementation of NCD.

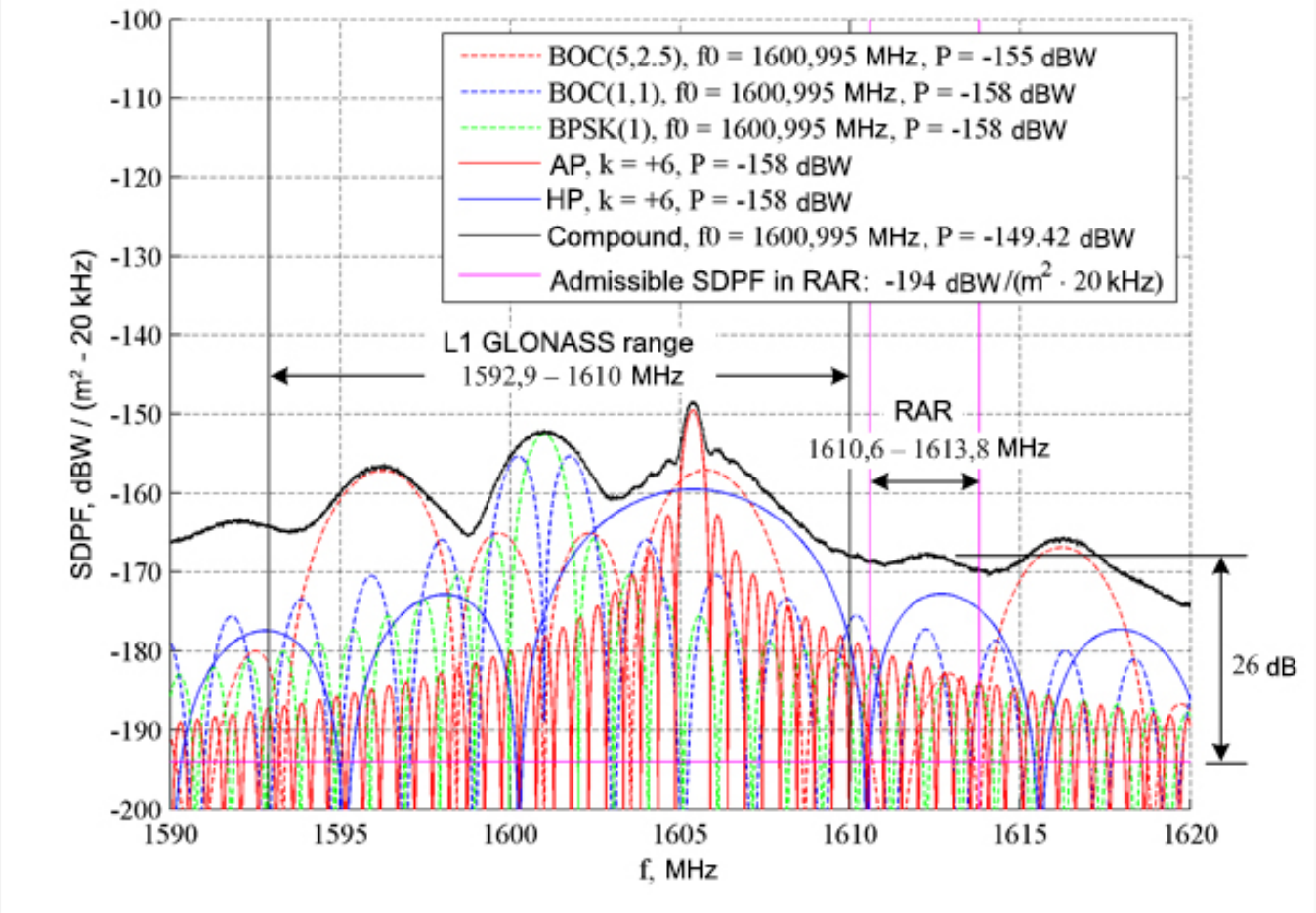

Fig. 4. SDPF of the compound L1 GLONASS signal for the number of the frequency of the AP and HP signals $k = 6$

References

1. Lestarquit L., Artaud G., Issler L-L. AltBOC for Dummies or Everything You Always Wanted to Know About AltBOC. *ION GNSS 21-st. International Technical Meeting of the Satellite Division*, 16-19, September 2008, Savannah, GA.
2. Kharisov V.N., Povalyev A.A. Optimal'noe vyravnivanie summy navigatsionnykh signalov v GNSS [Optimal Aligning GNSS Navigation Signals Sum]. *"Radiotekhnika"*, 2011, No. 7, pp. 65–75. (in Russian)
3. Kharisov V., Povalyaev A. Optimal aligning of the sums of GNSS navigation signals. *Inside GNSS*, 2012, Vol. 7, No. 1. pp. 56–67.

ROCKET-SPACE DEVICE ENGINEERING AND INFORMATION SYSTEMS
Vol. 5, Iss. 2, 2018, pp. 18–22

Analysis of Variability of Surface Heat and Impulse Fluxes and Water Vapor Content of the Atmosphere Over the North Atlantic Based on Satellite Microwave Data

A.G. Grankov, *Dr. Sci. (Phys.-Math.), agrankov@inbox.ru*
Kotel'nikov Institute of Radioengineering and Electronics of RAS, Moscow, Russian Federation
A.A.Milshin, *amilhin@list.ru*
Kotel'nikov Institute of Radioengineering and Electronics of RAS, Moscow, Russian Federation
N.K.Shelobanova, *nadezhda@ms.ire.rssi.ru:*
G.G. Yazeryan, *Cand. Sci. (Engineering), contact@spacecorp.ru*
Joint Stock Company "Russian Space Systems", Moscow, Russian Federation

Abstract. The estimates of spatial and temporal variations of monthly mean values of the near-surface vertical turbulent fluxes of sensible, latent heat and impulse, and the atmospheric total water vapor content in the North Atlantic were obtained based on the data from satellite microwave measurements. The Gulf Stream, Newfoundland, and Norwegian areas, which are characterized by the highest intensity of ocean-atmosphere heat exchanges, are the focus of this study. The long-term trends in water vapor changes over these areas were estimated. Some peculiarities of water vapor dynamics were observed in 2010, which manifested as intensive oil spills in the Gulf of Mexico in the spring of that year, as well as strong summer dryness over the European part of Russia.

Keywords: microwave radiation, brightness temperature, ocean–atmosphere system, energy active zones, sensible, latent heat and impulse, near-surface fluxes, water vapor of the atmosphere, radiometers SSM/I and AMSR-E

Introduction

Even 25-30 years ago when shipboard surveys were regularly conducted in the ocean, their frequency and scope were insufficient to solve an array of scientific and application-specific problems. A recent rapid decrease of the aforementioned measurements has increased the role of satellite-referenced surveying of the World Ocean. Satellite performance capabilities (measurement accuracy, spatial resolution and, most importantly, on-orbit life) have been incessantly improving. Modern satellites perform continuous measurements of the Earth's own microwave (MW) radiation with a diurnal or semidiurnal temporal resolution, thus, providing specialists with global and continuous meteorological and oceanographic information. At the same time, the nature of the tasks has changed from determining separate parameters of the ocean surface and atmosphere (ocean surface temperature, near-water wind velocity, atmospheric water vapor content) based on fragmentary measurements (obtained by first satellites: Kosmos-243, Nimbus-5, Kosmos-1056, Kosmos-1151) to using satellite estimates to determine their long-term variability (months, years).

The paper focuses on analyzing the spatial and temporal variations of monthly mean values of vertical turbulent fluxes of sensible, latent heat and impulses on the ocean surface and atmospheric total water vapor content – all of which comprise climate-forming factors.

The geographical area of research is the North Atlantic with coordinates 67°N, 95°W – 0°N, 0°W with a focus on the areas with the most intensive ocean–atmosphere heat exchanges: the Gulf Stream, Newfoundland, and Norwegian energy-active zones.

The results of regular measurements were obtained from the microwave radiometer (MR) SSM/I (Scanning Sensor Microwave/Imager) on the DMSP meteorological satellites and the AMSR-E (Advanced Microwave Scanning Radiometer) on the oceanographic satellite EOS Aqua. The technical characteristics of these satellites and their capabilities are presented in [1-3]; primary and thematic (secondary) processing of satellite measurement data is described in [4].

Separate findings on the possible usage of data gathered from satellite MR measurements for analyzing water vapor fields in the North Atlantic are set forth in works [5, 6].

Spatial and seasonal variability of monthly mean fluxes and water vapor in the North Atlantic

After processing the AMSR-E radiometer measurements (ascending and descending orbits of the EOS Aqua satellite) for November 2009 through December 2010 in the fragment of the North Atlantic with coordinates 67°N, 95°W – 0°N mean daily values of the sensible, latent heat and impulse fluxes were obtained. Subsequently, basing on them flux monthly mean values with a resolution of 0.25 degrees latitude and longitude (Figure 1 gives examples of processed data for February and August 2010) were calculated.

High temporal and spatial variability of all flux types can be noted in the North Atlantic. The highest flux intensity is exhibited during summer season, reaching peak values in July. The tropical zone east of Cuba in spring–summer seasons, as well as in October-September is characterized by increased values of this parameter. This zone belongs to the regions of tropical cyclone genesis, formation and passage. The seasonal peculiarity of impulse flux behavior lies in the minimal contrasts during summer season, whereas during fall–winter seasons contrasts essentially increase. The sensible heat fluxes are latitude-dependent: the most intensive fluxes are in the north of the Atlantic. Their value lowers on nearing equatorial latitudes.

Figure 1 illustrates a very important result — the possibility of monitoring the Gulf Stream in the sensible heat flux field from space with the spatial resolution of 0.25 x 0.25° provided by modern satellite microwave radiometric instruments.

Satellite estimates of the monthly mean values of total (sensible and latent) heat flux were compared with those of the famous OAFlux (oaflux.whoi.edu) archive in the location areas of ocean weather ship stations (weather ships) M (MIKE – 66° N, 0.5° W), D (DELTA – 44° N, 41° W) and H (HOTEL – 38° N, 71°W). These locations correspond to the Norwegian, Newfoundland and Gulf Stream energy-active zones. Comparison results demonstrate agreement between satellite and archive data.

Figure 2 shows estimates of the monthly mean values of total atmospheric water vapor content obtained by processing measurement data from the EOS Aqua satellite AMSR-E radiometer in 2009 and 2010.

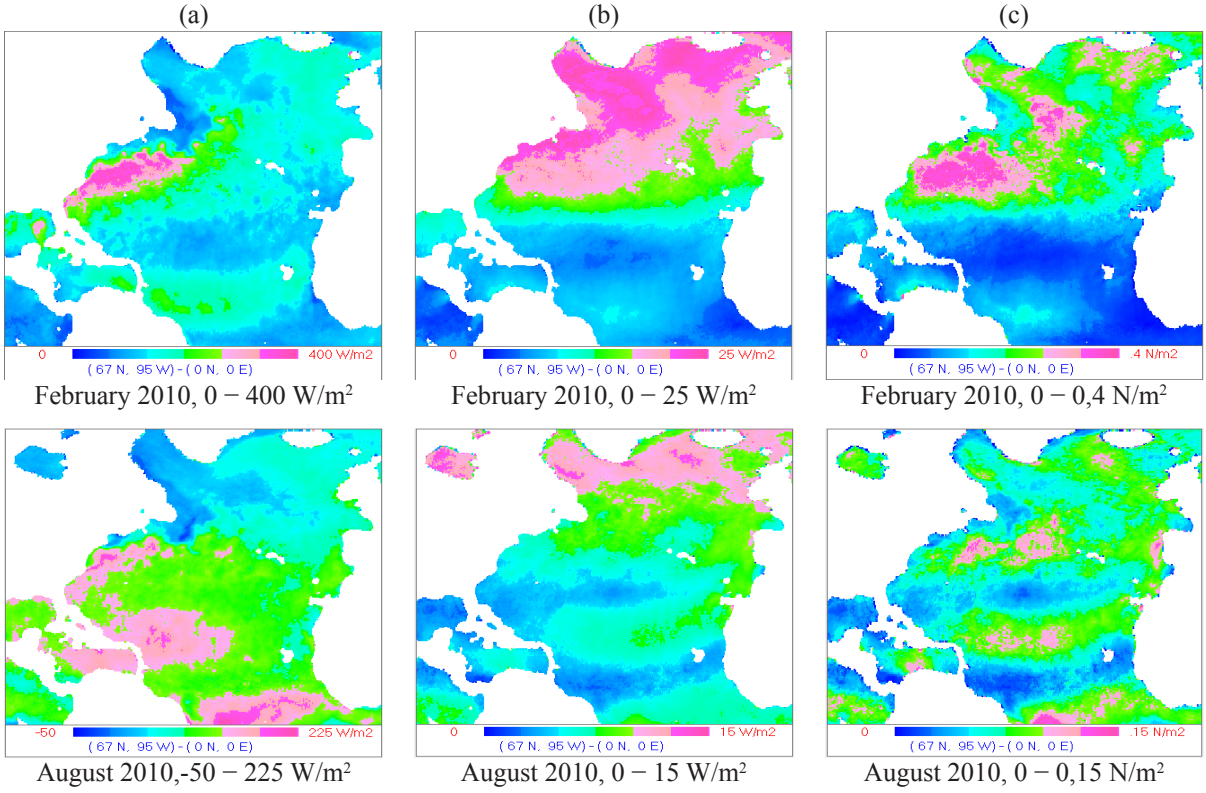

Fig.1. Spatial distribution of latent (a), sensible (b) heat fluxes and impulse (c) in the North Atlantic in 2010 according to AMSR-E radiometer data.

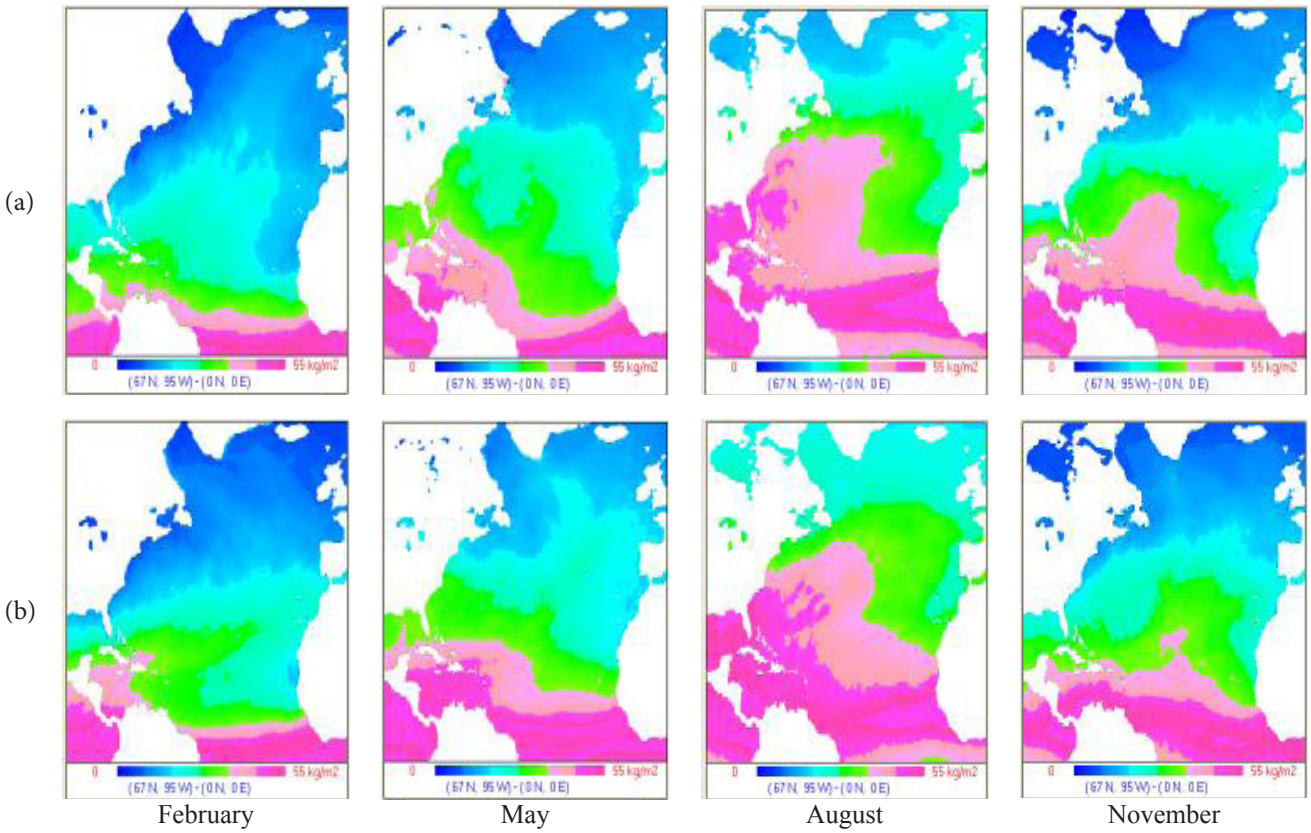

Fig.2 Spatial distribution of monthly mean values of total atmospheric water vapor content in the North Atlantic: (a) in 2009 (b) in 2010.

The picture of water vapor distribution in the North Atlantic is noticeably "striped" (delimited by latitudes). Figure 2. shows that the distribution has a well-defined latitudinal pattern (atmospheric humidity increases from lower latitudes to higher ones) and, yet, this parameter is highly contrasting as it varies from 15 to 55 kg/m^2 depending on the geographical latitude and season.

Interannual atmospheric water vapor variations in energy-active zones of the North Atlantic

The estimates of monthly mean atmospheric total water vapor content in the North Atlantic with a 0.25 latitude and longitude spatial resolution over the period 1988 – 2011 were obtained on the basis of the results of processing AMSR-E radiometer measurements over the period 2002–2011, supplemented by measurements of the radiometer SSM/I during the period 1988 – 2001. The temporal dynamics of water vapor in energy-effective zones M, D and H are given further in more detail.

Figure 3 gives monthly mean atmospheric total water vapor content values in North Atlantic zones M, D and H from 1988 to 2011 received in different years from SSM/I and AMSR-E radiometers

The illustration shows a noticeable effect of increasing water vapor quantity during these years that is clearly observed in zones D and H.

The increase of mean annual values of atmospheric water vapor content in the period 1996 – 2005, for example, in zones M, D, H amounted to 1, 1.1 and 1.5 kg/m^2 respectively. For the sake of comparison, we shall note that according to recent estimates received from GOME-SCIAMCHY (Global Ozone Monitoring Experiment-SCanning Imaging Absorption spectrometer for Atmospheric CHartographY) and HOAPS (Hamburg Ocean Atmosphere Parameters and Fluxes from Satellite Data) global variations of atmospheric water vapor during this period [7] were equal to 0.3–0.5 kg/m^2.

When evaluating global water vapor variations, probably, smoothing out the influence of such dynamic and contrasting, yet local, zones of the World Ocean, such as the energy-effective zones of the North Atlantic, the El Niño zone in the Pacific Ocean and others, plays a certain role.

Figure 4 illustrates mean interannual water vapor value variability in the Gulf Stream and Newfoundland energy-active zones over the period 1992 – 2011

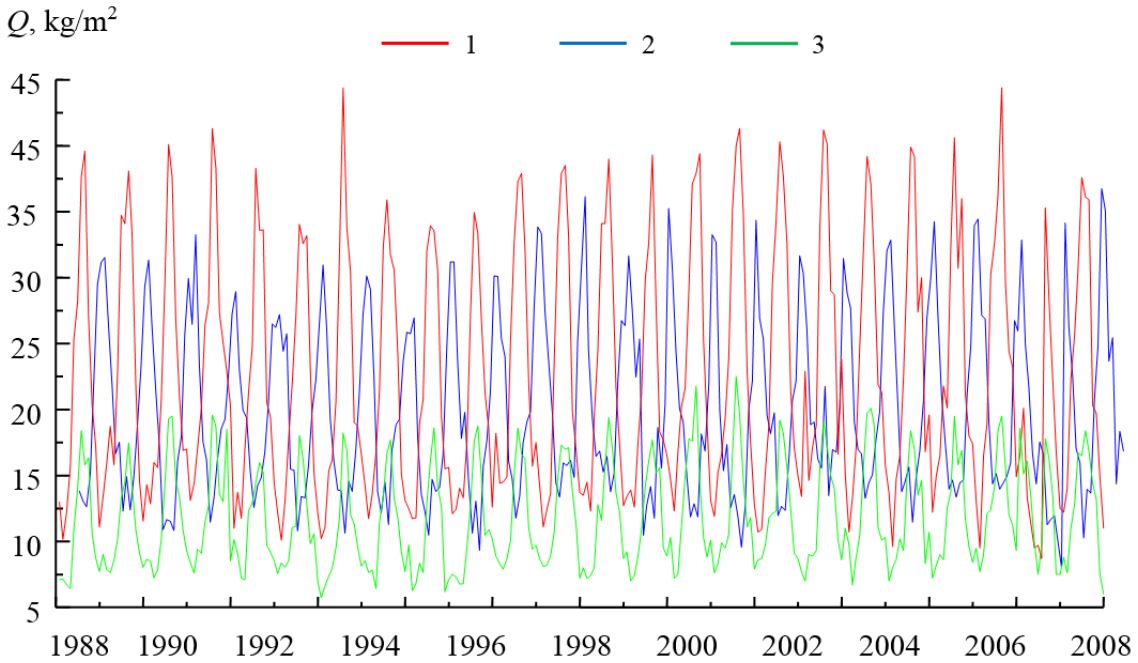

Fig.3 Long-term changes of monthly mean atmospheric total water vapor content values *Q* in North Atlantic zones H (1), D (2), M (3).

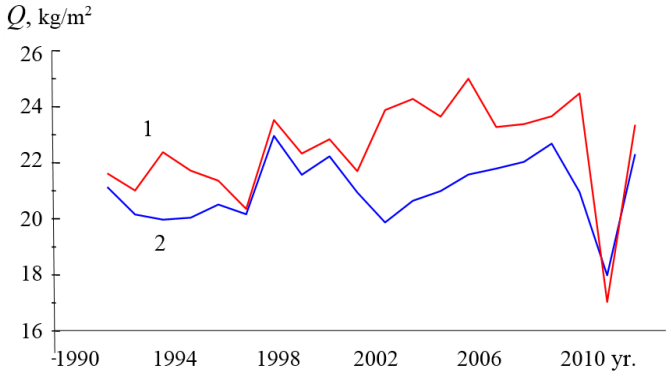

Fig.4. Variations of atmospheric total water vapor content in the Gulf Stream (1) and Newfoundland (2) energy-active zones of the North Atlantic during 1992–2011.

Zones H and D stand out in the illustration and are characterized by a sharp decrease of water vapor in 2010 (at the time of large oil spills in the Gulf of Mexico). The reduction of ocean surface evaporation in the Gulf Stream energy-active zone and the decrease in heat transfer to other zones in the Gulf Stream area explain this observation.

Conclusion

The main results obtained by analyzing AMSR-E and SSM/I radiometer measurement data:

1. The possibility of monitoring the Gulf Stream and its spatial/temporal variations in the sensible heat flux field from space with the spatial resolution of 0.25 x 0.25° was demonstrated.

2. An increase of monthly mean values of the atmospheric total water vapor content in the Gulf Stream, Newfoundland and Norwegian-Greenlandic energy-active zones of the North Atlantic from 1998 to 2011 was shown.

3. A sharp decrease of atmospheric total water vapor content in 2010 during intensive oil spills in the Gulf of Mexico in the spring, as well as strong summer dryness over the European part of Russia was discovered.

Therefore, radiometer scanners, such as the SSM/I and AMSR-E radiometers, are capable of serving as effective instruments for studying climate-forming factors: long-term spatial and seasonal variability of vertical turbulent heat, vapor and impulse fluxes on the ocean surface, atmospheric total water vapor content. This, in its turn, confirms the indispensability of space methods and Earth remote sensing systems in solving problems of hydrometeorology and climatology.

References

1. Hollinger P.H., Peirce J.L., Poe G.A. SSM/I instrument evaluation. *IEEE Trans. Geosci. Rem. Sensing*. 1990, Vol. 28, No. 5, pp. 781–790.
2. Kawanishi T., Sezai T., Ito et al. The advanced microwave scanning radiometer for the Earth Observing System (AMSR-E), NASDA's contribution to the EOS for global energy and water cycle studies. *IEEE Trans. Geosci. Remote Sens*. 2003, No. 48, pp. 173–183.
3. Grankov A.G., Mil'shin A.A. Sovremennoe sostoyanie sputnikovykh SVCh-radiometricheskikh sredstv dlya issledovaniya vzaimodeystviya okeana i atmosfery [The Modern Status of Satellite Microwave Radiometer Systems in the Studies of Ocean-Atmosphere Interaction]. *Problemy okruzhayushchey sredy i prirodnykh resursov* [Problems of Environment and Natural Resources]. 2016, No. 3, pp. 3–29. (in Russian)
4. Grankov A.G., Mil'shin A.A., Novichikhin E.P. *Radioizluchenie sistemy okean-atmosfera v ee energoaktivnykh zonakh* [Radio emission of the ocean-atmosphere system in its energy-active zones]. Saarbrucken, Lambert Academic Publishing, 2016, 314 p. (in Russian)
5. Grankov A.G., Mil'shin A.A., Shelobanova N.K., Chernyy I.V., Yazeryan G.G. Mnogoletnie variatsii vodyanogo para v Severnoy Atlantike po dannym sputnikovykh mikrovolnovykh izmereniy [Long-Term Variation of Total Vapor Over North Atlantic Using a Satellite Microwave Data]. *Raketno-kosmicheskoe priborostroenie i informatsionnye sistemy* [Rocket-Space Device Engineering and Information Systems]. 2015, Vol. 2, No. 2, pp. 47–52. (in Russian)
6. Mil'shin A.A., Shelobanova N.K., Grankov A.G. Mezhgodovye i vnutrigodovye variatsii vodyanogo para v Severnoy Atlantike po dannym sputnikovykh mikrovolnovykh izmereniy [Interannual and intraannual variations in total precipitable water over the North Atlantic from satellite microwave measurements]. *Meteorologiya i gidrologiya* [Russian Meteorology and Hydrology]. 2016, No. 8, pp. 18–25. (in Russian)
7. Mieruch S., Schroder M., Noltz S., Schulz J.S. Comparison of decadal global water vapor changes derived from independent satellite time series. *J. Geophys. Res*. 2014, No. 10, pp. 1–11.

ROCKET-SPACE DEVICE ENGINEERING AND INFORMATION SYSTEMS
Vol. 5, Iss. 2, 2018, pp. 23–30

Metrological and Methodical Aspects of Spectral-Energetic Calibrations of Optoelectronic ERS Equipment

D.O. Trofimov, *trofimov_do@spacecorp.ru*
Joint Stock Company "Russian Space Systems", Moscow, Russian Federation
Yu.M. Gektin, *Cand. Sci. (Engineering), petrov_sv@spacecorp.ru*
Joint Stock Company "Russian Space Systems", Moscow, Russian Federation
S.M. Zorin, *Cand. Sci. (Engineering), zorin_sm@spacecorp.ru*
Joint Stock Company "Russian Space Systems", Moscow, Russian Federation
A.A. Zaytsev, *zaytsev_aa@spacecorp.ru*
Joint Stock Company "Russian Space Systems", Moscow, Russian Federation

Abstract. The paper presents the results of modernization and the metrological characteristics of the Kameliya measuring complex of JSC "Russian Space Systems", as well as the methodological aspects of spectral-energetic calibrations of optoelectronic ERS equipment and the results of a brightness distribution study of the ribbon filament body of the TRU 1100-2350 lamp in operating mode. Optical circuits for measuring the spectral characteristics of optoelectronic ERS equipment, optical elements and blocks based on the Kameliya measuring complex are presented. The carried out work provided the possibility of obtaining the relative spectral characteristics of not only multi-zone scanning devices, but also measurements of transmission and reflection spectra of optical elements (spectral filters, mirrors, lenses) and optical units of remote sensing equipment in the wavelength range λ = 0.4-14 μm. In addition, a method has been developed for measuring the spectral characteristics of optical radiation sources (λ = 0.4-14 μm) and the results of the study of the brightness distribution of the filament of the TRU 1100-2350 lamp are presented.

Keywords: metrological characteristics, calibration, multispectral scanning device, measuring complex, spectral characteristic, optical layout, spectral radiance (SR)

Introduction

Radiometric measurements obtained with the help of Earth remote sensing (ERS) equipment are most relevant in such applications as:

- weather analysis and weather forecasting on a regional and global scale
- analysis and forecasting of the state of the seas and oceans
- analysis and forecasting of conditions for aviation flights
- detection and control of natural and man-made disasters and emergencies
- ecological control of the environment
- ensuring global monitoring in the interests of meteorology, climatology, and bioresource assessment.

The expansion of the nomenclature of multi-zone scanning devices (MSD) for hydrometeorological purposes (MSU-GS [1], MSU-MR [2], MSU-SR-M, MSU-MR-MP, MSU-O, RIVR) under development at JSC "Russian Space Systems", the increase in the number of flight models and in the pace of improvement of ERS-equipment design features dictate the corresponding development rates of the reference, experimental and stand, as well as, regulatory and methodological bases.

The demand for improvement of the hardware-methodical complex of metrological support and MSD radiometric parameter monitoring is conditioned by the following reasons:

- increase in radiometric accuracy, resolution and field-of-view of advanced ERS optical electronic equipment
- improvement of existing measuring tools and the creation of fundamentally new ones for assessing MSD characteristics
- the need to develop uniform, certified in accordance with metrological rules and standards, means and methods for calibrating and controlling MSD parameters
- the need to develop a system for ensuring unity and the accuracy required for the reproduction and transmission of differential quantities of multispectral and integrated optical radiation in the context of national standards and conditions of MSD standard operating in space.

The MSDs being developed at JSC "Russian Space Systems" produce high quality multizone video images in the wavelength range λ = 0.4-13.5 μm and undergo a ground-based radiometric calibration procedure. The procedure is necessary for the measurement of absolute values of effective radiance (ER) of objects L_{eff} (1) in the visible and near-infrared (IR) spectral range (λ = 0.4-2.5 μm) and of ER and radiation temperature in the thermal IR range (λ = 2.5-14 μm) for each spectral channel of the equipment.

$$L^n_{eff} = \int_0^\infty L(\lambda) S_n(\lambda) d\lambda \text{ , [W/(sr·m}^2\text{)]} \qquad (1)$$

where L^n_{eff} is the ER of the object, measured in channel n; $L(\lambda)$ is the spectral radiance (SR) of the object; $S_n(\lambda)$ – the relative spectral sensitivity of the MSD channel *n*.

MSD radiometric calibration is understood to be the procedure of forming a conversion characteristic for every spectral channel as the dependence of the output signal on the ER or the equivalent radiation temperature of the reference emitter (with account for the specified accuracy).

In accordance with the requirements of international documents [3] for advanced ERS radiometric equipment, it is required to ensure an ER measurement error of no more than 5% in the λ = 0.4-2.5 μm range and an absolute radiation temperature measurement error of 0.1-0.5 K in the range λ = 2.5-14 μm.

Metrological characteristics of the modernized complex *Kameliya*

The radiometric complex of JSC "Russian Space Systems" consists of:

1) the *Kameliya* measurement complex (Figure 1) engineered for the calibration of the monochromatic illuminant, diffuse illuminant and MSD, as well as for spectral characteristic measurement in the wavelength range λ = 0.4–2.5 (included in the State Register of Measuring Instruments and is checked annually by VNIIOFI as a reference measurement instrument);

2) IR measurement complex intended for radiometric calibration of MSD and measurement of spectral characteristics in a λ = 2.5–14 μm range.

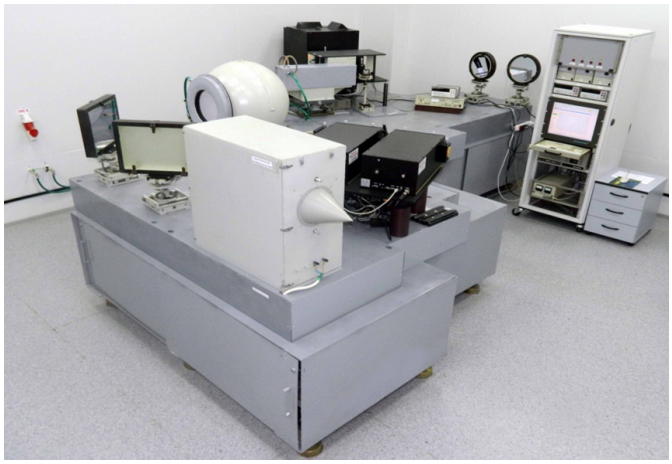

Fig. 1. The *Kameliya* measurement complex.

Currently, the metrological base of JSC "Russian Space Systems" for MSD development has been modernized.

The main areas of modernization, aimed at increasing radiometric calibration accuracy, are:

1) a class ISO8 clean room with antistatic protection of workplaces and automatic maintenance of the preset temperature (22 ± 2^{0}C, adjustable from 18 to 25^{0}C) and humidity (50 ± 10%) was certified and put in service in the assembly, adjustment, calibration and testing of optoelectronic equipment sections;

2) two digitally controlled modern monochromators in a subtractive configuration DM55S (λ = 0.4–2.5 μm) and MS257 (λ = 0.4–14 μm) were put into operation as part of the modernized *Kameliya* complex;

3) a universal program for controlling monochromators and data accumulation, which allows to automate the process of measuring spectral characteristics, has been developed. This considerably increases the capability for receiving and processing results along with reducing the random component of measurement errors;

4) the upgraded *Kameliya* complex has been certified and a pattern approval certificate for measuring instruments RU.E.377.A No. 55245, registration No. 57492-14 has been received (the metrological characteristics are set forth in Table 1);

5) an optical circuit with a maximum clear aperture of 230 mm for taking spectral characteristics of MSD in the range λ = 2.5–14 μm, where a model of an absolutely black body (ABB) type 67033 with a temperature range from +50^{0}C to +1050^{0}C (stability of ±0.02% in 24-hours) has been implemented;

Table 1. Metrological characteristics of the *Kameliya* complex, according to the results of the last calibration

Characteristic	Characteristic value
Wavelength range, μm	0.4–2.5
Absolute value of spectral radiance of the diffuse illuminant at the wavelength of 0.98 μm, W/(sr·m^3)	5.3·10^8
Maximum clear aperture of radiant flux, mm	230
Relative error in the results of measuring the absolute value of the spectral radiance of the diffuse illuminant at the wavelength of 0.98 μm, %	±6.4
Relative error in the results of measuring the relevant distribution of spectral radiance of the diffuse illuminant in the wavelength range from 0.4 to 2.5 μm, %	±5.1
Relative error in the results of measuring relative spectral distribution of radiation from a monochromatic illuminant in the wavelength range from 0.4 to 2.5 μm, %	±4.7

6) optical circuits and methods for measuring relative spectral characteristics of transmission and reflection of optical elements and blocks, as well as of optical emission sources in a spectral range of λ = 0.4–14 μm, have been developed;

7) a large-size temperature simulation chamber with a nitric environment (with an operating volume of 16 m^3 and an operating temperature range inside the chamber from +5^{0}C to +35^{0}C) for MSD radiometric calibration and for testing the impact of environment temperature changes on equipment has been commissioned and certified.

Methodological aspects of spectral-energetic calibrations of optoelectronic ERS equipment. Measurement of relative spectral characteristics in the wavelength range of λ = 0.4 – 14 μm

Figure 2 presents the typical optical schemes for measuring MSD spectral parameters based on the *Kameliya* measurement complex (Figure 2a: 1,3 – planar

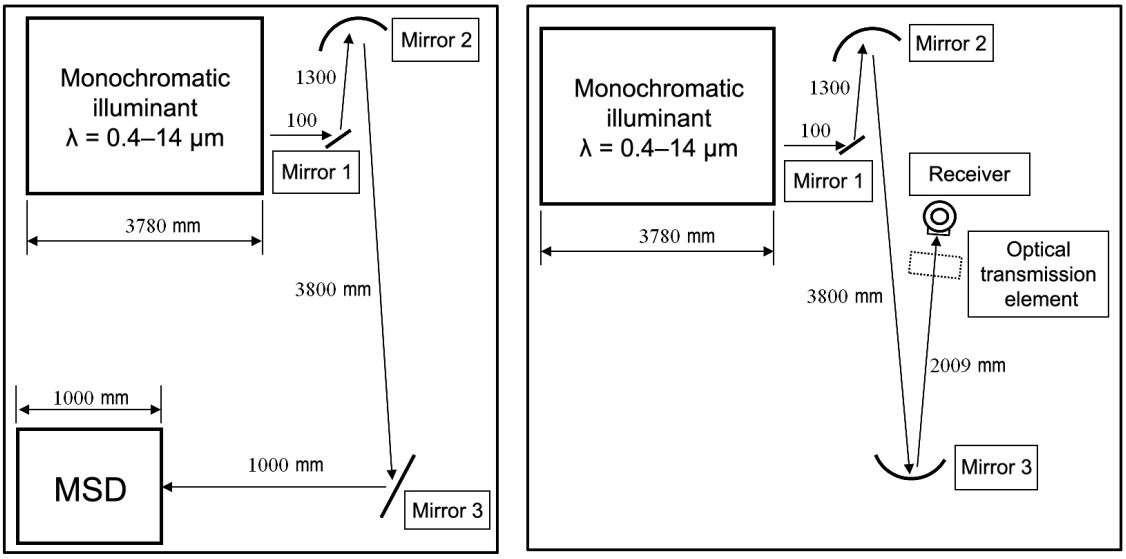

Fig. 2. Optical schemes of relative spectral characteristic measurements obtained by the *Kameliya* measurement complex.

mirrors, 2 – spherical mirror) (f = 1300 mm) and on the measurements of spectral characteristics of transmittance of optical elements and units (Figure 2b: 1 – planar mirror, 2 – spherical mirror (f = 1300 mm), 3 – spherical mirror (f = 2009 mm)).

Calibration of the monochromatic illuminant (MI) and MSD is carried out according to the measurement scheme given in Figure 2a.

According to the measurement scheme given in Figure 2b, two types of measurements are performed: illuminant calibration against a reference receiver and measurement of the transmission coefficient of optical elements (units).

Currently, the techniques for measuring the spectral characteristics of reflection of optical elements (for various angles) and sources of optical radiation in the λ = 0.4–14 μm spectral range have been implemented.

The monochromatic illuminant (MI) consists of the following elements: a TRU 1100- 2350 lamp (used for the λ = 0.4–2.5 μm range) or a type 67033 ABB model (used for λ = 2.5–14 μm range) as sources of radiation. They are connected with the help of a deflecting mirror, a condenser and a double monochromator of a subtractive configuration with digital control MS257 (spectral range: 0.4–14 μm).

In order to properly exclude the MI spectral characteristics together with the layer of air and to minimize measurement errors, it is necessary to provide the same optical path length for both stages: (MI + MSD measurement, Figure 2a) and (MI + reference receiver measurement, Figure 2b). Concurrently, the stability of measurement conditions (temperature, humidity and atmospheric composition (especially for the IR range)) is to be ensured.

In Figure 3, the results of measuring the spectral characteristics of one of the cut filters in the IR range of the spectrum λ = 8.0–9.5 μm, carried out in accordance with the scheme in Figure 2b, are given as an example.

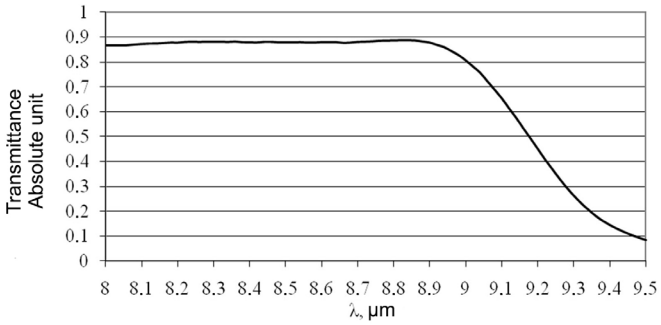

Fig. 3. Example of one of the cut filter's spectral characteristic in the IR range of the spectrum λ = 8.0–9.5 μm, obtained with the use of the *Kameliya* measurement complex in the IR range of the spectrum λ = 8.0–9.5 μm.

Such measurements (carried out in accordance with the scheme in Figure 2b) in the IR range of the spectrum (λ = 3.0–14 μm) have been made for each of the seven

IR channels of the fully manufactured MSU-GS beam splitting unit [1] (for the Electro-L No. 2 spacecraft). Also, the spectral characteristics (obtained in accordance with the scheme in Figure 2a) for all six channels (including IR channels) of the fully manufactured MSU-MR (for the Meteor-M No. 2 spacecraft [2]) have been received.

Figure 4 gives the relative spectral characteristics of one of the Al-based reflective coatings for various angles of reflection (10°, 45° and 60°) received with the use of the *Kameliya* measurement complex (with the implementation of an additionally designed instrument) in the IR range of the spectrum λ = 8.0–11.0 μm.

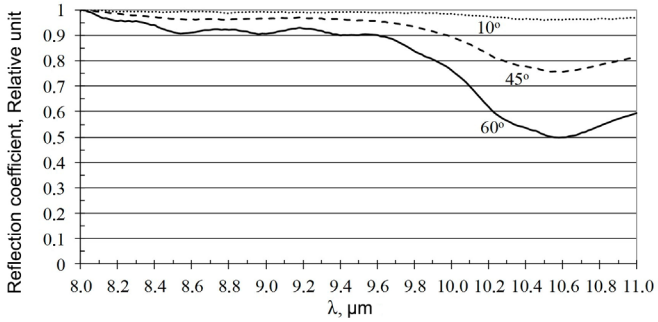

Fig. 4. Example of the spectral characteristics of one of the types of Al-based reflective coatings for different angles of reflection (10°, 45° and 60°) obtained with the help of the *Kameliya* measurement complex in the IR range of the spectrum (λ = 8.0–11.0 μm).

As the conducted studies show, the dependence of the spectral characteristic type of the reflective coating on the angle of reflection (Figure 4) in the IR range of the spectrum is explained by the absorption of the protective coating usually applied to Al mirrors. Despite the dielectric protective coating being amorphous, the IR vibrational spectra carry information about the short-range order of the atomic structure, which determines lattice absorption. In the case of normal incidence, only transverse optical phonons are recorded, whereas, in the case of oblique incidence, transverse and longitudinal phonons are recorded [4, 5]. The research results have demonstrated that, when choosing the reflective coating for mirrors designed to work at angles of more than 15° (deflecting and scanning mirrors for the IR range λ = 3–14 μm), the chemical composition, manufacturing technology, and thickness of the protective coating must be carefully considered to avoid dips in the value of the reflection coefficient in some wavelength ranges. Such dips substantially lower the quality of the optical path of infrared devices.

In Figure 5, measurements of the relative characteristics in the range λ = 400–2500 μm of a miniature halogen lamp with a rated power of 5 W (U_r = 12 V) for two different supply voltages (10 V and 6 V) is given.

Lamp filament brightness distribution of a TRU 1100-2350 lamp in operating mode

Absolute measurements of spectral radiance (SR) in the wavelength range λ = 0.4–2.5 μm during calibration of the diffuse illuminant (DI) from the *Kameliya* complex are carried out with the use of a reference TRU 1100-2350

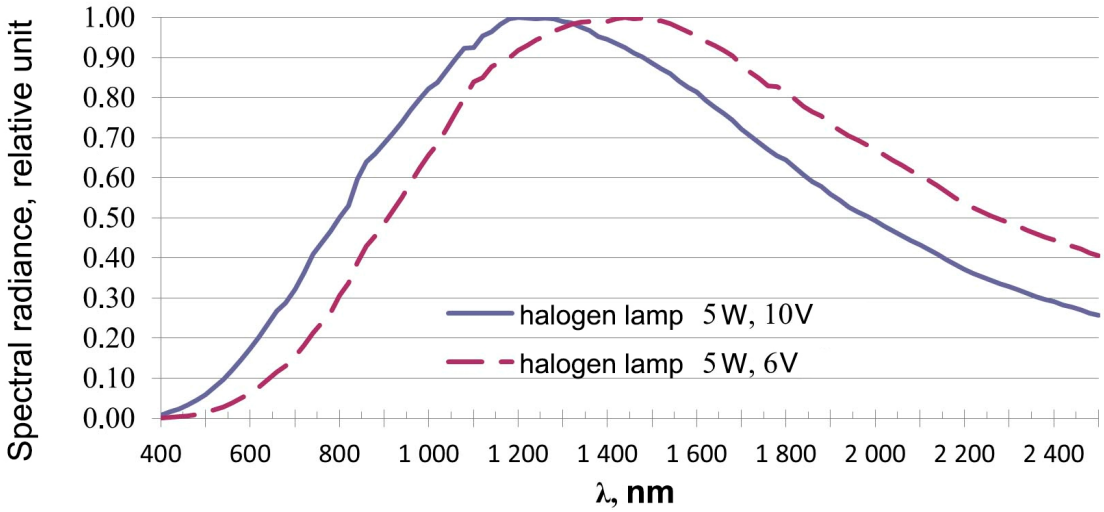

Fig. 5. Examples of relative spectral characteristics of radiation of a miniature halogen lamp with a rated power of 5 W (U_r = 12 V).

lamp (GOST 8.195-89 first category working standard), which is annually checked by VNIIOFI. The analysis of literature has shown the inconsistency of data on the distribution of brightness over the area of the ribbon lamp filament [6, 7].

The working area of the ribbon lamp filament of a TRU 1100-2350 is located opposite the pointer, facing the lamp envelope window (total ribbon size 2.8 x 20 mm). The limits of the working area are a distance of ±1 mm from the horizontal axis of the ribbon lamp filament, passing through the end of the pointer in accordance with the TU 16-546.108-76 technical specifications. In view of the strict requirements for the accuracy of SR absolute measurements, it is necessary to know how uneven the distribution of brightness across the lamp filament is.

Figure 6 illustrates a scheme for measuring the variance of lamp filament brightness. First of all, a laser module (operating at the wavelength λ = 637 nm) is installed behind the monochromator (MCh) entrance slit (opposite the center of the slit – Figure 6, laser). The entrance slit of the monochromator is limited in width to 0.6 mm and in height – to 0.5 mm.

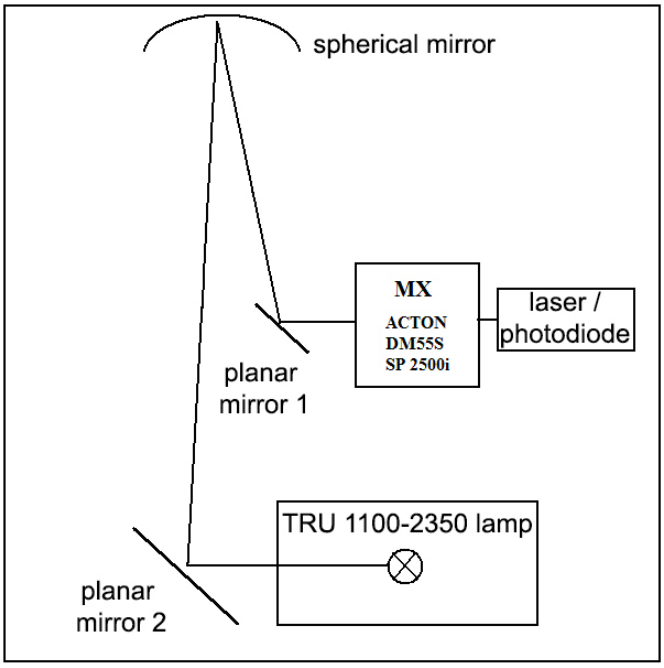

Fig. 6. Scheme for measuring the relative distribution of brightness across the area of a TRU 1100-2350 lamp filament.

After setting the monochromator wavelength to λ = 637 nm, the spot is aimed at the center of the mirrors horizontally and vertically (planar mirrors 1 and 2, spherical mirror) by adjusting the position of the mirrors and placing the laser spot in the center of the filament,

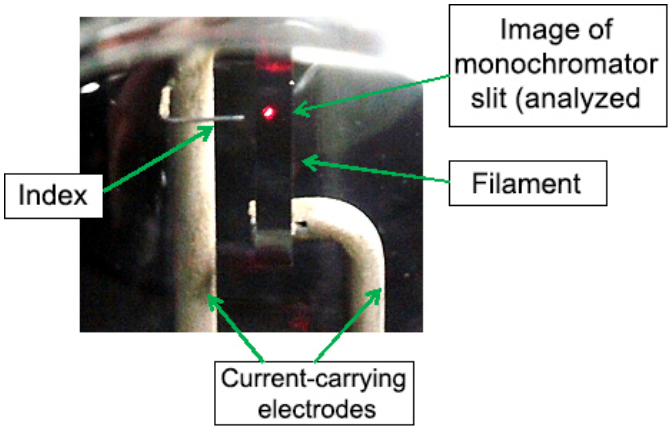

Fig. 7. Image of the monochromator slit in the plane of the filament during laser beam exposure (λ = 637 nm).

Later, the laser is turned on and a SZU 1337-1010BR photodiode (PD) is installed behind the exit slit of the monochromator (the laser module is not moved). The TRU 1100-2350 lamp is turned on (the rated current is 25 A ± 0.001 A) and the PD signal for a set point on the filament for λ = 980 nm (maximum SR for DI) with the help of an AGILENT 34401A multimeter. Analogous measurements are conducted at four more points of the filament body horizontally, and for each such point there are four more vertical points secured via shifting the laser light spot by movements of the lamp (Figures 8, 9).

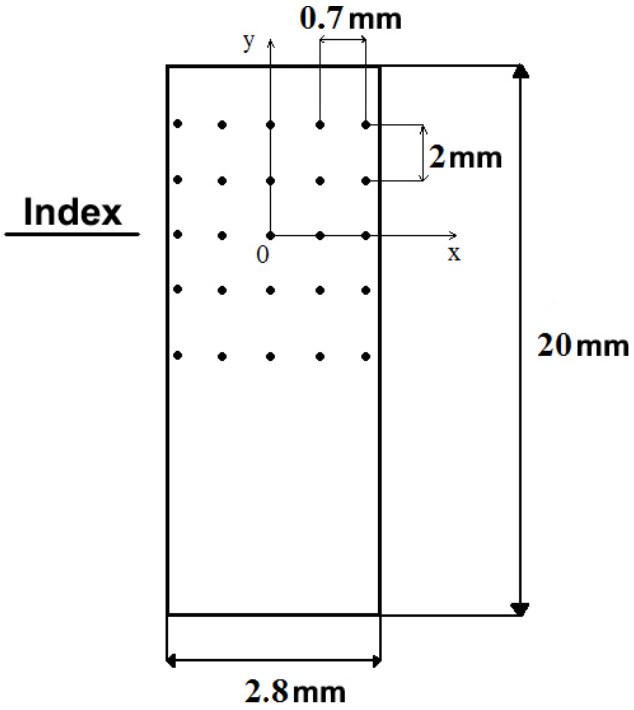

Fig. 8. Position of points for measuring the brightness across TRU 1100-2350 lamp filament.

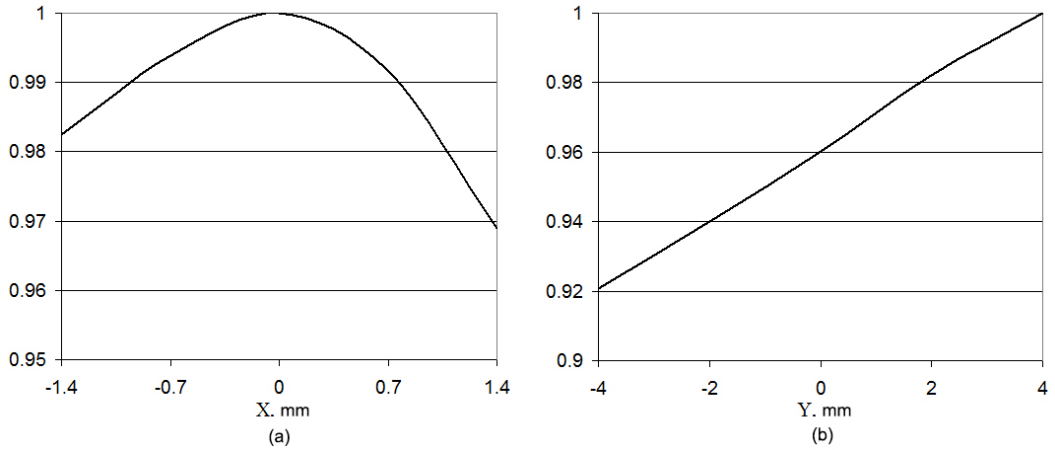

Fig. 9. Relative brightness distribution of TRU 1100-2350 lamp filament: (a) over ribbon width at index level, along axis X (Y = 0); (b) over ribbon height, along central Y axis (X = 0).

The obtained data reflects the existing non-uniformity of brightness along the vertical axis Y of the lamp filament body (about 8% for the measured area of the filament body, Figure 8, Figure 9b), while the brightness decreases in the direction from the top of the ribbon to the bottom. In the working area opposite the index along axis X, the non-uniformity is no more than 3% for the total width of the ribbon (Figure 8, Figure 9b), while the maximum brightness corresponds to the central point along the width of the ribbon.

Thus, the conducted measurements have demonstrated that implementing the given method and taking into account the measured brightness distribution near the working area of the lamp filament ensure the absolutizing of the DI. This is achieved by transmitting the SR from the reference TRU 1100-2350 lamp with high accuracy owing to the capability to position on the center of the working area of the lamp filament with an accuracy of no less than ±0.5 mm.

Conclusion

The results of modernizing the *Kameliya* measurement complex and the development of new methods of measuring spectral-energetic characteristics of optoelectronic ERS-equipment presented in the paper have ensured the practical implementation of optical circuits for taking the relative spectral characteristics of MSD. These methods have also proved to be adequate for measuring the transmission and reflection spectra (for various angles) of optical elements and optical blocks or ERS equipment in the range λ = 0.4–14 μm.

The new capabilities of the *Kameliya* complex have provided measurements for each of the seven IR channels of the fully manufactured light-splitting unit MSU-GS [1] (for the Electro-L No. 2 spacecraft), as well as for all six channels (three IR-channels) of the fully manufactured MSU-MR [2] (for the Meteor-M No. 2 spacecraft).

Apart from that, a method for measuring the spectral characteristics of optical emission sources (λ = 0.4–14 μm) in the range λ = 2.5–14 μm with the help of which the emission spectra of halogen lamps, light-emitting diode sources, gas discharge lamps were measured, has been developed.

Further upgrading of the *Kameliya* radiometric complex of JSC "Russian Space Systems" depends on the overall state of the metrological base in the space industry and in the country as a whole. The creation of advanced reference, measurement and testing equipment, especially in the IR part of the spectrum, as well as the development of a corresponding regulatory framework for competitive ERS equipment, which is an important government task, requires organizational decisions and financial support on a regular basis.

References

1. Andreev R. V., Akimov N. P., Badaev K.V., Gektin Yu.M., Zaytsev A.A., Ryzhakov A.V., Smelyanskiy M. B., Sulimanov N. A., Frolov A.G. Mnogozonal'noe skaniruyushchee ustroystvo dlya geostatsionarnogo meteosputnika "Elektro-L" [Multizone scanning apparatus for geosynchronous metrological satellite "Electro-L"] *Raketno-kosmicheskoe priborostroenie*

i informatsionnye sistemy [Rocket-Space Device Engineering and Information Systems], 2015, Vol. 2, No. 3, pp. 33-44. (in Russian)

2. Akimov N.P., Badaev K.V., Gektin Yu.M., Ryzhakov A.V., Smelyanskiy M.B, Frolov A.G. Mnogozonal'noe skaniruyushchee ustroystvo malogo razresheniya MSU-MR dlya kosmicheskogo informatsionnogo kompleksa "Meteor-M". Printsip raboty, evolyutsiya, perspektivy [Multiband Scanner of Low Spatial Resolution MSU-MR for space-based informational system "Meteor-M". The Principle of Operation and Development Prospects]. *Raketno-kosmicheskoe priborostroenie i informatsionnye sistemy* [Rocket-Space Device Engineering and Information Systems], 2015, Vol. 2, No. 4, pp. 30-39. (in Russian)
3. Panfilov A.S., Gavrilov V.R., Sapritskiy V.I. Usloviya podgotovki i provedeniya absolyutnykh radiometricheskikh izmereniy s pomoshch'yu optiko-elektronnoy apparatury nablyudeniya Zemli [Conditions for the Preparation and Conducting of Absolute Radiometric Measurements with the Use of Optoelectronic Earth Observation Equipment]. *Issledovaniya Zemli iz kosmosa* [Studies of the Earth from Space], 2014, No. 1, pp. 85-91. (in Russian)
4. Gritsenko V.A. Struktura granits razdela kremniy/oksid i nitrid/oksid [The structure of the silicon/oxide and nitride/oxide interfaces]. *Uspekhi fizicheskikh nauk* [Advances of physical sciences], 2009, Vol. 179, No. 9, pp. 921-930. (in Russian)
5. Gritsenko V.A. Atomnaya struktura amorfnykh nestekhiometricheskikh oksidov i nitridov kremniya [Atomic structure of amorphous nonstoichiometric oxides and silicon nitrides]. *Uspekhi fizicheskikh nauk* [Advances of physical sciences], 2008, Vol. 178, No. 7, pp. 727-737. (in Russian)
6. Vavaev V.A., Vavaev M.V., Polyanskiy I.V. Radiometricheskaya graduirovka kompleksa mnogozonal'noy sputnikovoy s"emki [Radiometric calibration of the complex of multizone satellite imagery]. Proceedings of scientific conference *Mekhanika, upravlenie i informatika. Sovremennye problemy opredeleniya orientatsii i navigatsii kosmicheskikh apparatov* [Mechanics, management and informatics. Modern problems of determining the orientation and navigation of space vehicles], held in Russia, Tarusa, 22-25 September 2008. Moscow: IKI RAN, 2009. pp. 549-561. (in Russian)
7. Kuinn T.D., *Temperatura* [Temperature] Moscow, Mir, 1985, 448 p. (in Russian)

ROCKET-SPACE DEVICE ENGINEERING AND INFORMATION SYSTEMS
Vol. 5, Iss. 2, 2018, pp. 31–35

Compact UHF Power Divider with Decoupling Between Inputs

V.G. Alybin, *Dr. Sci. (Engineering), otdelenie17@spacekorp.ru*
Joint Stock Company "Russian Space Systems", Moscow, Russian Federation
S.A. Zarapin, *otdelenie17@spacekorp.ru*
Joint Stock Company "Russian Space Systems", Moscow, Russian Federation
S.A. Yakhutin, *otdelenie17@spacekorp.ru*
Joint Stock Company "Russian Space Systems", Moscow, Russian Federation
S.V. Avramenko, *Cand. Sci. (Engineering), otdelenie17@spacekorp.ru*
Joint Stock Company "Russian Space Systems", Moscow, Russian Federation

Abstract. The paper deals with a new compact UHF power divider with decoupling between inputs, the amount of which may be chosen from 1 to 4, and a number of outputs can vary from 2 to 4. The input signal is fed to the one of the inputs and divided into equal parts between the outputs. Transmission factor from one of the inputs to any output independent of the number of the outputs does not exceed 6.8 dB. The power divider is implemented on four Lange bridges, which in the plane form the square. The construction of the model and experimental results are presented in the C-band. The power divider is successfully used in UHF units of the cross reservation for the onboard equipment of a command and measurement system.

Keywords: UHF power divider, directional coupler, Lange bridge, coupled lines

Introduction

To ensure a long active service life of the onboard equipment of spacecraft, it is required to unite up to four UHF devices by means of compact devices of cross reservation to provide decoupling between the inputs in the reserved group. Such devices are passive power dividers.

The power dividers of $n \times m$ made according to the binary scheme [1] are known. The dividers of this type are synthesized employing basic elements including a directed coupler, phase shifters, attenuators, etc. [2]. Disadvantages of such solutions are in the excess quantity of basic elements, restriction of the width of an operating band, complexity of coordination, and non-optimal mass-dimensional characteristics.

To apply spacecraft in the onboard equipment of a command and measuring system (OE CMS), it is required to use power dividers up to the power divider 3 × 3. Development of such power divider, which would allow one to employ it in the separate case or integrally as a part of the UHF device is expedient, as well as such device would possess the minimum losses, a good decoupling on inputs and outputs applicable to in the set frequency bands, and have the minimum dimensions and weight.

In a power divider 3 × 3, the defects peculiar to the dividers created according to the binary scheme that provides increase in number of the decoupled inputs up to four and decoupled outputs up to four are eliminated. It is especially important at coupling of the antenna-feeder device with receivers, when about 3 antennas with redundant low noise amplifiers and triplex receiving-transmitting devices are used. Multipolar distributors of UHF power, for example, 3 × 3, are used in OE CMS for cross reservation of triplex sets of receiving-transmitting devices and power amplifiers.

1. Power divider

Fig. 1 depicts the electric circuit of a power divider for the OE CMS [3] where 1, 2, 3, and 4 are the designations of the microstrip directed coupler with communication 3 dB. Microstrip pieces of the coupled lines 1 and 3 are coupled to the inputs 1, 2, 3, or 4, and microstrip pieces of the coupled lines 2 and 4 are coupled to the outputs 1, 2, 3, and 4, respectively.

Figs. 2–4 illustrate block diagrams of power dividers 4 × 4, 4 × 2, 3 × 2 representing modifications of the scheme 4 × 4.

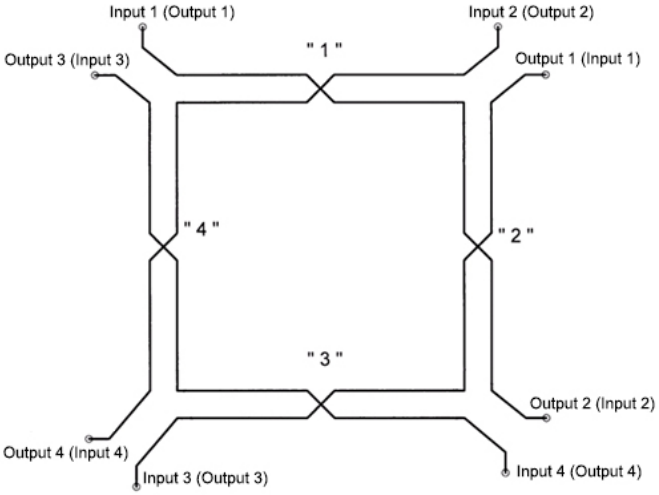

Fig. 1. The power divider 3 × 3

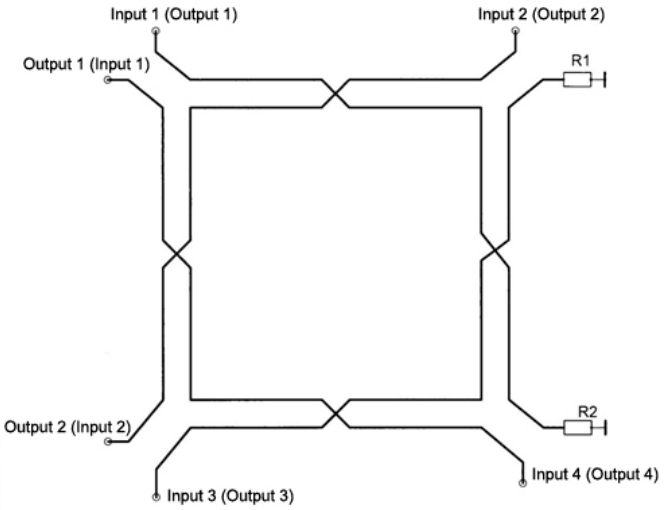

Fig. 2. The power divider 4 × 4

Generally, the divider 4 × 4 is for splitting of signal power given on one of four inputs on four outputs. Thus, at the outputs "Output 1", "Output 2", "Output 3", and "Output 4", there are signals weakened by 6 dB in relation to the power of the input signal P_a (without losses at the coupled lines 1, 2, 3, 4). The same way when giving a signal P_a on "Input 2", or on "Input 3", or on "Input 4", at the outputs "Output 1", "Output 2", "Output 3", "Output 4", there will be the signals weakened by 6 dB in relation to the signal power P_a. The submitted scheme of a divider 4 × 4 provides decoupling between the inputs "Input 1", "Input 2", "Input 3", and "Input 4", and also between the outputs "Output 1", "Output 2", "Output 3", "Output 4", not less than 20 dB. Thus, the possibility to use this divider operating according to the scheme 4 × 4 to ensure reservation of the onboard UHF equipment of spacecraft, in particular, a power amplifier of in OE CMS is confirmed.

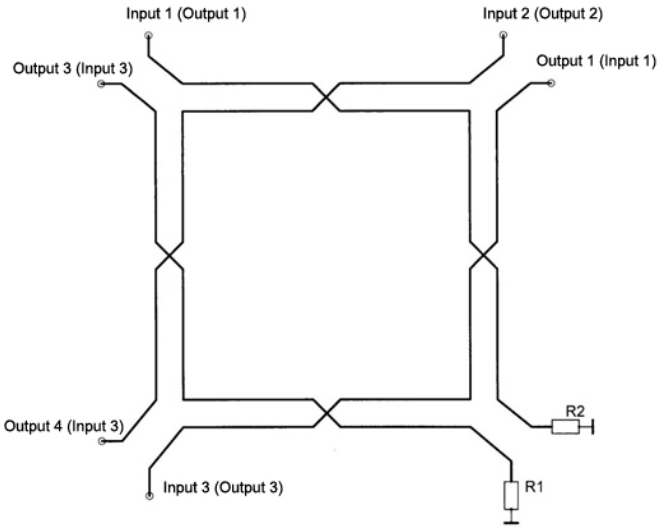

Fig. 3. The power divider 4 × 2

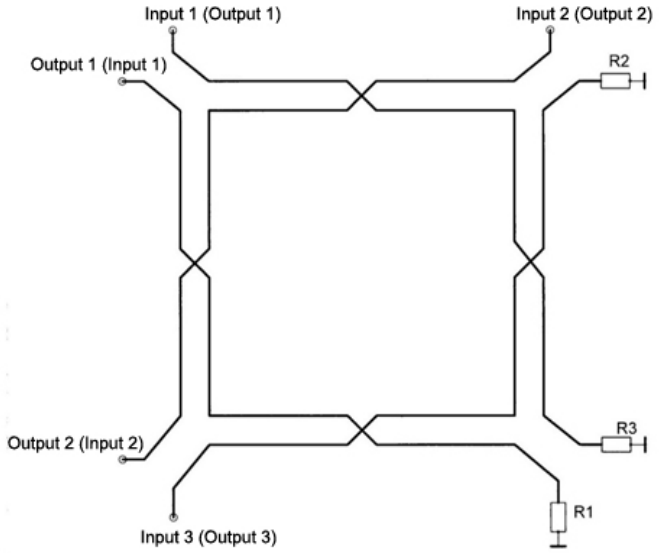

Fig. 4. The power divider 3 × 2

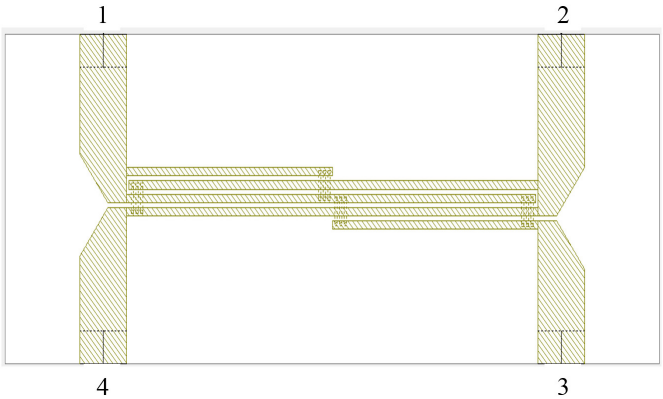

Fig. 5. The configuration of Lange bridge.

When coupling to one of the inputs of a power divider of the coordinated loading, the scheme 3 × 4 is implemented, and when coupling of the coordinated loadings to other ends of Lange bridges, it is possible to create other dividers: 4 × 3, 3 × 3, 3 × 2, 2 × 3. It is possible to create dividers 2 × 2 and 1 × 2, however for their realization there are more compact schemes.

The originality of a design of the offered power divider is in use of Lange bridges which existence of crossing of pieces of coupled lines in their middle, as shown in Fig. 5 is characteristic.

This property of Lange bridges has allowed one to realize a compact power divider with four Lange bridges located one in relation to next to it at right angle.

2. Simulation and experimental research of a power divider

When simulating a power divider 3 × 3, possible dispersions of parameters of ceramics and also dispersion of parameters of structural elements of the whole divider, including the form and length of the bridles connecting the corresponding conductors were considered. Simulating was carried out for the substrate of the Polikor material with the characteristics of $\varepsilon_r = 9.6 \pm 0.2$, $\mathrm{tg}\delta = 10^{-4}$, thickness $h = 1$ mm. At production of a printed circuit board, technological "constriction" of metal conductors was no more than 10 microns per side.

The appearance of a power divider is shown in the Fig. 6.

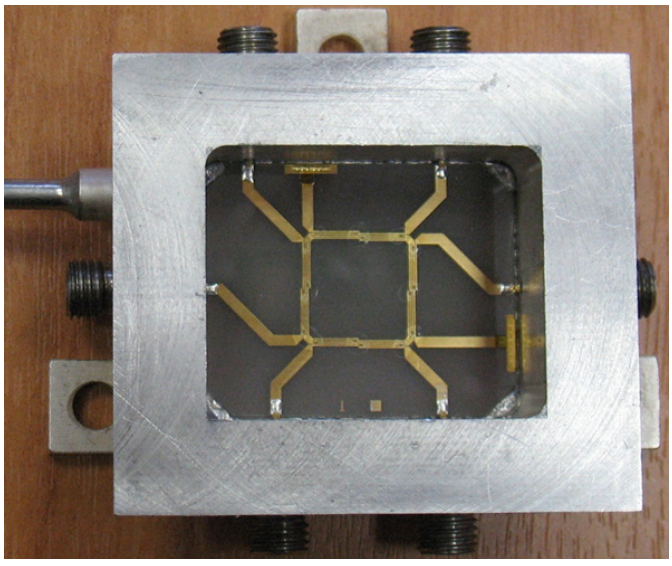

Fig. 6. The appearance of the power divider 3 × 3.

Production of a divider 3 × 3 placed in a separate tight case was made according to standard manufacturing techniques of plates of the UHF devices. Resistance of the spray ballast R1, R2 resistors was regulated by means of the laser.

Research data of the parameters of the built power dividers 3 × 3 are presented in Fig. 7–10. We can see that characteristics of power dividers 3 × 3 have an insignificant resonance frequency shift that is explained by the difference of ε_r from its nominal rate and a technological backlog on "constriction".

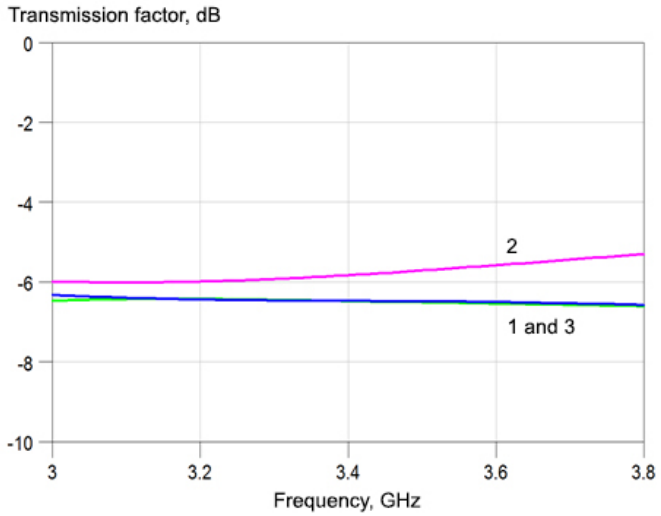

Fig. 7. Dependency of transmission factor in the power divider 3 x 3 on frequency: *1* is from the input 1 to the output 2; *2* is from the input 1 to the output 3; *3* is from the input 2 to the output 3.

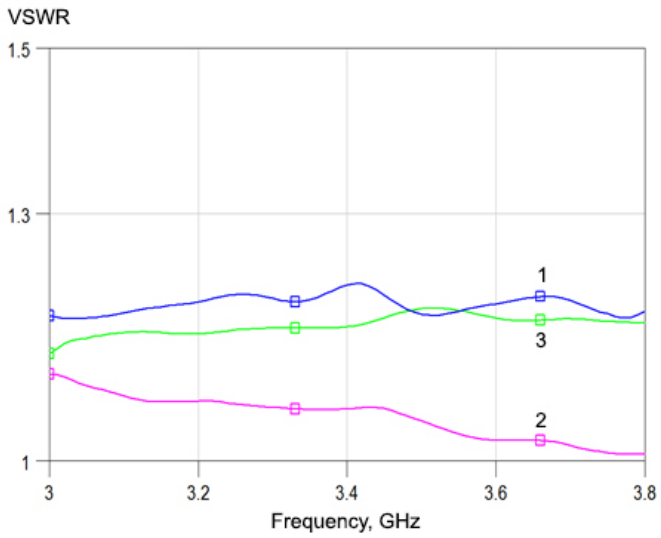

Fig. 8. VSWR Dependency of the inputs 1, 2, and 3 of the power amplifier 3 x 3 on the frequency.

As a result of the research, the values of key parameters of a divider are received:

- transmission factor from the input to the output is no more than –6.8 dB;
- decoupling between inputs and outputs is not less than 23 dB;
- VSWR of inputs or outputs is no more than 1.15 dB.

The measured electric characteristics of power dividers 3 × 3 validate the choice of parameters of a mathematical model and coincide well with the results of calculation.

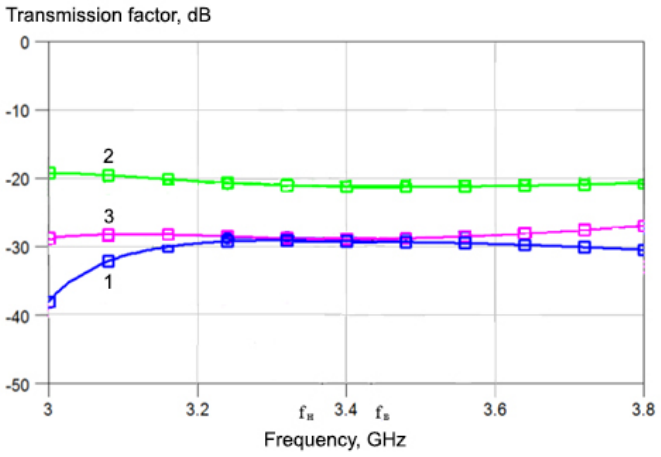

Fig. 9. Dependency of transmission factor (Kp) between the inputs of the power divider 3 x 3 on frequency: *1* is between the inputs 1 and 2, *2* is between the inputs 1 and 3, *3* is between the inputs 2 and 3.

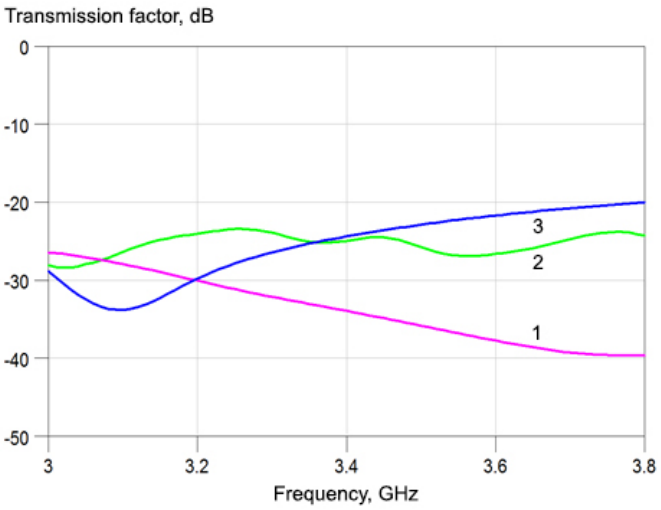

Fig. 10. Dependency of transmission factor (Kp) between the inputs of the power divider 3 x 3 on frequency: *1* is from the output 1 to the output 2, *2* is from the output 1 to the output 3, *3* is from the output 2 to the output 3.

Conclusion

The results of development of the compact power divider of the C-band capable to work with the number of inputs and outputs from 2 to 4 are shown. The feature of the design and the reached experimental parameters

allow one to use it both as a self-contained unit and as a component of the power amplifier of OE CMS as a device for cross reservation.

References

1. Model' Z.I. *Ustroystva slozheniya i raspredeleniya moshchnosti vysokochastotnykh kolebaniy* [The device for monitoring and distribution of UHF oscillations]. pp. 100 and 102. Moscow, Sovetskoye radio, 1980. (in Russian)
2. Sazonov D.M., Gridin A.N., Mishuchstin B.A. *Ustroystva SVCH* [UHF devices]. Vysshaya shkola, 1981, 259 p. (in Russian)
3. Alybin V.G., Zarapin S.A., Yakhutin S.A., Avramenko S.V. *Delitel' moshchnosti dlya bortovoy apparatury kosmicheskogo apparata* [A power divider for the onboard equipment of spacecraft]. Patent of the RF No. 2608978, 2017. (in Russian)

ROCKET-SPACE DEVICE ENGINEERING AND INFORMATION SYSTEMS
Vol. 5, Iss. 2, 2018, pp. 36–49

Principle of Formation of a Redundancy Parameter of the Information Stream from Analog Sensors of Slowly Changing Parameters and the Algorithm of its Implementation

V.V. Oreshko, *contact@spacecorp.ru*
Joint Stock Company "Russian Space Systems", Moscow, Russian Federation
V.A. Blagodyrev, *Cand. Sci. (Engineering), contact@spacecorp.ru*
Joint Stock Company "Russian Space Systems", Moscow, Russian Federation

Abstract. The article justifies and sets the task to develop the algorithms of information processing in onboard radio telemetry systems (RTS), which will define:
• the presence of redundancy of information from the sensors and its reduction;
• the redistribution of information packets from the sensors in transfer frames of onboard RTS in case of emergency.
The redundancy indicator of the information stream in onboard RTS is described. Based on the offered earlier adaptive difference algorithm (ADA) [1, 2], which allows one to eliminate redundancy resulting from the erroneous choice of measurement scale, an adaptive difference algorithm with decimation (ADAD) is developed. This algorithm makes it possible to reduce redundancy caused by the increased sampling frequency. The ADAD cumulative maximum redundancy reduction factor is formed by multiplication of the compression factor of the ADA and the maximum decimation factor.

Keywords: onboard processing of measurement results, reduction of data redundancy, information packet, onboard radio telemetry system

Introduction

Any type of time-division multiplex system and pulse-code modulation (PCM) telemetry systems, in particular, according to their definition, require the discretization of the original signal before its transmission. The assumed model of the sampling process comes down to quantizing an analog signal by duration with a uniform frequency that is defined by the duration considered to be short in comparison with the amplitude-modulated signal sampling frequency.

The discretized function (discrete original signal) de facto exists only at moments in time that coincide with the moment of analog signal quantizing. For this reason, the function cannot be ideally restored by linear approximation of selected points. If the repetition frequency of sampling values is high enough when compared to parameter dynamics, then it is possible to accurately restore the waveform and preserve its essential characteristics.

Moreover, the advantage of transmitting band-limited signals lies in the possible usage of the theorem known as the discrete representation theorem, which defines the conditions for determining the correct sampling frequency for sensor output signals. The theorem is also known as the Nyquist theorem, Kotelnikov theorem, sampling theorem.

According to this theorem, limited bandwidth signals (B) in the case of their discretization every t_s seconds can be correctly restored using the following inequality: $t_s £ 1/(2B)$, where B is the signal bandwidth limit. [3]

In other words, if a function in interval T does not contain frequencies exceeding 2W Hz, then it is completely determined by its instantaneous values of the 1/(2W) period with [4].

In telemetry, redundancy of the quantity of samples during data transmission is embedded at the time of parameter sampling frequency assignment, taking into account the a priori information regarding the signal intended for transmission through a communication link.

Initially, the so-called "compression ratio" (calculated as the ratio of the amount of original samples to the amount of samples at the output of the data compression device) was chosen to characterize the efficiency of the data compression algorithm in question. Nevertheless, soon it was understood that the data compression ratio is not solely dependent on algorithm efficiency — it is determined by the initially assigned parameter sampling frequency and by the waveform in the given time interval. In other words, the compression ratio, calculated as stated above, does not unambiguously characterize the data compression algorithm, as well as the choice of an efficient data compression algorithm and the classification of compression algorithms by efficiency.

Another condition for the study and comparison of data compression algorithms: the assumption that the analytic representation of the signal subject to the procedure of compression is a priori known — which is not the case when solving practical problems of rocket telemetry. Moreover, during emergency phases of flight the behavior of telemetry parameters is not stationary, which curtails the implementation of the statistical test method for choosing an effective data compression algorithm. [4]

Sampling rate of analog sensors of slowly changing parameters (SCP)

In [5] is noted that the sensors of the propulsion system are usually sampled with a 50 Hz and 100 Hz frequency. Yet, in order to receive information on the behavior of the engine in an emergency, the sampling frequency of the corresponding sensors should be increased up to 200400 Hz.

For increasing the sampling frequency of some sensors, parallel connection of one sensor output to several inputs of the message collection subsystem [6] can be used. In this case, the sensor measurement samples may be non-uniform. This is conditioned by the fact that the sampling cycle of the local switch (LS) is 5 ms and the framing cycle is 10-20 ms. This should be accounted for in the system operation algorithm when inserting information into the output frame from the buffer ("mirror") of the message collection subsystem in accordance with the measurement program.

The research set forth in [7] demonstrated that the sampling rate in LSs of analog sensors (LSA) could be increased by 2-4 times by way of selection of elements in the buffer cascade for reducing the time of the channel-switching transient. Thus, the maximum sampling frequency for analog sensors may be increased to 400 Hz or 800 Hz.

Still, with existing methods of placing sensor status information in transfer frames, for most sensors, increased sampling rates are useless because framing cycle duration

is already longer than the LSA sampling cycle by four-fold. In other words, the cumulative information content of all of the LSs is considerably higher than that of the radio channel. Currently for coordinating the information content of the message collection subsystem (MCS) (i.e., the aggregate of all of the LS) and the information content of the radio channel only a limited amount of interrogation programs is used. These programs determine the location in the frame and the sampling rate (repetition rate in frame) of every sensor. However, in the case of abnormal item operation, a higher sampling rate may be required for a sensor with a low frequency specified in the interrogation program because, after all, it is impossible to foresee every situation. Thus, arises the necessity to develop information-processing algorithms for onboard RTS that are to determine:

- the presence of redundancy of information from the sensors and its reduction;
- the redistribution of information packets from the sensors in transfer frames of onboard RTS.

The principle of forming the information stream redundancy parameter in onboard RTS

The telemetry system collects information from many sensors. Analog sensors make up the largest part (53% - 84%) of the information content of the information stream from the onboard RTS to the Earth. [1] An analog sensor switch usually has one analog-to-digital converter (ADC) for 64 sensors and all of them are sampled in turn with an equal frequency. The received data is transmitted to the buffer memory of the system central unit. The unit, in accordance with the programmed interrogation program, generates the output frame of the onboard RTS. When such a data generation method is implemented, information redundancy will be present in some channels, considering that not all channels require the same sampling frequency. Partially, this redundancy can be compensated for by decimating the information incoming into the buffer from some sensors at the time of system output frame generation.

In [1, 2] for reducing information redundancy from analog sensors the use of the adaptive difference algorithm (ADA) is suggested. It is a cumulative algorithm with packet data transmission. Fixed-sized packets are transmitted. Data is compressed by transmitting not the measurements themselves but by transmitting the differences between adjacent samples. At the same time, value Δ is formed, which is the maximum amount of bits that the difference between adjacent samples occupies within one packet during algorithm operation.

This value Δ is the information redundancy factor for inputs with less dynamic signals. Due to this, it is possible to implement selective decimation of information for inputs with less dynamic signals from sensors and use the newly available information content to transmit information from sensors with higher signal dynamics. This will lead to a proportional to the decimation factor increase of the maximum compression ratio.

Adaptive difference algorithm with decimation

As it can be seen from [1], the ADA eliminates redundancy when sampling a sensor at one frequency with a compression ratio of no more than four (4). The decimation algorithm eliminates redundancy with a factor equal to the ratio of the maximum and minimum sampling frequencies. Combining these algorithms will give an even higher redundancy elimination factor. Now, we turn our attention the adaptive difference algorithm with decimation (ADAD).

Assuming that the sampling frequency is always equal to 200 Hz, the minimum frequency of information output from sensors during decimation is equal to 12.5 Hz, i.e., the decimation factor is taken to be 16. The size of the data portion of a packet is equal to 16 bytes; ADC capacity – 8. The results of ADAD algorithm implementation are as shown in Table 1. Nine steps comprise a full ADAD cycle.

The first seven steps correspond to the full cycle of the ADA algorithm, coefficient Δ is calculated with respect to two adjacent measurements of a single parameter that are carried out with the frequency of 200 Hz. At first, 16 measurements are accumulated, the condition $\Delta_{max\ n} < 7$ bits is checked. If the condition is not met, then 16 measurements without compression are placed into the information packet. If the condition is met, then the accumulation of measurements continues.

After accumulating 18 measurements in the second step, the condition $\Delta_{max\ n} < 7$ bits is checked first. If the condition is not fulfilled, the packet formed during the first step is issued and the algorithm returns to step one. If the condition is fulfilled, then the specifying condition $\Delta_{max\ n} = 6$ bits is checked. If it is met, then an

Table 1. Example of the ADAD algorithm

Sampling frequency	Stage No.	Step No. (action)	Action for measurement collection buffer	Analysis of $\Delta_{max\,n}$ – maximum amount of bits required for representing the measurement value differences in binary form
200 Hz	0	1	Accumulation of 16 measurements	$\Delta_{max\,n}$ = 8 or 7 bits, 16 measurements in a packet $\Delta_{max\,n}$ < 7 bits, transition to action 2
		2	Accumulation of 18 measurements (MEAS) (+ 2 MEAS)	$\Delta_{max\,n}$ = 8 or 7 bits, issue of 1 packet with 16 measurements, transition to action 1 $\Delta_{max\,n}$ = 6 bits, issue of 1 packet with 18 measurements, transition to action 1 $\Delta_{max\,n}$ < 6 bits, transition to action 3
		3	Accumulation of 21 measurements (+ 3 MEAS)	$\Delta_{max\,n}$ = 8, 7 or 6 bits, issue of 1 packet with 18 measurements, transition to action 1 $\Delta_{max\,n}$ = 5 bits, issue of 1 packet with 21 measurements, transition to action 1 $\Delta_{max\,n}$ < 5 bits, transition to action 4
		4	Accumulation of 25 measurements (+ 4 MEAS)	$\Delta_{max\,n}$ = 8, …, 5 bits, issue of 1 packet with 21 measurements, transition to action 1 $\Delta_{max\,n}$ = 4 bits, issue of 1 packet with 25 measurements, transition to action 1 $\Delta_{max\,n}$ < 4 bits, transition to action 5
		5	Accumulation of 31 measurements (+ 6 MEAS)	$\Delta_{max\,n}$ = 8, …, 4 bits, issue of 1 packet with 25 measurements, transition to action 1 $\Delta_{max\,n}$ = 3 bits, issue of 1 packet with 31 measurements, transition to action 1 $\Delta_{max\,n}$ < 3 bits, transition to action 6
		6	Accumulation of 41 measurements (+ 10 MEAS)	$\Delta_{max\,n}$ = 8, …, 3 bits, issue of 1 packet with 31 measurements, transition to action 1 $\Delta_{max\,n}$ = 2 bits, issue of 1 packet with 41 measurements, transition to action 1 $\Delta_{max\,n}$ < 2 bits, transition to action 7
		7	Accumulation of 61 measurements (+ 20 MEAS)	$\Delta_{max\,n}$ = 8, …, 2 bits, issue of 1 packet with 41 measurements, transition to action 1 $\Delta_{max\,n}$ = 1 bit, transition to action 8
100 Hz	1	8	Accumulation of 62 measurements with a frequency of 200 Hz, decimation by a factor of 2 (equivalent of sampling frequency reduction), acquisition of 31 measurements with a frequency of 100 Hz	$\Delta_{max\,n}$ analysis analogous to step 5 for 31 decimated measurements $\Delta_{max\,n}$ = 8, …, 3 bits, issue of 1 packet with 61 measurements with a frequency of 200 Hz, transition to action 1 $\Delta_{max\,n}$ < 3 bits, transition to action 9
		9	Accumulation of 82 measurements with a frequency of 200 Hz, decimation by a factor of 2 (equivalent of sampling frequency reduction), acquisition of 41 measurements with a frequency of 100 Hz	$\Delta_{max\,n}$ analysis analogous to step 6 $\Delta_{max\,n}$ = 8, …, 3 bits, issue of 1 packet with 61 measurements with a frequency of 200 Hz, transition to action 1 $\Delta_{max\,n}$ = 2 bits, issue of 1 packet with 41 measurements with a frequency of 100 Hz, transition to action 1 $\Delta_{max\,n}$ < 2 bits, transition to action 10
		10	Accumulation of 122 measurements with a frequency of 200 Hz, decimation by a factor of 2 (equivalent of sampling frequency reduction), acquisition of 61 measurements with a frequency of 100 Hz	$\Delta_{max\,n}$ analysis analogous to step 7 $\Delta_{max\,n}$ = 8, …, 2 bits, issue of 1 packet with 41 measurements with a frequency of 100 Hz, transition to action 1 $\Delta_{max\,n}$ = 1 bit, transition to action 11

Table 1. Example of the ADAD algorithm

Sampling frequency	Stage No.	Step No. (action)	Action for measurement collection buffer	Analysis of $\Delta_{max\ n}$ – maximum amount of bits required for representing the measurement value differences in binary form
50 Hz	2	11	Accumulation of 124 measurements with a frequency of 200 Hz, decimation by a factor of 4 (equivalent of sampling frequency reduction), acquisition of 31 measurements with a frequency of 50 Hz	$\Delta_{max\ n}$ analysis analogous to step 8 $\Delta_{max\ n}$ = 8, …, 3 bits, issue of 1 packet with 61 measurements with a frequency of 100 Hz, transition to action 1 $\Delta_{max\ n}$ < 3 bits, transition to action 12
		12	Accumulation of 164 measurements with a frequency of 200 Hz, decimation by a factor of 4 (equivalent of sampling frequency reduction), acquisition of 41 measurements with a frequency of 50 Hz	$\Delta_{max\ n}$ analysis analogous to step 9 $\Delta_{max\ n}$ = 8, …, 3 bits, issue of 1 packet with 61 measurements with a frequency of 100 Hz, transition to action 1 $\Delta_{max\ n}$ = 2 bits, issue of 1 packet with 41 measurements with a frequency of 50 Hz, transition to action 1 $\Delta_{max\ n}$ < 2 bits, transition to action 13
		13	Accumulation of 244 measurements with a frequency of 200 Hz, decimation by a factor of 4 (equivalent of sampling frequency reduction), acquisition of 61 measurements with a frequency of 50 Hz	$\Delta_{max\ n}$ analysis analogous to step 10 $\Delta_{max\ n}$ = 8, …, 2 bits, issue of 1 packet with 41 measurements with a frequency of 50 Hz, transition to action 1 $\Delta_{max\ n}$ = 1 bit, transition to action 14
25 Hz	3	14	Accumulation of 248 measurements with a frequency of 200 Hz, decimation by a factor of 8 (equivalent of sampling frequency reduction), acquisition of 31 measurements with a frequency of 25 Hz	$\Delta_{max\ n}$ analysis analogous to step 11 $\Delta_{max\ n}$ = 8, …, 3 bits, issue of 1 packet with 61 measurements with a frequency of 50 Hz, transition to action 1 $\Delta_{max\ n}$ < 3 bits, transition to action 15
		15	Accumulation of 328 measurements with a frequency of 200 Hz, decimation by a factor of 8 (equivalent of sampling frequency reduction), acquisition of 41 measurements with a frequency of 25 Hz	$\Delta_{max\ n}$ analysis analogous to step 12 $\Delta_{max\ n}$ = 8, …, 3 bits, issue of 1 packet with 61 measurements with a frequency of 50 Hz, transition to action 1 $\Delta_{max\ n}$ = 2 bits, issue of 1 packet with 41 measurements with a frequency of 25 Hz, transition to action 1 $\Delta_{max\ n}$ < 2 bits, transition to action 10
		16	Accumulation of 488 measurements with a frequency of 200 Hz, decimation by a factor of 8 (equivalent of sampling frequency reduction), acquisition of 61 measurements with a frequency of 25 Hz	$\Delta_{max\ n}$ analysis analogous to step 13 $\Delta_{max\ n}$ = 8, …, 2 bits, issue of 1 packet with 41 measurements with a frequency of 25 Hz, transition to action 1 $\Delta_{max\ n}$ = 1 bit, transition to action 17

Table 1. Example of the ADAD algorithm

Sampling frequency	**Stage No.**	**Step No. (action)**	**Action for measurement collection buffer**	**Analysis of $\Delta_{max\,n}$ – maximum amount of bits required for representing the measurement value differences in binary form**
12.5 Hz	4	17	Accumulation of 496 measurements with a frequency of 200 Hz, decimation by a factor of 16 (equivalent of sampling frequency reduction), acquisition of 31 measurements with a frequency of 12.5 Hz	$\Delta_{max\,n}$ analysis analogous to step 14 $\Delta_{max\,n}$ = 8, …, 3 bits, issue of 1 packet with 61 measurements with a frequency of 25 Hz, transition to action 1 $\Delta_{max\,n}$ < 3 bits, transition to action 18
		18	Accumulation of 656 measurements with a frequency of 200 Hz, decimation by a factor of 16 (equivalent of sampling frequency reduction), acquisition of 41 measurements with a frequency of 12.5 Hz	$\Delta_{max\,n}$ analysis analogous to step 15 $\Delta_{max\,n}$ = 8, …, 3 bits, issue of 1 packet with 61 measurements with a frequency of 25 Hz, transition to action 1 $\Delta_{max\,n}$ = 2 bits, issue of 1 packet with 41 measurements with a frequency of 12.5 Hz, transition to action 1 $\Delta_{max\,n}$ < 2 bits, transition to action 19
		19	Accumulation of 976 measurements with a frequency of 200 Hz, decimation by a factor of 16 (equivalent of sampling frequency reduction), acquisition of 61 measurements with a frequency of 12.5 Hz	$\Delta_{max\,n}$ analysis analogous to step 16 $\Delta_{max\,n}$ = 8, …, 2 bits, issue of 1 packet with 41 measurements with a frequency of 12.5 Hz, transition to action 1 $\Delta_{max\,n}$ = 1 bit, issue of 1 packet with 61 measurements with a frequency of 12.5 Hz, transition to action 1

18-measurement packet is issued and packed into 16 bytes. If the specifying condition ($\Delta_{max\ n} < 6$ bits) is not fulfilled, then measurement accumulation is continued, and the transition to the third step of the algorithm is made.

Upon accumulation of 21 measurements in step three, first, the condition for transitioning from the second step is checked: $\Delta_{max\ n} < 6$ bits. If the condition is not met, the packet formed during step two is issued and the algorithm is returned to step one. If the condition is met, the specifying condition $\Delta_{max\ n} = 5$ bits is checked. If it is fulfilled, then a packet, packed in 16 bytes, with 21 parameter measurements is issued. If the specifying condition ($\Delta_{max\ n} < 5$bits) is not met, then measurement accumulation continues and transition to the fourth step of the algorithm takes place.

After accumulating 25 measurements in step four, first, the condition for transitioning from step three $\Delta_{max\ n} < 5$ bits is checked. If it is not met, the packet formed in step 3 is issued and the algorithm returns to the first step. If the condition is fulfilled, then the specifying condition $\Delta_{max\ n} = 4$ bits is checked. If it is met, then a packet with 25 parameter measurements packed in 16 bytes is issued. If the specifying condition ($\Delta_{max\ n} < 4$ bits) is not met, then measurements continue to be accumulated and the transition to the fifth step of the algorithm is made.

After accumulating 31 measurements in step five, the transition from step four condition $\Delta_{max\ n} < 4$ bits is checked. If the condition is not met, the packet, which was formed in step four, is issued and the algorithm returns to the first step. If the condition is fulfilled, the $\Delta_{max\ n} = 3$ bits specifying condition is met. If the specifying condition is fulfilled, then a packet with 31 measurements is issued that is packed in 16 bytes. If the specifying condition is not fulfilled ($\Delta_{max\ n} < 3$ bits), measurement accumulation is continued and the transition to the sixth step of the algorithm is made.

Upon accumulation of 41 measurements in step six the condition for transitioning from step five is checked: $\Delta_{max\ n} < 3$ bits. If the condition is not fulfilled, the packet, which was formed during step five, is issued and the algorithm returns to step one. If the condition is met, then the specifying condition $\Delta_{max\ n} = 2$ bits is checked. If it is fulfilled, a packet with 41 measurements is issued. The packet is packed in 16 bytes. If the specifying condition ($\Delta_{max\ n} = 1$ bit) is not met, the measurement accumulation is continued and the transition to step seven of the algorithm is carried out.

Summarizing the actions for all of the ADA steps (except for the first and the last ones): every step presumes that the condition for transition from the previous step ($\Delta_{max\ n} < Y - (n - 1)$, where Y is the ADC capacity and n is the number of the step) is checked after the required amount of measurements is assumed. Should the condition not be met, the packet that was formed during the previous step is issued and the algorithm returns to step one. If the condition is fulfilled, then the following specifying condition is checked: $\Delta_{max\ n} = Y - n$. If this condition is met, then a packet, which was generated during the current step, is issued. In the event of the specifying condition ($\Delta_{max\ n} = Y - n$) not being fulfilled, the condition for transitioning to the next step is fulfilled ($\Delta_{max\ n} < Y - n$), measurement accumulation is continued and a transition to the following step of the algorithm is carried out.

After the accumulation of 61 measurements in step seven (which corresponds to the last step of the ADA algorithm), the transition from step six condition ($\Delta_{max\ n} < 2$ bits) is checked first. If it is not fulfilled, the packet, which was formed during the sixth stage, is issued and the algorithm returns to step one. If the condition is met, that means that $\Delta_{max\ n} = 1$ bit. In the ADA algorithm a packet is issued with 61 measurements packed into 16 bytes and the algorithm returns to step one, i.e., the cycle starts over again. As for the ADAD algorithm – a transition to the information cycle is made, i.e., to step eight.

The accumulation of 62 measurements in step eight is carried out with a frequency of 200 Hz. The value Δ is calculated by the ratio of two adjacent sampling measurements, carried out with a frequency of 100 Hz. Thus, every other measurement from the original is taken – 31 measurements, in total, with a frequency of 100 Hz, which corresponds to the fifth step of the ADA algorithm. Further processing is carried out in a manner analogous to the fifth step; only measurements decimated by two-fold are processed.

Following the accumulation of 31 measurements with a 100 Hz frequency in step eight, a condition analogous to the one for transitioning from step five to step six is checked: $\Delta_{max\ n} < 3$ bits. If this condition is not met, the packet, generated in step seven (containing 61 measurements obtained with a frequency of 200 Hz and packed in 16 bytes) is issued. If the condition is fulfilled, the accumulation of measurements is continued and the transition to step nine of the ADAD takes place.

Table 2. Generalized ADAD algorithm

Sampling frequency, Hz	**Frequency decimation stage**	**Step No. (action)**	**Action for measurement collection buffer**	**Analysis of $\Delta_{max\,n}$ – maximum amount of bits required for representing the measurement value differences in binary form**
f_{max}	0	1	Accumulation of X/Y measurements	$\Delta_{max\,n}$ = Y or (Y – 1) bits, X/Y measurements per packet $\Delta_{max\,n}$ < (Y – 1) bits, transition to action 2
		2	Accumulation of ((X – Y) / (Y – 2) + 1) measurements	$\Delta_{max\,n}$ = Y or (Y – 1) bits, X/Y measurements per packet, transition to action 1 $\Delta_{max\,n}$ = (Y – 2) bits, issue of 1 packet with (X – Y) / (Y – 2) measurements, transition to action 1 $\Delta_{max\,n}$ < (X – Y)/(Y – 2) bits, transition to action 3
		3	Accumulation of ((X – Y) / (Y – 3) + 1) measurements	$\Delta_{max\,n}$ = Y, …, (Y – 2) bits, issue of 1 packet with (X – Y) / (Y – 2) measurements, transition to action 1 $\Delta_{max\,n}$ = (Y – 3), issue of 1 packet with (X – Y) / (Y – 3) measurements, transition to action 1 $\Delta_{max\,n}$ < (Y-3) bits, transition to action 4
		…		
		n	Accumulation of ((X – Y) / (Y – n + 1) + 1) measurements	$\Delta_{max\,n}$ = Y, …, (Y – (n – 1)) bits, issue of 1 packet with ((X – Y) / (Y – (n – 1)) + 1) measurements, transition to action 1 $\Delta_{max\,n}$ = (Y – n) bits, issue of 1 packet with ((X – Y) / (Y – n) + 1) measurements, transition to action 1 $\Delta_{max\,n}$ < (Y – n) bits, transition to action (n + 1)
		…		
		Y – 1	Accumulation of ((X – Y) / 2 + 1) measurements	$\Delta_{max\,n}$ = Y, …, 2 bits, issue of 1 packet with ((X – Y) / 3 + 1) measurements, transition to action 1 $\Delta_{max\,n}$ = 1 bit, issue of 1 packet with ((X – Y) / 2 + 1) measurements, transition to action Y

Table 2. Generalized ADAD algorithm

Sampling frequency, Hz	**Frequency decimation stage**	**Step No. (action)**	**Action for measurement collection buffer**	**Analysis of $\Delta_{max\ n}$ – maximum amount of bits required for representing the measurement value differences in binary form**
$f_{max}/2$	1	У	Accumulation of ((X – У) / 4 + 1) x 2 measurements with $f_{max\ n}$, frequency decimation by a factor of 2 (equivalent of sampling frequency reduction), acquisition of ((X – У) / 4 + 1) measurements with $f_{max\ n}/2$ frequency	$\Delta_{max\ n}$ analysis analogous to step У – 3 for ((X – У) / 4 + 1) decimated measurements $\Delta_{max\ n}$ = У, …, 3 bits, issue of 1 packet with ((X – У) / 2 + 1) measurements with $f_{max\ n}$ frequency, transition to action 1 $\Delta_{max\ n}$ < 3 bits, transition to action У + 1
		У + 1	Accumulation of ((X – У) / 3 + 1) x 2 measurements with $f_{max\ n}$ frequency, decimation by a factor of 2 (equivalent of sampling frequency reduction), acquisition of ((X – У) / 3 + 1) measurements with $f_{max\ n}/2$ frequency	$\Delta_{max\ n}$ analysis analogous to step У – 2 $\Delta_{max\ n}$ = У, …, 3 bits, issue of 1 packet with ((X – У) / 2 + 1) measurements with $f_{max\ n}$ frequency, transition to action 1 $\Delta_{max\ n}$= 2 bits, issue of 1 packet with ((X – У) / 3 + 1) measurements with $f_{max\ n}/2$ frequency, transition to action 1 $\Delta_{max\ n}$ < 2 bits, transition to action У + 2
		У + 2	Accumulation of ((X – У) / 2 + 1) x 2 measurements with частотой $f_{max\ n}$, decimation by a factor of 2 (equivalent of sampling frequency reduction), acquisition of ((X – У) / 2 + 1) measurements with $f_{max\ n}/2$ frequency	$\Delta_{max\ n}$ analysis, analogous to step У – 1 $\Delta_{max\ n}$ = У, …, 2 bits, issue of 1 packet with ((X – У) / 3 + 1) measurements with $f_{max\ n}/2$ frequency, transition to action 1 $\Delta_{max\ n}$= 1 bit, transition to action У+3
…				

Table 2. Generalized ADAD algorithm

Sampling frequency, Hz	**Frequency decimation stage**	**Step No. (action)**	**Action for measurement collection buffer**	**Analysis of $\Delta_{max\,n}$ – maximum amount of bits required for representing the measurement value differences in binary form**
f_{max}/K_d	$m = \log_2 K_d$	y + 3m – 3	Accumulation of ((X – y) / 4+1) x K_d measurements with $f_{max\ n}$ frequency, decimation by a factor of K_d (equivalent of sampling frequency reduction), acquisition of ((X – y) / 4+1) measurements with $f_{max\,n}/K_d$ frequency	$\Delta_{max\ n}$ = y, …, 3 bits, issue of 1 packet with ((X – y) / 2+1) measurements with $2x\,f_{max\,n}/K_d$ frequency, transition to action 1 $\Delta_{max\,n}$ < 3 bits, transition to action (y + 3m - 2)
		y + 3m – 2	Accumulation of ((X – y) / 3 + 1) x K_d measurements with $f_{max\,n}$ frequency, decimation by a factor of K_d (equivalent of sampling frequency reduction), acquisition of ((X – y) / 3 + 1) measurements with $f_{max\,n}/K_d$ frequency	$\Delta_{max\ n}$ = y, …, 3 bits, issue of 1 packet with ((X – y) / 2 + 1) measurements with $2x\,f_{max\,n}/K_d$ frequency, transition to action 1 $\Delta_{max\,n}$ = 2 bits, issue of 1 packet with ((X – y) / 3 + 1) measurements with $f_{max\,n}/K_d$ frequency, transition to action 1 $\Delta_{max\,n}$ < 2 bits, transition to action (y + 3m – 1)
		y + 3m – 1	Accumulation of ((X – y) / 2 + 1) x K_d measurements with $f_{max\,n}$ frequency, decimation by a factor of K_d (equivalent of sampling frequency reduction), acquisition of ((X – y) / 3 + 1) measurements with $f_{max\,n}/K_d$ frequency	$\Delta_{max\ n}$ = y, …, 2 bits, issue of 1 packet with ((X – y) / 3 + 1) measurements with f_{max}/K_d frequency, transition to action 1 $\Delta_{max\,n}$ = 1 bit, transition to action y + 3m
		…		

Table 2. Generalized ADAD algorithm

Sampling frequency, Hz	**Frequency decimation stage**	**Step No. (action)**	**Action for measurement collection buffer**	**Analysis of $\Delta_{max\ n}$ – maximum amount of bits required for representing the measurement value differences in binary form**
f_{max}/K_{d_max}	$m_{max} = \log_2 K_{d\_max}$	У + 3m_{max} – 3	Accumulation of ((X – У) / 4 + 1) x K_{d_max} measurements with f_{max} frequency, decimation by a factor of K_{d_max} (equivalent of sampling frequency reduction), acquisition of ((X – У) / 4 + 1) measurements with f_{max}/K_{d_max} frequency	$\Delta_{max\ n}$ = У, …, 3 bits, issue of 1 packet with ((X – У) / 2 + 1) measurements with 2x f_{max}/K_{d_max} frequency, transition to action 1 $\Delta_{max\ n}$ < 3 bits, transition to action (У + 3m_{max} – 2)
		У + 3m_{max} – 2	Accumulation of ((X – У) / 3 + 1) x K_{d_max} measurements with f_{max} frequency, decimation by a factor of K_{d_max} (equivalent of sampling frequency reduction), acquisition of ((X – У) / 3 + 1) measurements with f_{max}/K_{d_max} frequency	$\Delta_{max\ n}$ = У, …, 3 bits, issue of 1 packet with ((X – У) / 2 + 1) measurements with 2x f_{max}/K_{d_max} frequency, transition to action 1 $\Delta_{max\ n}$ = 2 bits, issue of 1 packet with ((X – У) / 3 + 1) measurements with f_{max}/K_{d_max} frequency, transition to action 1 $\Delta_{max\ n}$ < 2 bits, transition to action (У + 3m_{max} – 1)
		У + 3m_{max} – 1	Accumulation of ((X – У) / 2 + 1) x K_{d_max} measurements with f_{max} frequency, decimation by a factor of K_{d_max} (equivalent of sampling frequency reduction), acquisition of ((X – У) / 2 + 1) measurements with f_{max}/K_{d_max} frequency	$\Delta_{max\ n}$ = У, …, 2 bits, issue of 1 packet with ((X – У) / 2 + 1) measurements with f_{max}/K_{d_max} frequency, transition to action 1 $\Delta_{max\ n}$ = 1 bit, transition to action 1

N0 – input number of measurements; N – number of measurements issued in packet;
n – step number of the adaptive difference algorithm with decimation, $1 \le n \le$ У + 3m_{max} – 1;
X – packet data portion size, bit; У – ADC capacity, uncompressed measurement size;
$\Delta_{max\ n}$ – number of bits necessary for displaying the differences of two adjacent measurements in step n; f_{max} – maximum sampling frequency, Hz
f_{min} – minimum sampling frequency, Hz; K_d – decimation factor, multiple of 2, $1 \le K_d \le K_{d\_max}$;
K_{d_max} – maximum decimation factor ($f_{min} = f_{max}/K_{d\_max}$); m – frequency decimation stage, m = 0, 1, 2, …, m_{max}
m_{max} – final stage of frequency decimation, corresponds to the maximum decimation factor K_{d_max}

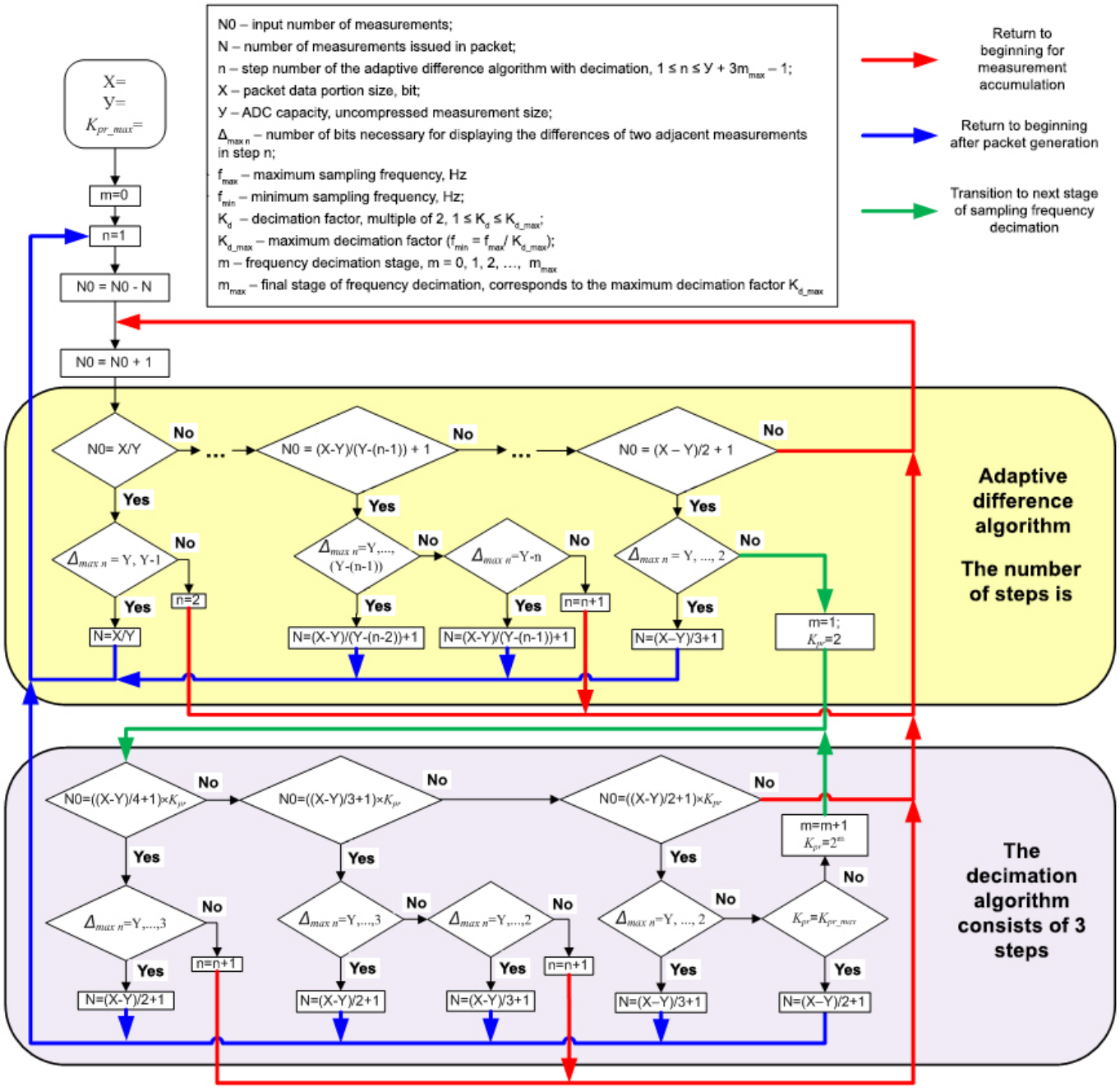

Figure. Adaptive difference algorithm block diagram.

Eighty-two measurements are accumulated in step nine with a frequency of 200 Hz and they are decimated by a factor of two. The 41 measurements that are thus obtained are processed by analogy with step six. At first, the condition for transitioning from the previous step $\Delta_{max\ n} < 3$ is checked. If the condition is not fulfilled, the packet formed in step seven (61 measurements with a frequency of 200 Hz packed in 16 bytes) is issued and the algorithm returns to step one. If the condition is met ($\Delta_{max\ n} < 3$ bits), a specifying condition is checked: $\Delta_{max\ n} = 2$ bits. In the case of its fulfillment, a packet with 41 measurements received with a frequency of 100 Hz and packed in 16 bytes is issued. If the specifying condition ($\Delta_{max\ n} = 2$ bits) is not met, then $\Delta_{max\ n} = 1$ bit and the measurements are continued to be accumulated. After this, the transition to the tenth step of the ADAD algorithm is performed.

During the tenth step 122 measurements are accumulated with a frequency of 200 Hz and are decimated by two-fold. The 61 measurements that are obtained with a frequency of 100 Hz are processed in an

analogous manner to step seven. At first, the condition for transitioning from the previous step $\Delta_{max\ n} < 2$ bits is checked. If the condition is met, a packet generated in step nine (i.e., 41 measurements with a frequency of 100 Hz and packed in 16 bytes) is issued and the algorithm returns to the first step. Upon the fulfillment of the condition, measurement accumulation continues and the ADAD algorithm transitions to step eleven.

The results of ADAD algorithm operation are given in Table 1. According to Table 1, all of the subsequent steps are subdivided into repeating groups of three steps that differ from one another only in the sampling frequencies of output data packets.

The actions in steps eleven, twelve and thirteen are analogous to those of steps eight, nine, and ten with the only difference that the equivalent sampling frequency of the measurements being packed into packets is, once again, lowered by a factor of two. These iterating groups can symbolically be called *steps of an adaptive algorithm with decimation (AAD) operating with ADA, or with decimation stages*.

In the final step of the ADAD algorithm instead of a transition to the following step of decimation, a packet is issued, consisting of 61 measurements (with a frequency of 12.5 Hz) packed in 16 bytes of the data portion of the packet. After that, the ADAD cycle repeats itself from the beginning.

In generalized form the ADAD algorithm is given in Table 2.

A block diagram of the generalized ADAD is given in the Figure.

Conclusion

Therefore, not only does the ADAD algorithm that has been developed allow for a decrease in redundancy, owing to a reduced number of transmitted bits – as is done by the ADA, but it also is able to compensate the redundantly assigned sampling frequency. The ADAD cumulative maximum redundancy reduction factor is formed by multiplying the ADA compression ratio and the maximum factor of decimation. The ADA compression ratio depends on the size of the packet data portion and the ADC capacity. In the example provided, the ADA compression ratio is equal to 3.8125 and the decimation factor is equal to 16. If the sensor signal changes insignificantly and in such a manner that processing by means of ADAD reaches the final step, then instead of 976 accumulated measurements with a frequency of 200 Hz , a packet containing only 61 measurements with a frequency of 12.5 Hz is issued. Due to the fact that the data portion of the packet is chosen to contain 16 measurements without decimation, then the redundancy reduction factor is equal to 976/16=3.8125×16=61.

References

1. Oreshko V.V. Algoritmy ustraneniya izbytochnosti informatsii, peredavayemoy ot bortovykh telemetricheskikh sistem na Zemlyu [Algorithms for Elimination of the Redundancy of the Information Transmitted from Onboard Telemetry System to the Earth]. *Raketno-kosmicheskoe priborostroenie i informatsionnye sistemy* [Rocket-Space Device Engineering and Information Systems]. 2017, Vol. 4, No. 2, pp. 75–84. (in Russian)
2. Oreshko V.V. Algoritm formirovaniya adaptivnoy struktury dannykh v informatsionnykh paketakh dlya bortovykh radiotelemetricheskikh sistem [Algorithm to form an adaptive data structure in information packets for onboard radio telemetry systems]. *Sbornik trudov VII Vserossiyskoy nauchno-tekhnicheskoy konferentsii "Aktual'nye problemy raketno-kosmicheskogo priborostroeniya i informatsionnykh tekhnologiy"* [Proceedings of the VII All-Russian scientific and technical conference "Current problems of rocket and space device engineering and information technologies]. Moscow, AO "Rossiyskie kosmicheskie sistemy", June 2–4, 2015, 584 p. (in Russian)
3. Horan S. *Vvedenie v telemetricheskie sistemy s impul'sno-kodovoy modulyatsiey* [Introduction to telemetry systems with pulse code modulation]. 1997. Eds. Kukushkin S.S., Blagodyrev V.A. (Translated by Kondrat'eva Yu.I.). (in Russian)
4. Pobedonostsev V.A. Teoreticheskie voprosy izmereniya kolichestva informatsii nepreryvnykh signalov na konechnykh intervalakh [Theoretical Questions in Measuring the Amount of Information in Continuous Signals on Finite Intervals]. *Raketno-kosmicheskoe priborostroenie i informatsionnye sistemy* [Rocket-Space Device Engineering and Information Systems]. 2014, Vol. 1, No. 2, pp. 47–58. (in Russian)

5. Khromov O.E., Blagodyrev V.A. Nauchno-metodicheskie osnovy sistemnogo podkhoda k postroeniyu informatsionno-izmeritel'nogo kompleksa [The Methodological Fundamentals of a System Approach to Construction of an Information-Measuring Complex]. *Raketno-kosmicheskoe priborostroenie i informatsionnye sistemy* [Rocket-Space Device Engineering and Information Systems]. 2014, Vol. 1, No. 1, pp. 68–77. (in Russian)
6. *ИЮ0.071.076. Struktura videosignala* БИТС*2*-МА-*9*МКТМ [ИЮ0.071.076. Structure of a videosignal БИТС2-МА-9МКТМ]. 1985. (in Russian)
7. Oreshko V. V., Kulikov A. I., Romanov P. E. Vliyanie svoystv kabel'noy seti i datchiko-preobrazuyushchey apparatury na tochnost' izmereniya analogovykh medlenno menyayushchikhsya parametrov bortovymi radiotelemetricheskimi sistemami [Influence of properties of a cable network and sensing transducers on accuracy of measurement of analogue slowly changing parametres onboard radiotelemetering systems]. *Informatsionno-izmeritel'nye i upravlyayushchie sistemy* [Information-measuring and Control Systems]. 2016, Vol. 14, No. 8. (in Russian)

ROCKET-SPACE DEVICE ENGINEERING AND INFORMATION SYSTEMS
Vol. 5, Iss. 2, 2018, pp. 50–60

Methodology for the Creation of an Innovative Scientific and Technical Reserve in the Rocket and Space Industry

V.Yu. Klyushnikov, *Dr. Sci. (Engineering), Senior Researcher, klyushnikovvy@tsniimash.ru*
Central Research Institute for Machine Building (FGUP TSNIIMASH), Moscow, Russian Federation
A.A. Romanov, *Dr. Sci. (Engineering), Prof., romanov@spacecorp.ru*
Joint Stock Company "Russian Space Systems", Moscow, Russian Federation
A.E. Tyulin, *Cand. Sci. (Engineering), contact@spacecorp.ru*
Joint Stock Company "Russian Space Systems", Moscow, Russian Federation

Abstract. The paper analyzes the problem of creating an innovative scientific and technical reserve (STR) in the rocket and space industry. A general methodological approach to the creation of STR is proposed. The main provisions of the STR establishment methodology are formulated. Innovative uncertainty and some limitations are taken into account. Restrictions due to the structure of technological way of life in the economy, the phase of the cycle of economic conjuncture and the general laws of the development of technical systems are analyzed.

Keywords: innovative scientific and technical reserve, rocket and space industry, innovative restrictions, technological paradigm, general laws of the development of technical systems

Introduction

All the outstanding achievements of scientific and technological progress, including the successes of astronautics in the twentieth century, were achieved by advancing and solving problems of the development of science and technology. The basis of all innovations is an innovative scientific and technical reserve (STR), created long before the start of implementation of large projects [1].

The design stage (including the development of customer requirements and the concept of a space system) in real costs does not exceed 20% of the total cost of creating a product. At the same time, the significance of the work performed at this stage reaches 95% [2]. In this regard, the existence of an STR is crucial to the success of a project.

In Russia, the most theoretically developed subjects are the methodologies for creating an STR in the field of weapons and military equipment (WME) [3, 4, etc.]. However, the basic methodological provisions for the creation of an STR in the field of weapons and military equipment are poorly applicable to the creation of rocket and space technology (RST) for the following reasons:

- in the defense field, the problem of goal setting is much easier to solve than the problem of goal setting in space activities;
- the uncertainty of the directions of development of weapons and military equipment is significantly lower than the uncertainty of the directions of development of astronautics;
- space activities directly and indirectly affect many aspects of the society, while maintaining the national defense capability only creates conditions for normal operation of state institutions, organizations, establishments and citizens;
- the methodology for creating an STR for the development of weapons and military equipment does not take into account the limitations imposed by the structure of techno-economic paradigms in the economy, the phase of the economic cycle and the general laws governing the development of technical systems.

There are no countries in the World than have a regulated general procedure for creating an STR in various areas: different enterprises and organizations do it in their own way. As the analysis of the problem shows, the project principle of work organization when creating an STR, and especially goal programming, have significant limitations.

The project approach is limited in the areas of activity where the final result, the required resources and time are determined insufficiently or not at all. In the general case, the creation of an STR is a process, not a project (that is, the work on the creation of an STR should be carried out continuously!). Moreover, the process is creative, initiated by insights of scientists and engineers. Sometimes the creation of an STR can be a project, but only in a small number of cases, then when it comes to the purposeful creation of a basis for solving a specific task. However, in this case this activity can be considered a pre-project research aimed at the implementation of a specific project, rather than development of an STR.

The project approach is fixated on the tasks of managing the design process, involves rigidly defined procedures and, generally speaking, does not require considerable intellectual effort. There is a temptation to resolve the difficulties associated with the development of fundamentally new design solutions, either using the old technological basis, or by making trivial decisions by analogy.

With the wide introduction of the project approach, in combination with the general decline in the level of education, there is a threat of washing out of the creative element, and first of all, at the stage of creating the STR, replacing high-class specialists with managers and executives.

Goal programming in the conditions of accelerating technological development and deepening innovative uncertainties in the development of science and technology can inhibit the creation of an STR that implements truly innovative principles.

Nevertheless, in our opinion, some general directions for solving the problem of creating an STR for the rocket and space industry, not related to the project approach or goal programming, which can serve as the basis for a number of regulatory industry papers, can be proposed.

The purpose of this article is to substantiate the main directions of the methodology for the creation of an STR in the rocket and space industry.

1. The structure of the innovative scientific and technical reserve

In accordance with the definition given in GOST R 57194.1-2016 [5], an innovative scientific and technical reserve (hereinafter STR) refers to promising products of the intellectual activity of enterprises and organizations in the field of science and technology, critical and

breakthrough technologies, the development and implementation of which in industrial production and products will lead to an increase in the efficiency of the industry and the introduction of technical systems with new properties and qualities. An innovative STR includes (Fig. 1) a scientific reserve (SR), a scientific and technical reserve (STcR) and a scientific and technological reserve (STlR).

At the initial stage of development of a specific system (space technology product), a previously developed STR can be represented as a network hierarchy of technical components (elements) of a *PBS* (*Product Breakdown Structure*) that are mutually coordinated by interfaces and which are integrated into the target system with the help of support systems. Each of the components of the PBS hierarchy in the life cycle includes the entire set of representations, from computer models to physical implementation.

The STcR includes promising products focused on creating a target technical system that can be described as a hierarchical product structure and is a mutually coordinated network hierarchy of technical subsystems and components integrated into the target technical system using support systems. The STcR is focused on a specific target system, which can be a specific product with a full life cycle, or a conceptual development project of advanced equipment. The result of the creation of STcR can be a research and development report, a system project, a patent, know-how and other innovative scientific and technical products.

The STlR includes advanced products focused on the creation of a support system that advances the target engineering system through its life cycle and is a coordinated network hierarchy of activities performed using current or advanced organizational, technical and technological mechanisms. At the same time, the advancement of the target system by the support systems along its life cycle (LC) is regulated by GOST R ISO / IEC 15288 [6] and GOST R ISO / IEC 12207 [7]. The STlR is a network hierarchy of tasks mutually coordinated by interfaces, a *WBS* (*Work Breakdown Structure*). The tasks are potentially implemented by technical and organizational mechanisms of the support systems for advancing the target system through its life cycle. Maturity, as the ability of a specific technology of a scientific and technological reserve to carry out work to advance target systems, is determined by the *TRL* (*Technology Readiness Levels*).

The result of the creation of STlR can be scientific and engineering products of the same type as in the case of NTNZ, but with an emphasis on technology (How to implement STcR? What production and technological capabilities, technologies, will this be required?).

SR, STcR and STlR in the general case may or may not be interconnected. SR, STcR and STlR can be interpreted as the degree of maturity of the STR: the cause-and-effect (production) dynamics of the creation of the STR can be described as a sequence: general theoretical concept (SR) ® technical solution (STcR) ® implementation tools (STlR).

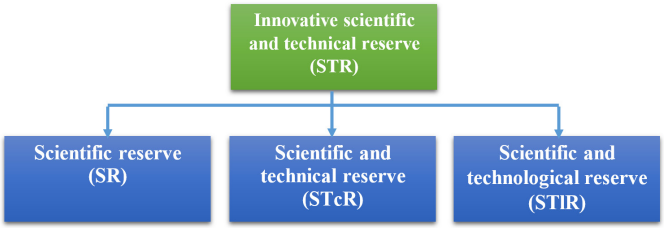

Fig. 1. The structure of the innovative scientific and technical reserve

Lastly, the NZ is the result of fundamental scientific research (new knowledge about phenomena, effects, laws, patterns, etc.) that is not directly related to the existing or advanced artifacts, technical means and technologies. Forms of presenting the SR as a commodity are research reports, articles, monographs and other sources of information in standardized forms, including archives of electronic documentation, designed for machine processing. The scientific reserve is focused on fundamental research and studies that do not directly imply subsequent research and development work (R&D) for the creation of a specific product of rocket and space technology.

Thus, the formation of the STR should be considered as a complex systemic activity that creates the scientific, technical and technological basis for the industry, carried out mainly by research organizations and individual researchers, together with the rocket and space industry and organizations of other industries, necessary for the creation (development, modernization) of various types and products of space technology. The STR includes the results of theoretical and experimental research, as well as exploratory development.

The structural components of the STR are [8]:

- new knowledge obtained in the course of studying the properties of material objects, processes and phenomena in the field of space exploration, including the results of theoretical and experimental research: a knowledge base for the areas of scientific and technical activities;

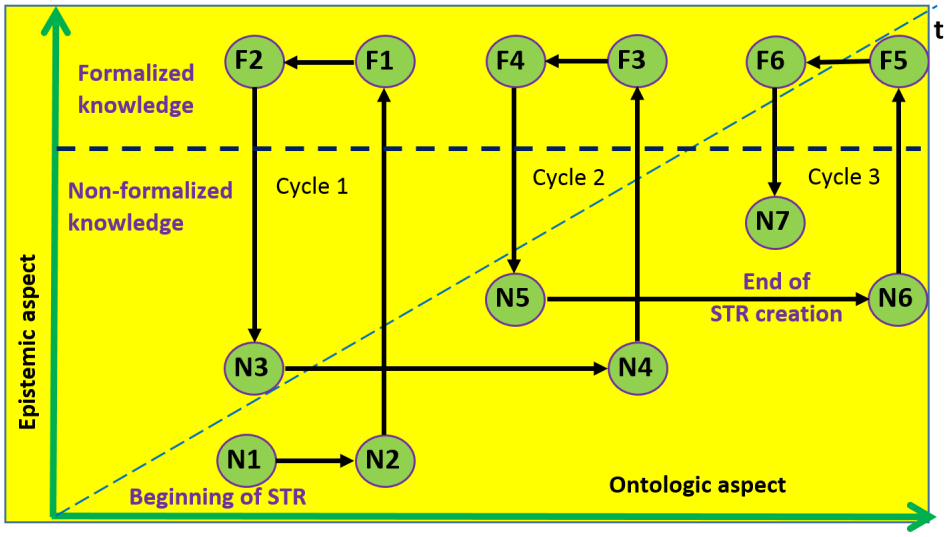

Fig. 2. The spiral of knowledge creation in the dynamics of the development of scientific and technical reserve

- new technical solutions (results of exploratory development), including design documentation, prototypes of new designs, elements and components of space technology (in the general, parts of target systems);

- technological processes and specialized equipment necessary for the development, production and testing of rocket and space technology, including processes and equipment for the design, production and processing of materials, assembly, quality control, testing. This component of the STR exists in the form of relevant regulatory and technical documentation and equipment (in general, supporting systems).

The process of creating an STR can be described by the so-called "knowledge spiral", which shows the transition of knowledge from one type to another. In particular, formalized (conscious) and non-formalized (unconscious) knowledge are distinguished. The creation of an STR is a continuous interaction of implicit and explicit knowledge through various forms of transformation. One of the main conditions driving the "knowledge spiral" (Fig. 2) is the redundancy of the STR. That is why leading countries are paying so much attention to creating a reserve. In the United States, in particular, the commitment to the creation of the STR in advance led to the fact that knowledge became a commodity as well as material objects [9].

The implementation of this principle leads to the fact that the number of research and development activities carried out by an enterprise deliberately surpasses the nomenclature of samples of rocket and space technology to be created. Therefore, when holding tenders for a contract for the creation of a new space technology, there will always be options to choose from. If the tenders are made multi-stage or at least two-stage (for example, the first stage is a tender for the implementation of an advance project or technical proposal, and the second stage, according to the results of the first, is the implementation of the remaining stages of product design), then there is competition, which is based on the STR, in advance created by each of the participants of the competition. Enterprises of the industry, creating an STR, are already competing with each other, although in an implicit form.

In our opinion, the creation of the STR can be financed either at the expense of the enterprise (most likely) or on the basis of budget financing. The amount of financing for creating an STR can be tied to achievements in this area, for example, it can be based on the results of the year: the higher is the volume of STR created, the higher is the next year funding for these purposes. It is imperative to create targeted financial incentives of specific scientists and specialists, developers of the STR.

The current results of the continuous process of creating an STR in the form of specific documents can be combined into an information base such as a depository. The semantic structure of such a depository is presented in fig. 3

The meaning of the term "depository" is that the information base of the STR not only stores STR documents, but also guarantees the copyrights of their developers with all the ensuing consequences. An STR depository contains building blocks that (with appropriate "processing") can be used as the basis for a specific project.

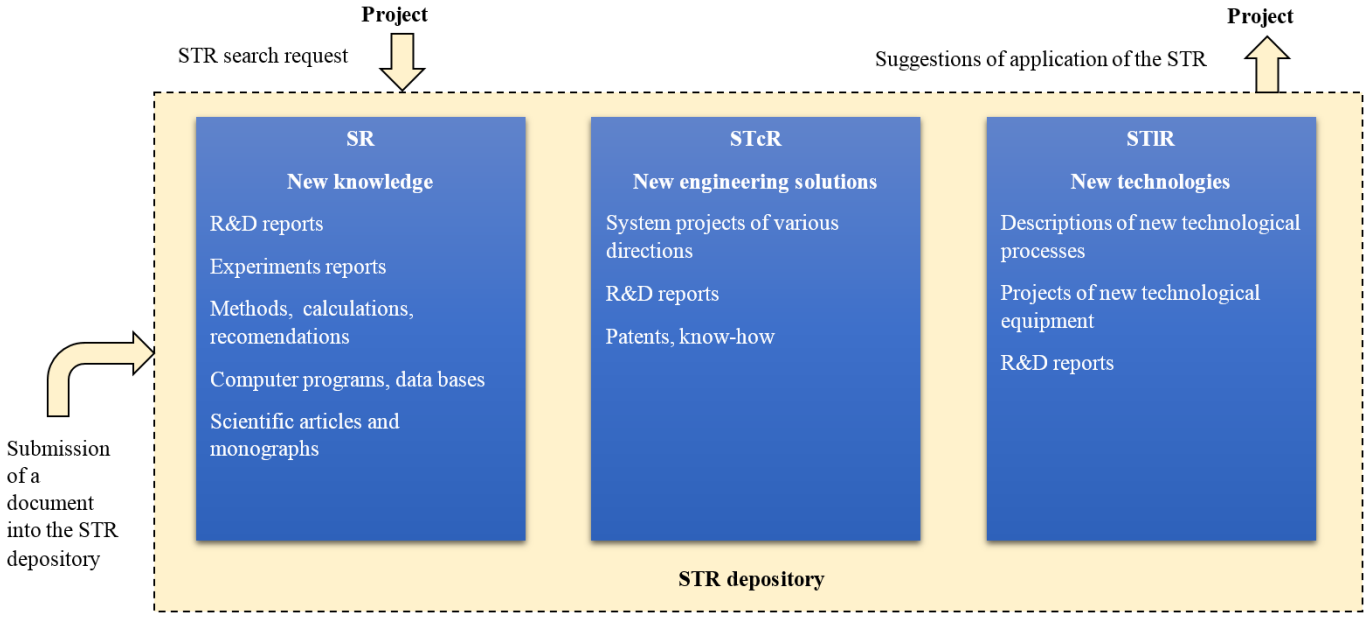

Fig. 3. The semantic structure of an STR depository

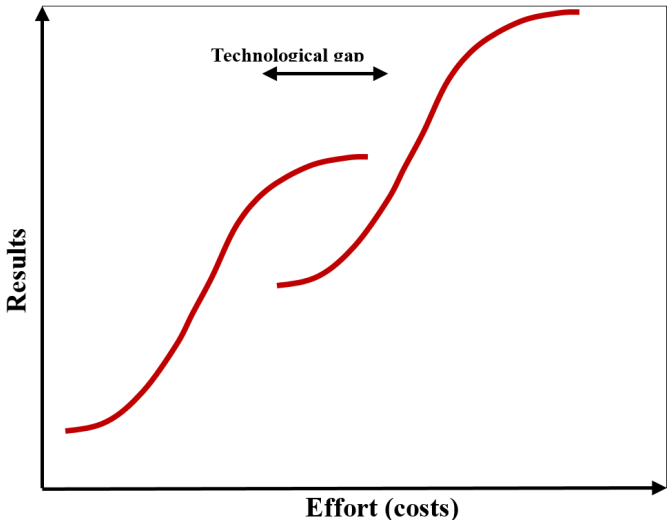

Fig. 4. Illustration of the technological gap concept

2. General principles for the creation of an innovative scientific and technical reserve

The main problem of creating an innovative STR is the so-called innovation uncertainty, which arises as a measure of ignorance of potential directions and opportunities for technological development, in particular, taking into account possible technological gaps that break the momentum of the development of science and technology (Fig. 4). The technological gap in the development of a technical system is understood as a qualitative leap in the dynamics of the target (forecast) characteristics of the system, a gap in its evolutionary development due to new achievements of basic science or new design solutions. Development of any technical system sooner or later reaches a level where, in spite of the efforts made, its characteristics hardly improve. As an example, a liquid rocket engine can be given: its technical evolution has reached the limit: any design solutions are able to raise the specific impulse by no more than 10-15%, but the costs increase geometrically. In such a situation, further development of the system is possible only on the basis of a technological gap. A technological gap eliminates the innovation uncertainty.

The methodology of the continuous creation of the STR becomes particularly important in connection with the impending problem of singularity (Problem 2045)[1], illustrated by the Panov–Snooks curve [10]: there is a pronounced tendency for the innovation uncertainty border to approach the duration of the R&D stages [11]. In our case, the problem of singularity can be interpreted as the desynchronization of the duration of the cycles for creating an innovative STR, the development of technologies (from TR=0 to TR=9) and the lifetime of a space technology product. The technological gap will occur long before the end of the product life cycle.

[1]Technological singularity is a hypothetical moment, after which, in the opinion of supporters of this concept, technical progress will become so fast and complex that it will be inaccessible to human understanding. Reality, apparently, will not be so intimidating. It is possible to talk about the threat of singularity, about the asymptotic approach to it. In any case, the information explosion will be somewhat stretched in time.

In this regard, firstly, the process of creating an STR, resolving innovation uncertainty, should be continuous, and secondly, it should be ahead of the current R&D projects. At the same time, the method of selection of critical technologies stops working in its pure form: all technologies fall into the category of critical ones.

At first glance, taking into account all the above, the task of creating an STR can be characterized by the idiom "Go I know not wither and fetch I know not what." Nevertheless, the task can be successfully solved if the following principles are put in the basis of the methodology for creating an STR, (Fig. 5):

1. The general directions for the creation of an STR should be determined based on objectively existing critical system conflicts in the development of rocket and space technology and space activities in general. As a rule, overcoming such conflicts is accompanied by a discontinuity in the smooth evolutionary development of a technical system, a technological gap. However, there may be several directions of technological gaps. In such cases, is proposed to consider the most acceptable way to overcome conflicts the one that best meets the expectations of the society [12]. In this way, the level of innovation uncertainty can be reduced.

It should be noted that focusing only on the technological environment in the process of identifying critical conflicts and choosing ways to resolve them is unproductive. It is necessary to take into account the synchrological[2] nature of potential conflicts in all social environments [13].

I.e., in determining the prospects and directions for the development of the space technology, the humanitarian issues of working with social environments are involved, which in general terms corresponds to the ideas of the VII technological paradigm[3] [14, 15].

2. Definition of the corridor for creating of an innovative STR in the field of technological and economic opportunities [16], determined by the technological paradigm in the economy and the phase of the cycle of the economic conditions[4].

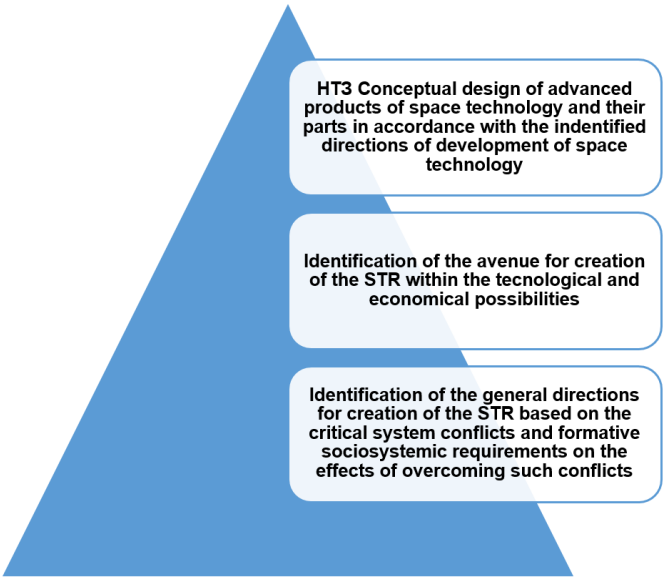

Fig. 5. Methodological principles for the creation of an STR

3. Conceptual design of advanced space technology products, their components, instruments, systems and units in accordance with previously identified fields for creation of an innovative STR. Conceptual design, generally speaking, should be the initial stage of the project to create a specific space technology product. However, within the framework of the creation of an STR, conceptual design tasks are not practically specified; they should be much more redundant and extensive compared to pre-project research tasks.

The proposed principles for the creation of an STR respond to the main challenges of the time, take into account the predicted changes in the technological base of the space technology, such as technological gaps and the impending problem of singularity.

3. The main provisions of the methodology of creating an innovative scientific and technical reserve in the rocket and space industry

Identifying of critical system conflicts

Identifying critical system conflicts and forming socio-system requests for the effects of overcoming these conflicts in the rocket and space industry is a rather difficult task due to the impossibility of its formal solution. Table 1 presents some preliminary results of expert identification of critical system conflicts and forming socio-system requests for the effects of overcoming them in the rocket and space industry.

[2]Synchrological - establishing the relationship between phenomena and processes occurring at the same time in different parts of one state or in several states.

[3]VII technological paradigm is called socio-humanitarian or cognitive. Its main feature is the convergence of nano-, bio- and information technologies, aimed at transforming human consciousness into a productive force (conscious control of reality, creation of new realities: technological, cultural, social).

[4]This refers to the phases of economic cycles of different periodicity: Kondratiev, Kuznets, Kitchin, Zhiglyar, etc. The main of them is the Kondratiev cycle (Kondratiev waves).

Table 1 - Results of the expert identification of critical system conflicts and the forming socio-system requests for the effects of their overcoming in the rocket and space industry

No.	Critical system conflict	Possible socio-system request for the effects of overcoming the conflict
1	The conflict between the biological nature of man and the factors of outer space	The pursuit of space expansion, including the industrial exploration of space, the transfer of polluting and dangerous industries into space, the development of the mineral resources of planets and asteroids, the efficient use of solar energy, the colonization of the solar system. Striving for sublimation of such human qualities as passionarity and aggressiveness in solving problems of research, exploration and use of space
2	The conflict between the unclear goal-setting of space activities and the large resource costs for the space exploration and space expansion	
3	The conflict between the demand for space products and space services and the high cost of space technology products	Striving for the availability of the entire range of space services anytime and anywhere
4	The conflict between the high speed of development of science and technology and the impossibility of spacecraft modernization during orbital flight	The desire to receive higher quality space services

Definition of the corridor of technological development

The possible directions for creating an innovative scientific and technical reserve in any field, including the rocket and space industry, are limited by the existing and advanced structure of technological paradigms in the economy, the phase of the economic cycle and the general laws governing the development of technical systems.

In the long term (10–30 years), Kondratiev cycles [17], which are directly related to innovation, apparently have the greatest influence on the development of technology (Fig. 6). Since the beginning of the twenty-first century, after the global crisis of 2001-2002, the fifth technological paradigm and the corresponding Kondratiev cycle entered a downward phase. At the same time, began the development of the first generations of technology of the 6th technological paradigm, which will become predominant in the advanced countries in 2020-2050s. The total duration of Kondratiev cycles (Kondratiev long waves) ranges from 45-60 to 50-70 years. The problems of the 6th technological paradigm with respect to space activities are considered in [18, 19].

Based on the theory of large cycles of the economic situation, it can be expected that on the downward wave of the Kondratieff cycle, the depth and duration of economic crises will increase. Their peak may fall on the beginning of the 2020s, after which the reverse trend will prevail.

In general, in the next 25 years, the avenue of the technological development of the space industry, due to the current economic structure and the associated innovation cycle, is characterized by a generally favorable economic environment.

As the key factors for the development of the space technology products of the 6th technological paradigm, one can identify from five to twenty of the most promising breakthrough technologies of the beginning of the 21st century, including:

- computer-controlled processes of production and operation of rocket and space technology at all stages of its life cycle;
- microminiaturization and multifunctionalization of information and communication, sensor and actuating devices with a high degree of accuracy;
- autonomous intellectual modules and spacecraft (SC), including multi-agent spacecraft systems;
- alternative and combined energy sources, ways of highly efficient energy transportation, energy saving, compliance with environmental standards;
- biotechnological development in the interests of manned space flight;
- nanotechnology of a wide range of applications;
- implementation of the bionic principles (life-technologies) of creating space technology, etc.

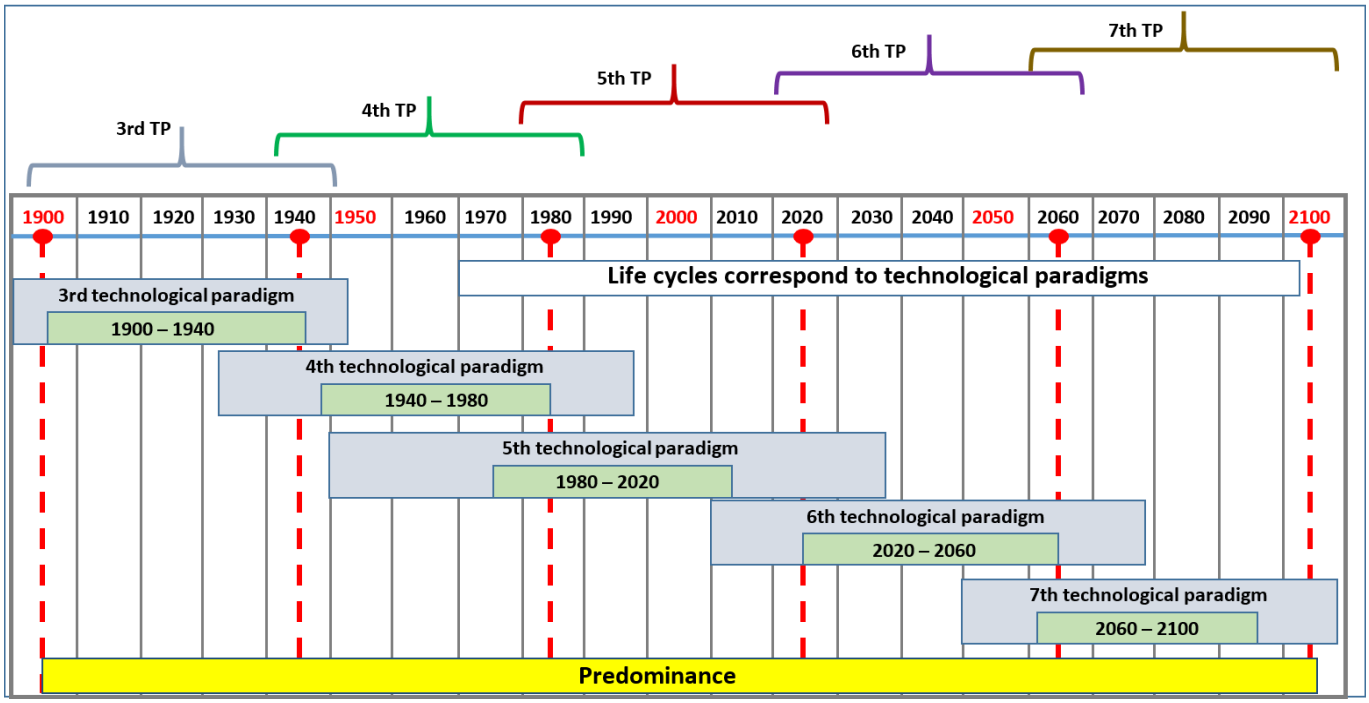

Fig. 6. Dynamics of change of technological paradigms [19]

Conceptual design

Conceptual design complements and specifies the general directions for the creation of the STR. Conceptual design is carried out by industry research and design organizations, individual scientists and specialists.

Examples of possible directions of conceptual design when creating the STR in the rocket and space industry are presented in Table 2.

As methods of conceptual design in the process of creating the STR, the following can be used:

- heuristic methods;
- methods of iterations (sequential approximation);
- decomposition methods;
- methods of inducing questions;
- various brainstorming technologies;
- methods of the theory of inventive problem solving (TIPS);
- methods of functional cost analysis, etc.

The most promising methods of conceptual design are the methods of TIPS, based on the general laws governing the development of technical systems [20]. In this case, under a concept we understand the description of the way to achieve a goal. Concepts include physical or functional principles of action, principles of change, principles of conflict elimination, improving pairs of interrelated indicators of a technical system, as well as sets of optimal values of parameters of system elements. Description of the concept should be sufficient for the development of design solutions.

Currently, new varieties of computer-aided design (CAD), focused on conceptual design - CAI-systems [5] are being created. Distinctive features of CAI systems include:

- management of innovative activity of the enterprise;
- development of concepts (technical ideas);
- management of patents of the enterprise.

The main function of CAI systems is concept design. The conceptual design method combines all known invention strategies and covers the entire concept development cycle. It uses complex formal algorithms and a large base of general technical and scientific knowledge [1]. However, it should be noted that numerous development projects of CAI-systems (inventing software) could not significantly increase the productivity of creative activities due to the lack of a formal method that covers all stages of the concept development: from the choice of the initial goal to the definition of the areas for application of the developed concepts.

[5]CAI – Computer Aided Invention – the search for innovative solutions using a computer.

Table 2 - Examples of possible directions and objects of conceptual design when creating the STR in the rocket and space industry

No.	Conceptual Design Directions	Conceptual Design Objects
1	Putting space objects into the Earth orbit and departure trajectories	New ways of launching space objects to the Earth orbit and departure trajectories. Constructive layout of the launch vehicles. Reusable launch vehicles. Platforms for launching payloads of up to several thousand tons. Small and micro-sized launch vehicles for launching small (ultra-small) spacecraft.
2	Rocket engines	Thermochemical rocket engines: - detonation liquid rocket engines (LRE); - LRE with a central body; - one-component LRE, including using micro- (nano-) encapsulated fuel. Nuclear rocket engines: - impulse engines; - heterogeneous gas-phase engines. Thermonuclear rocket engines. Electric propulsion engines: - ion engines; - plasma engines, including engines with free plasma confinement. Cross-media engines (atmosphere - space). Rocket engines on new physical principles (anti-gravity, control of the space-time continuum, etc.).
3	Manned space flight	Ensuring the safety of long-distance space flight and comfortable habitability of manned spacecraft. Emergency crew rescue. Means of landing on the planet (return vehicles). Closed-circuit biological life support systems. Technologies of hibernation (anabiosis) during long-distance space flights. Avatar technologies for extravehicular activity and planetary exploration.
4	Remote sensing of the Earth from space	New ways of sensing the Earth from space. Ultra-compact optical systems. Distribution of the target function of Earth sensing among a cluster of small (ultra-small) spacecraft.
5	Space communications, broadcasting and retransmission	New ways of transmitting (relaying) data through space communication channels. Methods of reception and transmission of weak signals with levels comparable to or lower than the level of natural noise. Quantum communication. Communication between spacecraft. The distribution of the objective function of communication, data transmission and relaying in a cluster of small (ultra-small) spacecraft.
6	Space navigation	Methods of precision space navigation for terrestrial consumers. Navigation methods in high near-earth orbits (H > 2000 km), including geostationary orbit. Deep space navigation methods: - within the solar system; - outside the solar system. Methods of navigation on the surface of the planets.

Conclusion

Thus, the main features of the new methodology for creating an STR in the industry have been formulated, taking into account the existing innovation uncertainty and limitations arising from the structure of technological paradigms in the economy, the phase of the cycle of economic situation and the general laws governing the development of technical systems.

The proposed methodology can be used as a basis for a new research and production system for the rocket and space industry, designed to give impetus to its further innovative development.

The main provisions of the developed methodology should be reflected in the regulatory and methodological documents of the industry, paying particular attention to the creative, informal, systemic nature of the creation of the STR, the grassroot initiative, the need for targeted incentives for this process, careful observance of copyright, as well as the requirement of redundancy of the STR in relation to those R&D projects, which are aimed at the creation of specific space technology products.

The creation of the STR should be based on informal heuristic procedures and CAI systems, which makes it possible:

- to determine the general directions of the creation of the STR, taking into account the critical system conflicts and sociological demands for the effects of overcoming these contradictions;

- to identify the areas of technological and economic opportunities that set the "corridor" for the creation of the STR, taking into account the current and future technological paradigm in the economy and the phases of the cycle of the economic situation;

- to predict at the conceptual level the design profile and the main characteristics of promising design solutions in accordance with the previously identified directions for the creation of the STR; the procedures of the conceptual design can be based on the methods of the theory of inventive problem solving (TIPS), based on the general laws governing the development of technical systems.

References:

1. Romanov A.A. Smena paradigmy razrabotki innovatsionnoy produktsii: ot razroznennykh NIOKR k tsifrovym proektam polnogo zhiznennogo tsikla [Paradigm Shift in the Development of Innovative Products: from Disparate R&D to Full Life Cycle Digital Projects]. Raketno-kosmicheskoe priborostroenie i informatsionnye sistemy [Rocket-Space Device Engineering and Information Systems], Vol. 4, No. 2, 2017, pp. 68–84. (in Russian)
2. Romanov A.A., Shpotya D.A. Bazovyy podkhod k identifikatsii kriticheskikh tekhnologiy: opredelenie vazhneyshikh inzhenernykh kharakteristik izdeliya [Basic Approach to Identification of Critical Technologies: Estimation of the Most Important Engineering Attributes of a Product]. Raketno-kosmicheskoe priborostroenie i informatsionnye sistemy [Rocket-Space Device Engineering and Information Systems], 2016, Vol. 3, No. 3, pp. 63-75. (in Russian)
3. Burenok V.M. Tekhnologicheskie i tekhnicheskie osnovy razvitiya vooruzheniya i voennoy tekhniki [Technological and technical basis for the development of weapons and military equipment]. Moscow, Granitsa, 2010, 216 p. (in Russian)
4. Burenok V.M., Ivlev. A.A., Korchak V.Yu. Programmno-tselevoe planirovanie i upravlenie sozdaniem nauchno-tekhnicheskogo zadela dlya perspektivnogo i netraditsionnogo vooruzheniya [Program-targeted planning and management of the creation of a scientific and technical reserve for prospective and non-conventional weapons], Moscow, Granitsa, 2007, 408 p. (in Russian)
5. GOST R 57194.1-2016 Transfer tekhnologiy. Obshchie polozheniya. [Transfer of technologies. General provisions]. (in Russian)
6. GOST R ISO/MEK 15288-2005 Informatsionnaya tekhnologiya (IT). Sistemnaya inzheneriya. Protsessy zhiznennogo tsikla sistem. [Information technology (IT). System engineering. Processes of the life cycle of systems]. (in Russian)
7. GOST R ISO/MEK 12207-2010 Informatsionnaya tekhnologiya (IT). Sistemnaya i programmnaya inzheneriya. Protsessy zhiznennogo tsikla programmnykh sredstv. [Information technology (IT). System and software engineering. Software life cycle processes]. (in Russian)
8. Krivoruchenko V.S. Terminologiya sozdaniya NTZ [Terminology for the creation of STR]. Aktual'nye problemy gumanitarnykh i estestvennykh nauk [Actual problems of the humanities and natural sciences], No. 10-1, 2015, pp. 114-119. (in Russian)

9. Kravchenko A.Yu., Smirnov S.S., Reulov R.V., Khovanov D.G. Rol' nauchno-tekhnicheskogo zadela v innovatsionnykh protsessakh sozdaniya perspektivnogo vooruzheniya: problemy i puti resheniya [The role of the scientific and technical reserve in the innovative processes of creating long-range weapons: problems and solutions]. Vooruzhenie i ekonomika [Arms and Economics], No. 4 (20), 2012, pp. 41-55. (in Russian)
10. Panov A.D. Singulyarnaya tochka istorii [Singular point of history]. Obshchestvennye nauki i sovremennost' [Social sciences and modernity]. 2005, No. 1, pp.122–137. (in Russiant)
11. Rezhimy s obostreniem: Evolyutsiya idei. Sbornik statey [Modes with peaking: Evolution of the idea. Collected papers]. Ed. by G.G.Malinetskiy, 2nd Ed. revised and enlarged. Moscow, Fizmatlit, 2006, 312 p. (in Russian)
12. Malinetskiy G.G., Timofeev N.S. O metodologii prognoza razvitiya aerokosmicheskogo kompleksa [On the methodology for forecasting the development of the aerospace complex]. Preprinty IPM im. M.V.Keldysha [Preprints of Institute of Applied Mathematics named after Keldysh]. 2012, No. 72, 16 p. Available at: http://library.keldysh.ru/preprint.asp?id=2012-72 (in Russian)
13. Pereslegin S.B. Novye karty budushchego [New maps of the future]. Moscow, 2009. (in Russian)
14. Lepskiy V.E. Refleksivno-aktivnye sredy innovatsionnogo razvitiya [Reflexively active mediums of innovative development]. Moscow, 2011. (in Russian)
15. Prokhorov I. A. Nachalo 7-go tekhnologicheskogo uklada [The beginning of the 7th technological paradigm]. Available at: http://www.energoinform.org/pointofview/prohorov/7-tech-structure.aspx (Last accessed: 21.07.2017) (in Russian)
16. Klyushnikov V.Yu. Metodologiya kompleksnogo prognozirovaniya tekhnologicheskogo razvitiya raketno-kosmicheskoy tekhniki [Methodology of complex forecasting of technological development of rocket and space technology]. Kosmonavtika i raketostroenie [Cosmonautics and rocketry]. No. 2 (95), 2017, pp. 13-25. (in Russian)
17. Kondrat'ev N.D. Bol'shie tsikly kon»yunktury i teoriya predvideniya. Izbrannye Trudy [Large cycles of conjuncture and theory of foresight. Selected works]. Moscow, Ekonomika, 2002, 767 p. (in Russian)
18. Romanov A.A., Tyulin A.E. Shestoy tekhnologicheskiy uklad v kosmicheskom priborostroenii [Sixth Technological Paradigm in Space Device Engineering]. Raketno-kosmicheskoe priborostroenie i informatsionnye sistemy [Rocket-Space Device Engineering and Information Systems], 2017, Vol. 4, No. 4. pp. 64–82. (in Russian)
19. Prognoz innovatsionno-tekhnologicheskogo razvitiya Rossii s uchetom mirovykh tendentsiy na period do 2030 goda [Forecast of innovation and technological development of Russia taking within world trends until 2030]. Ed. by B.N. Kuzyk, Yu.V. Yakovets, A.I. Rudskoy. Moscow, MISK, 2008. (in Russian)
20. Zlotin B.L., Zusman A.V. Zakony razvitiya i prognozirovanie tekhnicheskikh sistem: Metodicheskie rekomendatsii [Laws of development and forecasting of technical systems: Methodical recommendations]. Kishinev, Kartya Moldovenyaske, 1989, 114 p. (in Russian)
21. Glazunov V.N. Kontseptual'noe proektirovanie: Teoriya izobretatel'stva. Uchebnoe posobie [Conceptual design: The theory of invention. Textbook]. Moscow, LENAND, 2018, 512 p. (in Russian)

ROCKET-SPACE DEVICE ENGINEERING AND INFORMATION SYSTEMS
Vol. 5, Iss. 2, 2018, pp. 61–67

The Concept of Building an Expert-Diagnostic Complex for Analysis of Information Systems

V.V. Betanov, *Dr. Sci. (Engineering), Prof., betanov_vv@spacecorp.ru*
Joint Stock Company "Russian Space Systems", Moscow, Russian Federation
V.K. Larin, *Cand. Sci. (Engineering), vklarin@mail.ru*
Joint Stock Company "Russian Space Systems", Moscow, Russian Federation

Abstract. The article considers the concept of an expert-diagnostic complex (EDC) for analyzing the operation of information systems (IS). The current state of the problem regarding the development of an expert-diagnostic system (EDS) for the analysis and failure recovery in the work of each unit of an IS is studied. The study included the development of an appropriate knowledge base and other parts of an EDS, such as a database, operation area, and solver. All these led to significant material and technical costs, complicating the issue of correspondent software performance. The proposed integration of single-profile EDS into an EDC including the monitoring of failure addressing using diagnostic labels will greatly simplify the user's work without large expenditures on product creation. The EDC design differs from that of the EDS by the presence of several knowledge bases and an add-in in the form of an interface for convenience of the user. The article presents the technology of EDC building including several single-profile knowledge bases. An example of building an EDC is given.

Keywords: subject area, concept, expert-diagnostic complex, diagnostic labels

Introduction

The use of an EDS for tackling non-formalized issues in different areas of the national economy has found wide application. The efficiency of such implementation depends on the relation between the provided benefits and the creation, implementation and operational costs of the instrument. One should note that, owing to certain constraints concerning the structural components of the system, EDS is used for solving problems in a narrow subject area. This particularly concerns the central body of the EDS – the knowledge base, the application range of which depends on the gained experience in solving such problems and on the interpretation of this experience by the production model. For this reason, the combined use of several EDS with proper hardware and software is necessary for full-fledged expert service of complex systems. All of this impairs the efficiency of using EDS for complex systems. A possible solution in this situation (in other words, the efficient service of complex systems with the implementation of expert assessment) lies in the development and introduction of expert-diagnostic complexes (EDC) based on separate elements of single-profile EDSs. What is more, the fundamental difference between the designs of the EDC and the EDS is the presence of several knowledge bases describing the situation in the chosen system and an add-in in the form of a control program for creating technological activation chains of corresponding program units.

The present paper gives a conceptual description of an EDC for the performance evaluation of an IS. The BNS ASC is considered in the paper as an example of EDC application.

The choice of the system was conditioned by the following reasons:

- sufficient complexity of the constituent types of ballistic – navigation support that justifies the use of EDC;
- availability of EDS developments for analyzing issues of concern that arise in some BNS concepts;
- BNS is the most studied (for the authors) hardware and software system in terms of performance issues.

The following terms and notions are used in the present paper:

Ballistic-navigation support (BNS) – an aggregate of hardware-software components and technologies for ballistic information reception that is essential for spacecraft flight control.

TIPP KB – knowledge base of the trajectory information pre-processing program.

Subject area (SA) – an aggregate of interconnected elements, which ensure the fulfillment of the assigned task.

Object – any element of the system.

Object property – a certain quantity that characterizes the state of the object at any moment in time.

Concept — (from Latin *conceptus* – thought, idea) – constituent part of the subject area.

Information parameters – the characteristics of a concept, the deviation from which may lead to system malfunctions.

Diagnostics – the identification of object operation failures by means of comparing the current values of its parameters with normal values.

EDS – an expert-diagnostic system is for solving problematic issues that arise from the operation of separate parts of an IS.

EDC – an expert-diagnostic complex is for solving problematic issues that arise from the operation of information systems.

Distinctive features of the EDC in comparison with the EDS:

- the presence of several KBs;
- the availability of a setup program for the complex meant for solving specific problems;
- the presence of a problem analysis and decision algorithm unit.

ASC – automated software complex

MS – mathematical software

TNPM – trajectory navigation parameter measurements

LD – location determination

Prerequisites for setting up an EDC

1. The system in question should be introduced in the form of a hierarchical structure.
2. For further EDC building, the system should be divided into functional parts that correspond to the last level of the hierarchy.
3. In the course of system operation, it is necessary to carry out monitoring with the help of special labels that characterize the operation of system parts. As the labels are filled out, an output signal is generated that initiates the EDC technological cycle.

4. The constituent parts of the level should be described as subject areas.

5. Each subject area is to be given in the form of an aggregate of concepts with the description of information parameters.

6. A corresponding knowledge base with the ability to connect to the EDS circuit (the elements of which are accounted for in the given structure) should be formed within each subject area.

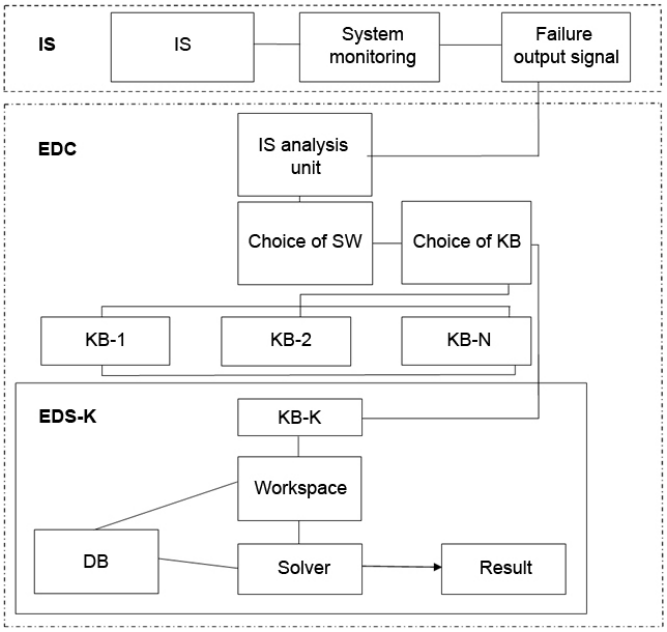

Fig. 1. EDC block diagram.

Description of the EDC block diagram

The EDC diagram given in Figure 1 consists of two parts: 1 – an information system as a source of information (includes a monitoring system that generates an output signal in the case of an IS failure) and 2 – an EDC as an instrument for processing the aforementioned information.

The following components are part of the EDC:

— IS analysis unit. The function of the unit is to analyze the characteristics of the output signal with the aim of choosing a correspondent KB. The descriptions of SAs that characterize the main parts of the IS are part of the analysis unit. Considering this, KBs that correspond to the content and quantity of SAs are formed.

At this point, the most difficult part of the task is the choice of SAs that would correspond to the system's main parts. With the purpose of clarifying this issue we shall turn to the IS typical diagram (Figure 2).

The choice of the main parts of an IS is analogous to the choice of the level of detail of the IS structure that is determined by autonomously functioning units. In this case, the 3rd level consists of units, the functioning of which does not depend on the specifics of the IS. For every 3rd level unit a set of information parameters that characterize its stability may be determined, and accordingly, production models for filling up knowledge bases are formed.

KB (1…N) containing formalized operating experience of such ISs are part of the EDC. Based on the selected SA, the KB is determined according to the following rule: "SW index should match the KB – $SA_{\underline{к}}$ - $\underline{KB_{к}}$ index", which is used in the further solution of the problem according to the EDS-K scheme (Figure 1).

A detailed description of EDS units is given in [1].

As an example, we shall consider the design of an EDC for BNS ASC.

Figure 3 provides a diagram of BNS, where the ASC is located on the 2nd level (as a component of the MS).

A block diagram of the ASC is given in Figure 4 for further consideration.

Each ASC unit is a separate subsystem independent of the specifics of input parameters. It may be considered as an object for separate analysis by the EDS. Subsequently, a separate KB should be developed for every unit.

More specifically, in works [2, 4, 5] the description of EDS prototypes for ASC operation failure analysis and correction is provided. Namely, "EDS for the search and correction of non-difference phase measurement jumps" is one of the sections of the TIPP unit, "knowledge base for receiver location determination software module" is a BVP section, and "EDS for trajectory measurement information analysis" is a section of TIPP.

In normal operating mode (when failures are absent) the result of ASC functioning are refined orbit parameters saved in corresponding DB tables and file archives. Apart from that, intermediate results are formed TNPM sessions (before and after filtering), sessions of difference measurements, LD results and statistics, etc. In the event of failure, the ASC either stops (variant A) or carries on providing results of unsatisfactory quality (variant B). For successful troubleshooting it seems appropriate to, first, determine which ASC component the failure concerns and, after that, it will be possible to pass on to analyzing the causes of failures and failure recovery.

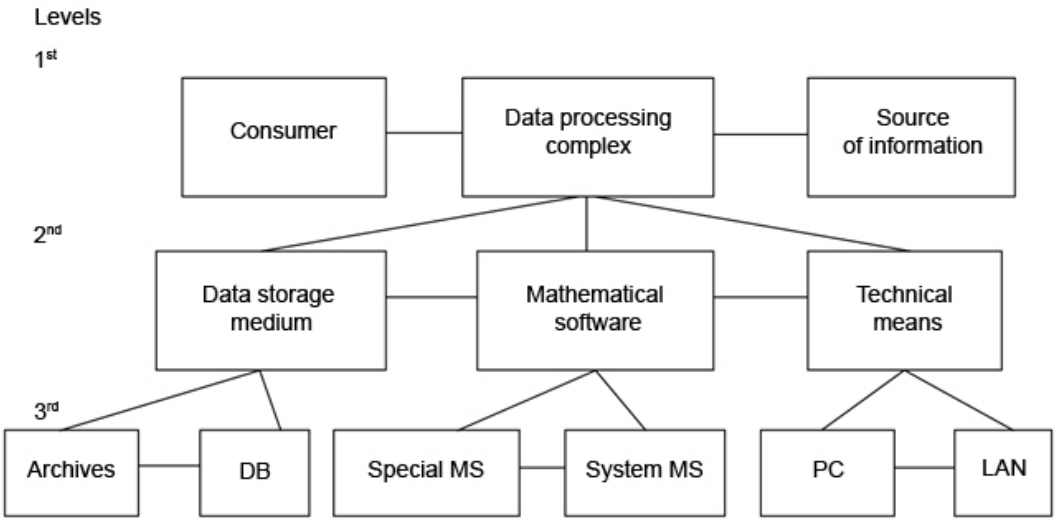

Fig. 2. IS typical diagram.

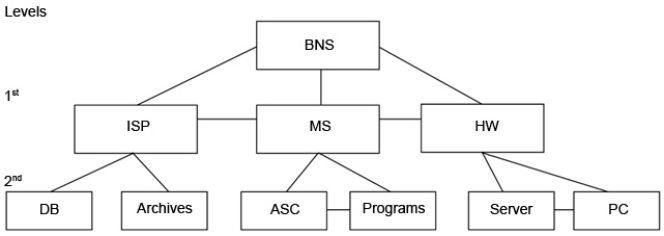

Fig. 3. BNS.

Let us consider the principles of building an EDC-TIPP for analyzing performance of a part of ASC-TIPP (variant A).

The EDC-TIPP building technology cycle consists of the following stages:

1st stage. Determination of detail level for IS hierarchical structure. In accordance with BNS and ASC structure analysis (Figures 3, 4), initially the 2nd level of BNS was defined – within it an ASC was selected for further work.

2nd stage. The division of selected system into functionally independent parts (Figure 4) to a certain level of detail.

3rd stage. Building a SA for corresponding parts.

4th stage. Failure address determination (name of the corresponding ASC, the TIPP in particular).

For failure address determination we introduce *diagnostic labels (DL),* which are, in essence, named cells at the end of each subprogram that take on values of 0 or 1. "1" shows that the program performs calculations. "0" signifies that calculations by the given subprogram have stopped (subprogram – a functionally complete part of the general program that has input and output data).

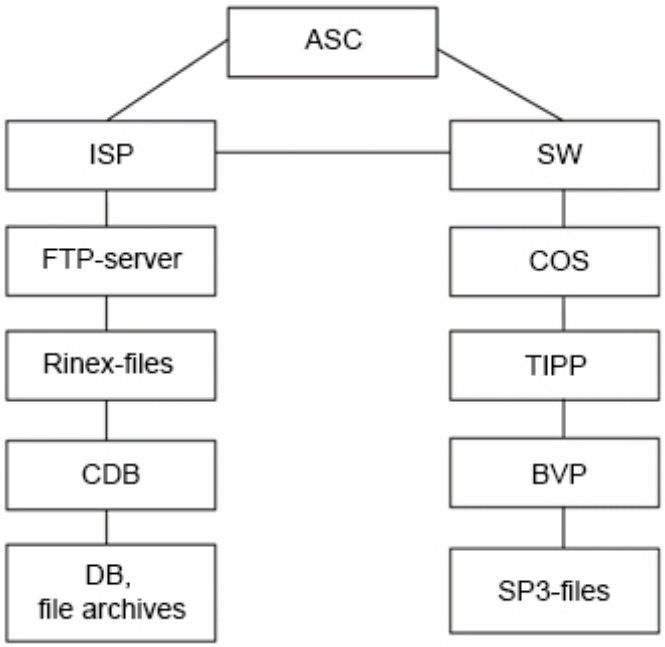

Fig. 4. ASC diagram.

Explanatory notes to Figure 4:

ISP – Information support

SW – Software

FTP–server – website with measurement data

COS – program for configuring operating settings of the complex

Rinex–files – trajectory measurement information

TIPP – trajectory information pre-processing program

CDB – central database

BVP – boundary-value problem (orbit parameter determination program)

DB, file archives – current information repositories

SP3–files– orbit parameters in a generally accepted format

5th stage. Formation of KBs that correspond to SAs. The technology for filling up KBs consists in the sequential performance of the following operations: SA building, concept definition, setting of information parameters and their specific values, production model formation – the KB.

6th stage. Addition of KB to the technological scheme of the EDS for analyzing and correcting particular failures.

As an example, we will consider the stage-by-stage formation of a KB for an ASC unit, omitting stages 1 and 2 (Figures 3, 4).

The TIPP subject area consists of:

— Trajectory measurement information (TMI);

Subprogram [5]:

— measurement session formation
— processing and filtering of measurement sessions
— formation of baseline sets
— difference measurement formation
— filtering of difference measurement sessions
— LD based on code range measurements
— statistical evaluation of location results

For our convenience, the concepts are grouped the following way:

1st group – trajectory measurements
— trajectory measurements (TM)
— measurement session formation
— processing and filtering of measurement sessions

2nd group – difference TM (DTM):
— formation of baseline sets
— difference measurement formation
— filtering of difference measurement sessions

3rd group - LD
— LD based on code range measurements
— statistical evaluation of location results

The TM group is characterized by the following information parameters (IP):
— nominal quantity of measurements per session
— measurements received via noisy signals
— marginal errors of receiving station coordinates
— critical values of phase cycle “jumps”
— measurement filtering threshold values

The DTM group is characterized by the following information parameters:
— baseline threshold values
— nominal settings for difference formation
— nominal settings for reduction of measurements
— matching factor for measurement reduction settings and difference formation

Table. F_i reaction description

IP group	V_i	F_i reaction
1	V_{11}	Sessions, the number of measurements of which is less than the nominal value, excluded from processing
	V_{12}	Measurement obtained at $\gamma \leq 70$, excluded from processing
	V_{13}	Receiving stations with coordinate errors exceeding limit values, do not participate in processing
	V_{14}	Phase measurements with critical jump values, excluded from processing
	V_{15}	Measurements not included in filtering thresholds, not included in processing
2	V_{21}	Baselines, the length of which differs from the nominal value, excluded from further decision-making
	V_{22}	Phase differences, the settings of which differ from the nominal value, excluded from processing
	V_{23}	If the current measurement reduction does not match the nominal measurement, the corresponding measurement range is excluded from processing
	V_{24}	If the value of the matching factor for reduction settings and difference formation is less then given, measurements belonging to this range are excluded

Since the parameters of the 3rd group (LD) do not directly influence the decision-making process of the unit in question and are information on the quality of the overall decision, they will not be analyzed any further.

The next stage is the creation of a knowledge production model.

A production model (PM) is a rule-based model for the representation of knowledge in the form of sentences: "if (condition) then (action)". In this case, the main elements of the production model are the information parameters of the 1st and 2nd groups.

For the sake of convenience we will introduce the following notations: 1st group IPs – V_{1i}, 2nd group IPs – V_{2i}.

Then, the conditions for analyzing production model data can be presented in the following form:

A. If $V_C = V_{1i}$ then 0.

B. If $V_C \neq V_{1i}$ then F_{1i},

where V_C is the current IP value, F_{1i} is the reaction to the discrepancy between IP current and control values, which indicate failure, "0" stands for a normal decision, reaction F_i is absent.

The given actions are analogous for the 2nd IP group provided that index "1_i" is changed to "2_i".

The table gives action descriptions (reactions EDS - F_i) for condition B.

The next stage is KB formation.

Production rules are the main part of a KB. They are needed for reaction formation upon the occurrence of non-standard situations during ASC operation. The information base of TIPP KB formation are conditions "A" and "B", as well as the formulations of reactions F_i set forth in the Table. Thus, the TIPP KB consists of two groups of production rules: TM and DTM. They are capable of functioning as a part of ASC BNS EDS jointly with other KBs [2, 4, 5].

By analogy with the described above, example COS KB and BVP KB can be built.

In the light of all of the above and considering the previous developments of the authors in EDS building [2, 4, 5], we will introduce a general diagram of an EDC for ASC BNS software (Figure 5).

Explanatory notes to Figure 5:

ASC SW – ASC software;

COS, TIPP, KB, SP3 – constituent part of ASC (see explanatory notes to Figure 4);

"Program operation analysis" – ASC operation failure memory unit and ASC operation "failure" address identification by the values of diagnostic labels;

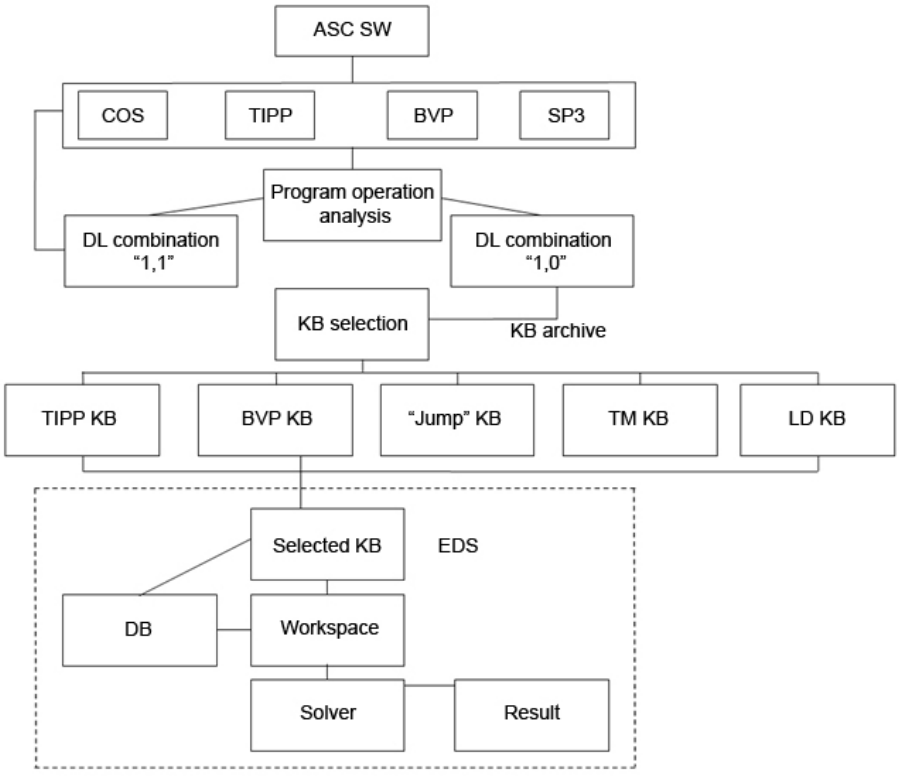

Fig. 5. TIPP EDC general diagram.

DL combination "1, 1" – stands for the normal execution of the current subprogram;

DL combination "1, 0" - stands for solution failure in the current subprogram.

It should be noted that before running a solution program all DLs are set to "1, 0". During normal execution of the subprogram "0" is replaced by "1".

KB selection – the selection of a knowledge base is carried out by "failure" address that is identified by a DL conditional name identifier and subprogram names, the table of which is located in the body of the unit in question.

KB archives:

TIPP KB – pre-processing knowledge base (description is given in this article)

BVP KB – boundary-value problem knowledge base (yet to be developed)

"Jump" KB – phase measurement jump identification and correction knowledge base (developed, set forth in [4])

TM KB – trajectory measurement knowledge base (developed, given in [5])

LD KB – location determination knowledge base (developed, given in [2])

Selected KB – the KB selected from the archives, corresponding to the DL identifier

Standard EDS units: database, workspace, solver with their descriptions provided in [1].

Conclusion

Based on the materials given in the present paper, the following conclusions can be made:

1. The technology for building expert-diagnostic complexes (EDC) for analyzing the operation of an IS that allows to create expert systems for several subject areas (thus, significantly broadening the capabilities for system analysis in comparison with EDS) was developed.

2. The replacement of several EDS by a single complex will allow to considerably speed up IS operation problematic issue solving, as well as reduce time and resources required to develop corresponding software.

3. The proposed procedure for searching for addressing "failures" involving diagnostic labels allows for the prompt identification of the emergency subprogram and response formation for blocking the arisen situation.

4. The technology for building a KB for the "pre-processing" ASC unit that is considered in the paper may be used for forming KBs for other ASC units, thus, noticeably reducing the time required for developing programs analyzing the complex as a whole.

5. The development and implementation of an EDC based on existing EDSs will allow for problems occurring during IS operation to be solved more efficiently.

References

1. Gavrilova T.A., Khoroshevskiy V.F. *Bazy znaniy intellektual'nykh sistem* [Knowledge bases of intellectual systems]. Saint-Petersburg, Izd-vo "Piter", 2000. (in Russian)
2. Betanov V.V., Larin V.K., Pozyaeva Z.A. Baza znaniy dlya programmnogo modulya opredeleniya mestopolozheniya priyemnika [A database for a program module for determination of beacon location]. *Sbornik statey ITMiVT im. Lebedeva* [Proceedings of Lebedev IPMCE]. 2015. (in Russian)
3. Betanov V.V., Larin V.K., Pozyaeva Z.A. K voprosu analiza prichin vozniknoveniya sboev v AKP [Analysis of Error Occurrence Causes in the Hardware-Software Complex]. *Raketno-kosmicheskoe priborostroenie i informatsionnye sistemy* [Rocket-Space Device Engineering and Information Systems]. Moscow, 2015, Vol. 1, No. 3. (in Russian)
4. Betanov V.V., Larin V.K., Pozyaeva Z.A. Prototip ekspertno-diagnosticheskoy sistemy poiska i korrektsii skachkov bezraznostnykh fazovykh izmereniyakh [The Prototype of an Expert Diagnostic System for Cycle Slip Detection and Correction]. *Raketno-kosmicheskoe priborostroenie i informatsionnye sistemy* [Rocket-Space Device Engineering and Information Systems]. Moscow, 2014, Vol. 1, No. 3. (in Russian)
5. Larin V.K. Postroenie prototipa ekspertno-diagnosticheskoy sistemy analiza traektornoy izmeritel'noy informatsii KA [Building of a Prototype of Expert-Diagnostic System for the Analysis of Spacecraft Flight Path Measurement Information]. *Raketno-kosmicheskoe priborostroenie i informatsionnye sistemy* [Rocket-Space Device Engineering and Information Systems]. Moscow, 2017, Vol. 4, No. 1. (in Russian)

ROCKET-SPACE DEVICE ENGINEERING AND INFORMATION SYSTEMS
Vol. 5, Iss. 2, 2018, pp. 68–78

Advanced Technique of Spacecraft Flight Control of One Orbital Constellation Using Intersatellite Radio Links

I.N. Panteleymonov, *panteleymonov_in@spacecorp.ru*
Joint Stock Company "Russian Space Systems", Moscow, Russian Federation

Abstract. The paper is devoted to the problem of boosting the effectiveness of the flight control system for spacecraft in an orbital constellation. The paper offers to apply modern transferring methods using the TCP/IP protocol stack and to employ up-to-date methods of remote control. The concept of creating orbital constellations with spacecraft interrelated by intersatellite radio links will allow one to control the entire orbital constellation in quasi-real time. Thus, the orbital constellation will be a digital network of data transfer, where each spacecraft will function as a relay satellite to transfer control data to any spacecraft, as well as serve as an object to be controlled. The article gives a justification to use the above-mentioned technologies, and graph and network schemes for linkage to control spacecraft flight.

Keywords: communication, spacecraft, orbital constellation, flight control system, radio link, command and measurement station, onboard equipment, antenna system

Introduction

One of the main requirements for spacecraft flight control systems is efficiency. Our country's traditional spacecraft flight control systems permit to pass control data to and from the satellite only when the spacecraft is in the radio coverage zone of one of the ground-based command and measurement complexes (CAMC). Thus, for most of the flight time there is no connection to the spacecraft. One of the solutions to this problem is creating a two-tier configuration of control and communication with the use of three–four geostationary relay satellites (GRS) [1, 2, 3, 4, 5]. With the help of an intersatellite radio link, it is possible to provide one CAMC with a 24-hour link to any satellite (to one, several or all at once). This direction of development of spacecraft (SC) flight control is present-day and advanced, yet it does not lack such limitations as latency. The altitude of geostationary relay satellite orbits (circa 36,000 km) conditions latency. This results in large distances between two orbital slots.

Figure 1 depicts the link configuration (orbital segment) for connecting to a satellite via four GRS.

Figure 2 shows the generalized scheme of the link configuration for connecting to a satellite via three GRS.

1. Topological model of a communication and flight control system for an orbital constellation using intersatellite radio links

1.1 Communication link configuration and network architecture

The orbital arrangement of a single satellite constellation is a certain amount of spacecraft located in several orbital planes (OP) — e.g., satellite constellations for Earth remote sensing (ERS), satellite communication systems in medium-Earth orbit (MEO SCS) or low-Earth orbit relay satellites (LEO RS), satellite navigation systems.

Neighboring spacecraft belonging to one constellation should be connected using intersatellite radio links in such a manner so that every spacecraft is connected to four neighbor satellites in a single or in adjacent OPs. Therefore, the orbital constellation will form a fully connected satellite network for data transmission, where every spacecraft is a satellite router with its own information input/output ports:

– 1 global network port – connection to a command and measurement station (CAMS) – radio data downlink

– 4 global network ports – for retransmitting data to neighbor satellites using intersatellite radio links

– 1 local network port – for transmitting control data to spacecraft's own onboard equipment.

Such architecture is employed on the Iridium satellite system and has the following advantages:

1) it allows to create a flexible network, where adaptive routing protocols can be implemented to build any data transfer route:

a) with a minimum length path for real-time traffic;

b) with optimal throughput with account for onboard relay system (ORS) loading – for broadband traffic;

c) with routes bypassing faulty SC or SC that are located in special areas (e.g., on the dark side of the orbit, in disaster areas and war zones);

2) shows high survivability and adaptivity;

3) allows a single command and measurement station (CAMS) to have real-time access to any of the constellation SC.

The communication link configuration (consisting of six OPs with twelve SC on each OP) for flight control of a space communication system (SCS) orbital constellation (OC) is given in Figure 3. The system uses LEO relay satellites.

Figure 4 shows the orbital constellation flight control network architecture.

1.2 Intersatellite radio link (IRL)

For communication via an IRL, it is sensible to use bands K, Ka, V and Q, and, eventually, switch to transmitting data using frequencies of the optical spectrum.

The use of bands K, Ka, V or Q will permit to do the following [10]:

– reduce the dimensions of antenna-feeder devices (AFD) and UHF-equipment;

– reduce the energy consumption of AFD and UHF-equipment pointing systems;

– broaden bandwidth and increase data rates (from 300 Mbit/s to 1 Gbit/s);

– surmount the limitations of radio link energetics that exist for lower frequency ranges due to high load levels.

Therefore, for communication via IRL using bands K, Ka, V or Q, it is reasonable to employ four pencil beam

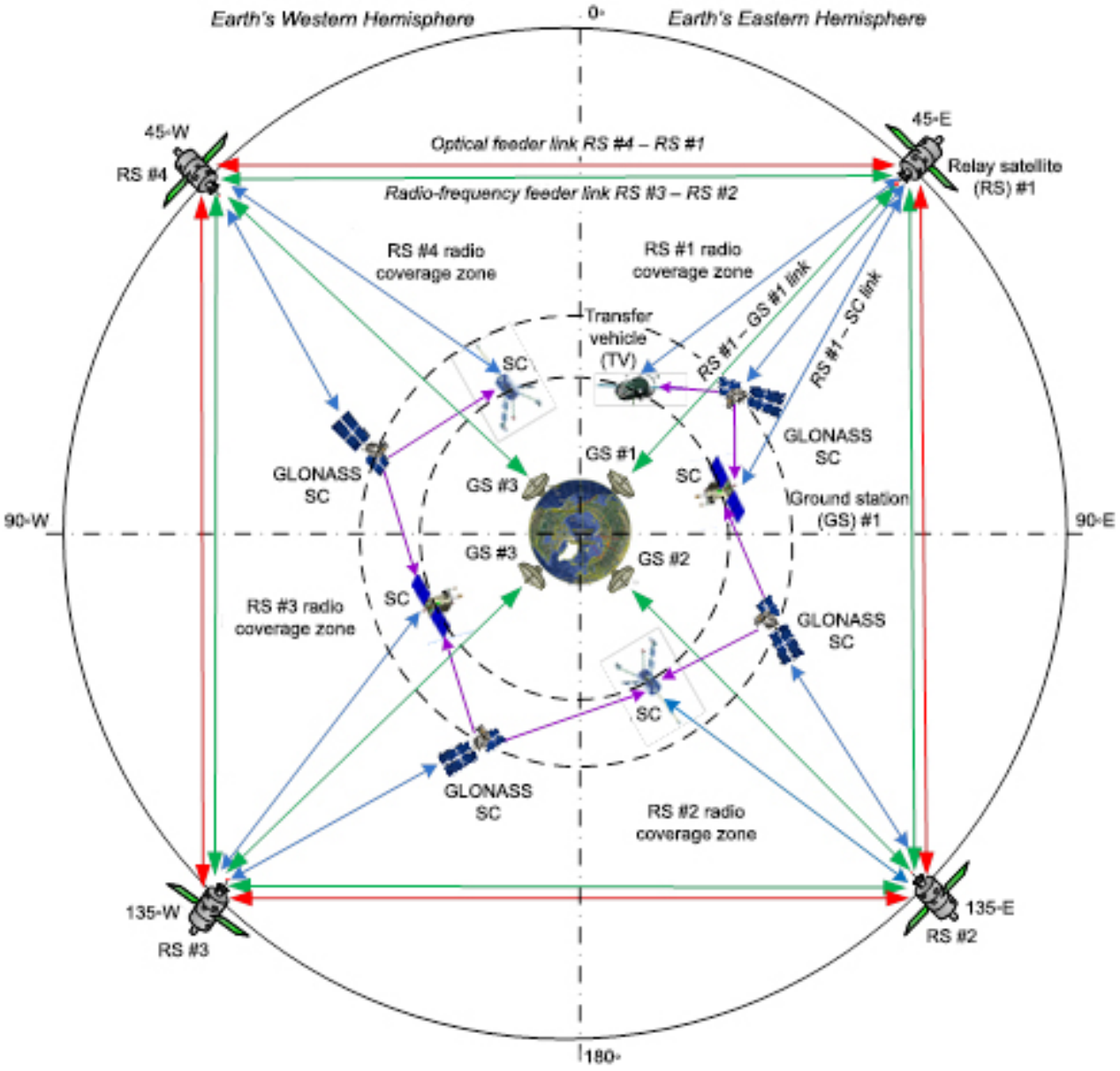

Fig. 1. Link configuration (orbital segment) for connecting to a satellite via four GRS

reflector antenna arrays (AA) with a small diameter (up to 0.3–1 m) [10] located along spacecraft X and Z axes of symmetry.

The use of the optical spectrum will allow us to:

– reduce future AA and UHF-equipment dimensions by four-fold;

– cut down energy consumption of AA and UHF-equipment pointing systems;

– substantially broaden bandwidth and increase data transfer rates (up to 10 GGbit/s);

– lift the existing restrictions of radio link energetics for radio frequency bands.

At first, optical communication systems for IRLs can be used in parallel with radio band communication systems.

Laser receiving-transmitting antenna arrays should be located along axes X and Y of the spacecraft.

1.3 Radio uplink

For communicating via a radio uplink, it is reasonable to use bands Ka, V or Q and, with time, pass on to creating an optical data transmission backup link. Due to the fact that each SC has a sizeable radio coverage

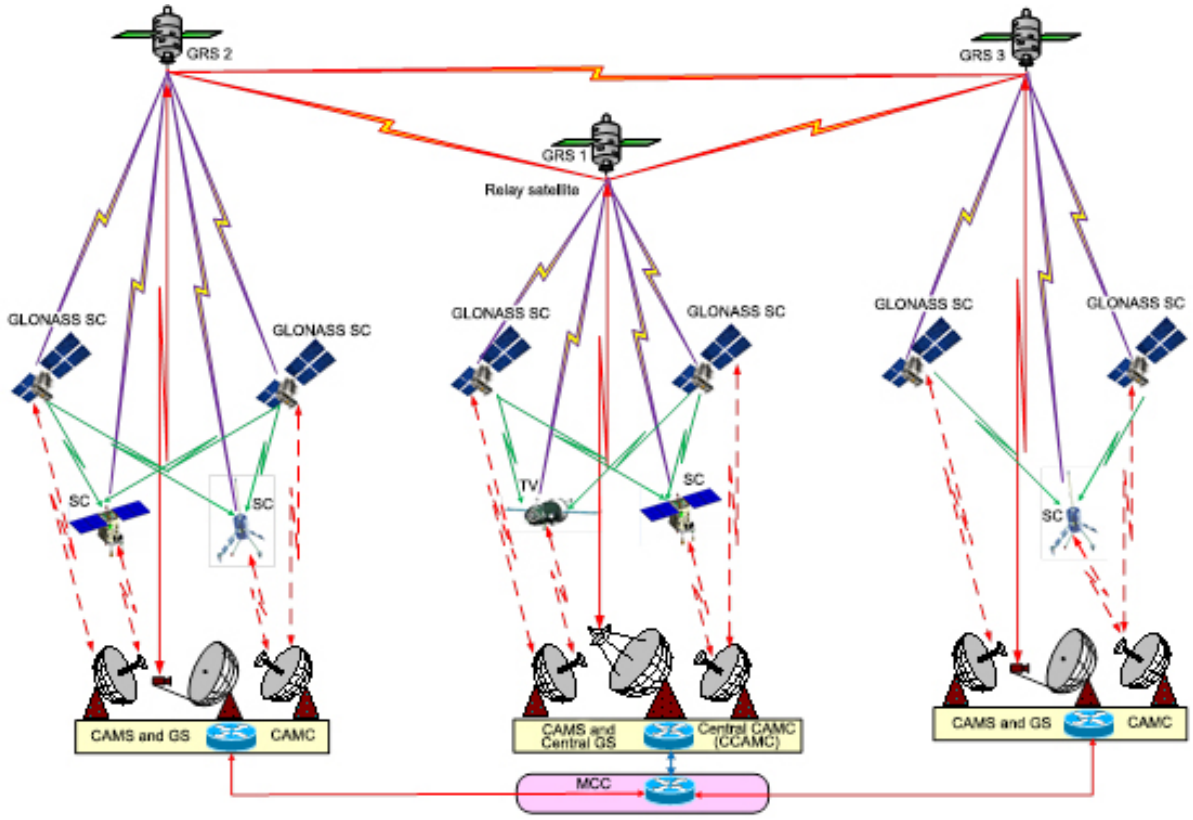

Fig. 2. Generalized scheme of link configuration for satellite connection via GRS

zone (RCZ), it is rare to have zone-wide poor weather conditions influencing atmospheric light transmission. Optical data traffic will be transmitted to a CAMS situated in favorable atmospheric light transmission conditions. Even if optical communication proves to be impossible in the given RCZ, it is possible to connect to CAMSs located in other RCZs via IRL.

Thus, for a radio uplink in the Ka, V or Q bands it is, once again, more sensible to use one pencil beam reflector antenna array of a small diameter (up to 0.3–1 m). Reflector antenna arrays, laser receiving-transmitting antenna arrays should also be Earth-oriented and located along the minus-Y axis of the SC.

1.4 Link organization topological diagram

For a more detailed look at the configuration of CAMS–SC communication, a topological model of the scheme is given below in the form of a graph. The configuration scheme of intersatellite links is depicted in Figure 5. In Figure 4, we see that in the presence of intersatellite links in the SC–SC communication channel the graph becomes fully connected. Full-connectedness indicates that there are several routes from the CAMS-1 initial vertex to the SC-N terminal vertex. This improves communication system flexibility and fault-tolerance. Dynamic routing protocol implementation will be instrumental in fulfilling the tasks of routing and connection set-up in automatic mode [7, 8, 9].

The logical topology of the SC–SC connection scheme is "every satellite with every adjacent satellite", while the logical topology of the SC–CAMS communication is "point-to-point". This statement is the result of the SC connection logic given below.

The topological diagram of MCC–SCS OC SC on LEO via IRL communication configuration is presented in the form of a graph in Figure 5.

1.5 SC and CAMS IP-addressing

Protocol IP v.6 is applied for addressing in an OC network.

The first 48 bits of the IP-address (numbers in the first, second and third octets) are the address of the OC network and are assigned by the international committee to the entire network.

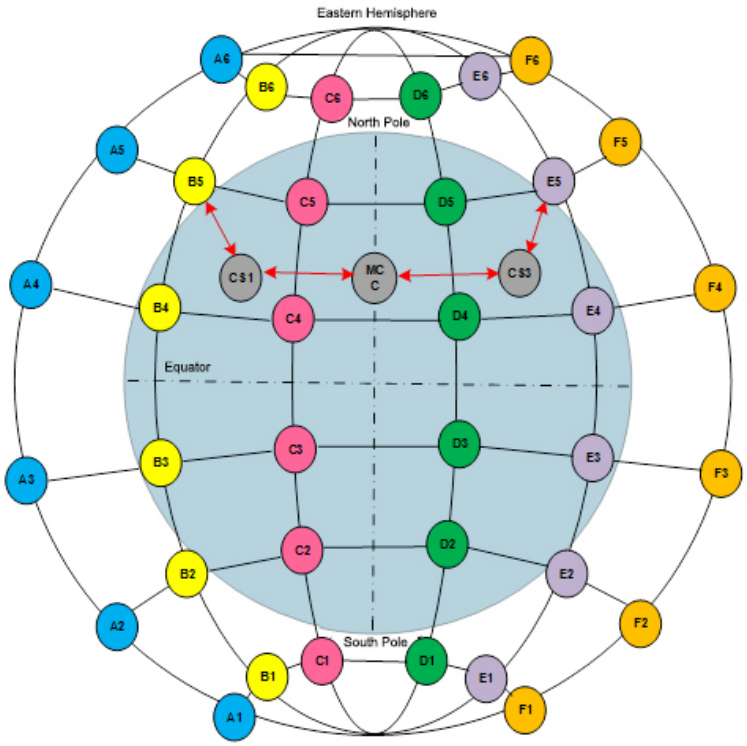

Fig. 3. Communication link configuration for flight control of SCS OC using LEO RS

Notation keys:
MCC – Mission Control Center (MCC)
CS 1 – CS 2 – CAMS #1 – CAMS #3
A1 – A6 – low-Earth orbit SC of OC #1, lettered A
B1 – B6 – low-Earth orbit SC of OC #2, lettered B
C1 – C6 – low-Earth orbit SC of OC #1, lettered C
D1 – D6 – low-Earth orbit SC of OC #1, lettered D
E1 – E6 – low-Earth orbit SC of OC #1, lettered E
F1 – F6 – low-Earth orbit SC of OC #1, lettered F.

The last 48 bits of the IP-address (fourth quartet) are the node address.

The middle 32 bits of the IP-address are the subnet address and are reserved for specific tasks.

For illustrative purposes, the SC and CAMP IP-address structure is given in the form of a table (Table 1).

The first number in the fifth octet represents SC priority; the second number in the fifth octet stands for traffic priority.

The third and fourth numbers of the fifth quartet denote the number of the SC, where the first number defines the orbital plane and the second number denotes the SC number on the orbital plane, e.g., A2.

For specifying the CAMS, the number of the CAMS should be indicated.

Radio link identifiers should be given in the sixth and seventh octets.

The first number in the sixth quartet represents the RL type and takes on the following values:

– 1 – for radio uplink;

– 2 – for intersatellite radio link (IRL);

The second number of the sixth quartet stands for the band, which can either be radio or optical-spectrum frequency:

– number 1 denotes optical spectrum frequency,

– number 2 stands for radio band.

The third number of the sixth quartet represents the number of the AA, the fourth number in the sixth quartet shows the type of tranceiving equipment:

Table 1. SC IP-address structure

1				2				3				4				5				6				7				8			
1	2	3	4	1	2	3	4	1	2	3	4	1	2	3	4	1	2	3	4	1	2	3	4	1	2	3	4	1	2	3	4
OC network												Reserved				Priority		SC #		Radio link								Reserved		SC equipment #	
																SC	Traffic			RL type	Radio/optical	AA #	RCV/XMIT	Equipment unit #	Band	Subband					

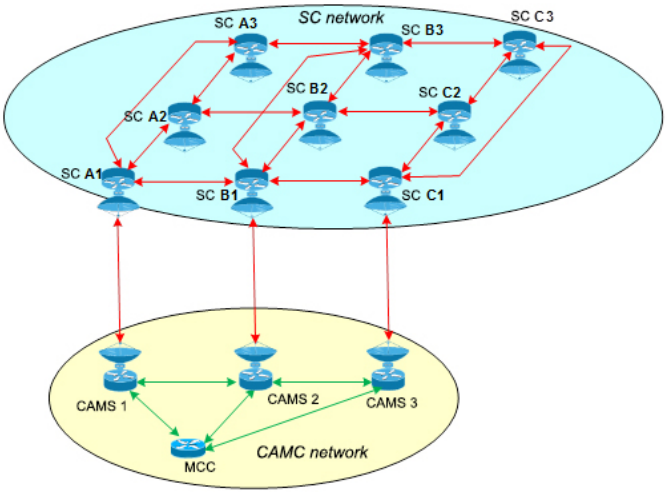

Fig. 4. Orbital constellation flight control network architecture

– number 1 – receiver,

– number 2 – transmitter.

The first number in the seventh quartet stands for the tranceiving equipment unit number; the third and fourth numbers represent the bandwidth and subband, respectively.

The first and second numbers of the eighth octet denote the spacecraft equipment type:

– number 1 – service,

– number 2 – special.

The third and fourth numbers of the eighth octet are the SC equipment number.

2. OC SC flight control system operation algorithms

2.1 The use of IRL for real-time SC flight control

Connected via IRL, orbital constellation SC form a global satellite data communication network. A CAMS, by establishing communication with a single SC in its radio coverage zone, gains access to all of the spacecraft in the constellation. Full-time communication with any SC using one or several CAMS is achievable by switching from one SC to another.

To give an understanding – the implementation of the TCP/IP protocol stack (widely used in present-day local area and distributed communication networks [1, 2]) is considered to be an advanced approach to data processing and transmission (carried out by the onboard equipment (OE) of the spacecraft as well as by ground-based wired and satellite communication networks).

The basic flight control mode is remote access to the central controlling machine (CCM) of the SC OE by means of setting up VPN tunnels connecting the MCC local computer network (LCN) and the spacecraft LCN via wired and intersatellite links [7, 8, 9]. Thus, MCC personnel are provided with remote access from their computers to the SC system control servers (controllers) and are able to promptly manage the OE of the SC by using specific software. A convenient windowed interface displaying images, graphs and tables will simplify the

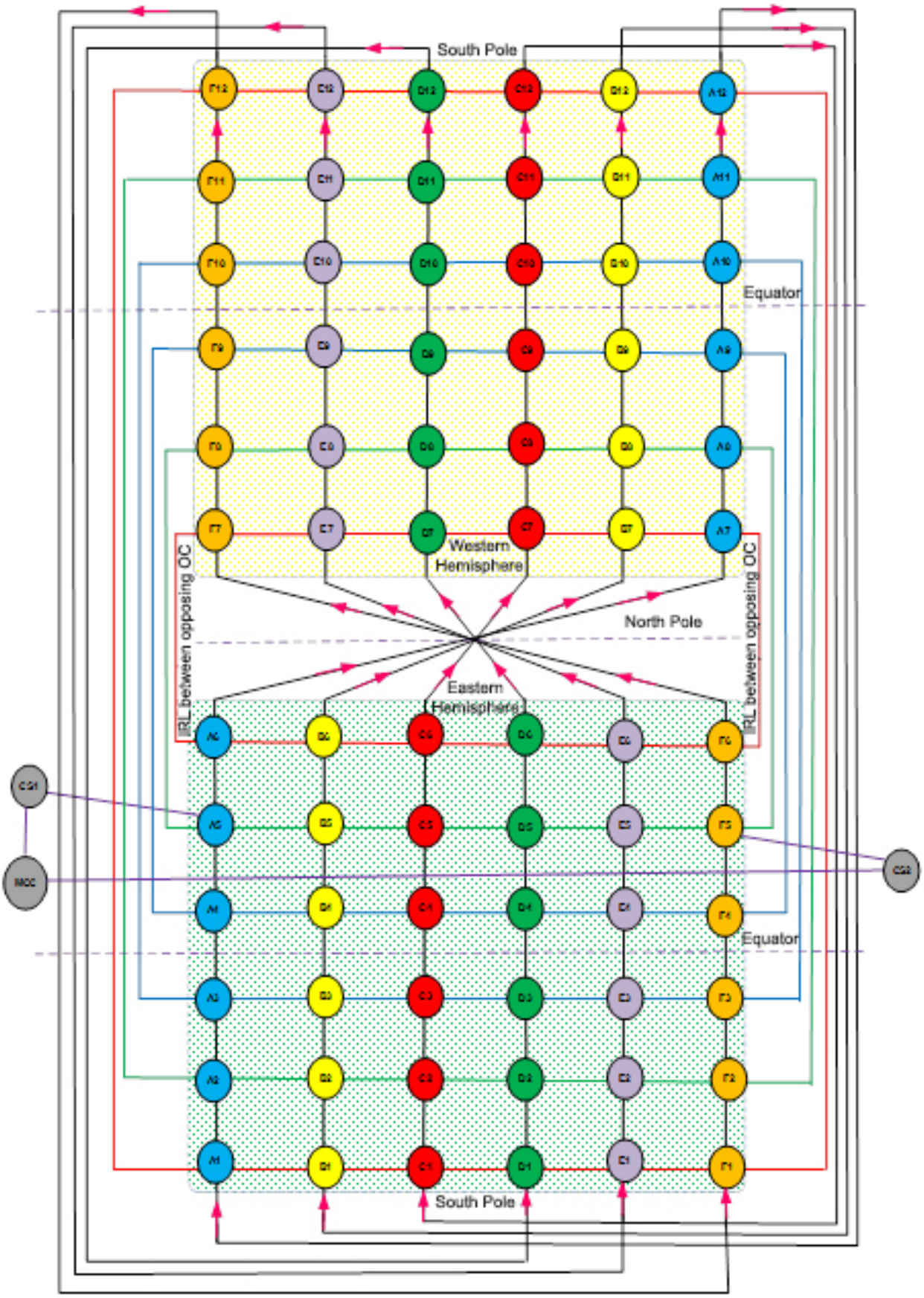

Fig. 5. MCC–SCS OC SC on LEO via IRL communication configuration scheme in the form of a graph

Table 2. Requirements for control data transmission rates through a link

Mode	Access Protocol	
Text	remote control – Telnet protocol implementation	from 9.6 kbit/s
Graphics	WEB-interface access	from 64 kbit/s
	Telemetry data reception, imaging and command – SNMP protocol implementation	from 64 kbit/s
	Desktop access – VNC system and RDP protocol implementation	from 128 – 256 kbit/s
	Telemetry data reception, imaging and command – SCADA system implementation	from 9.6 kbit/s

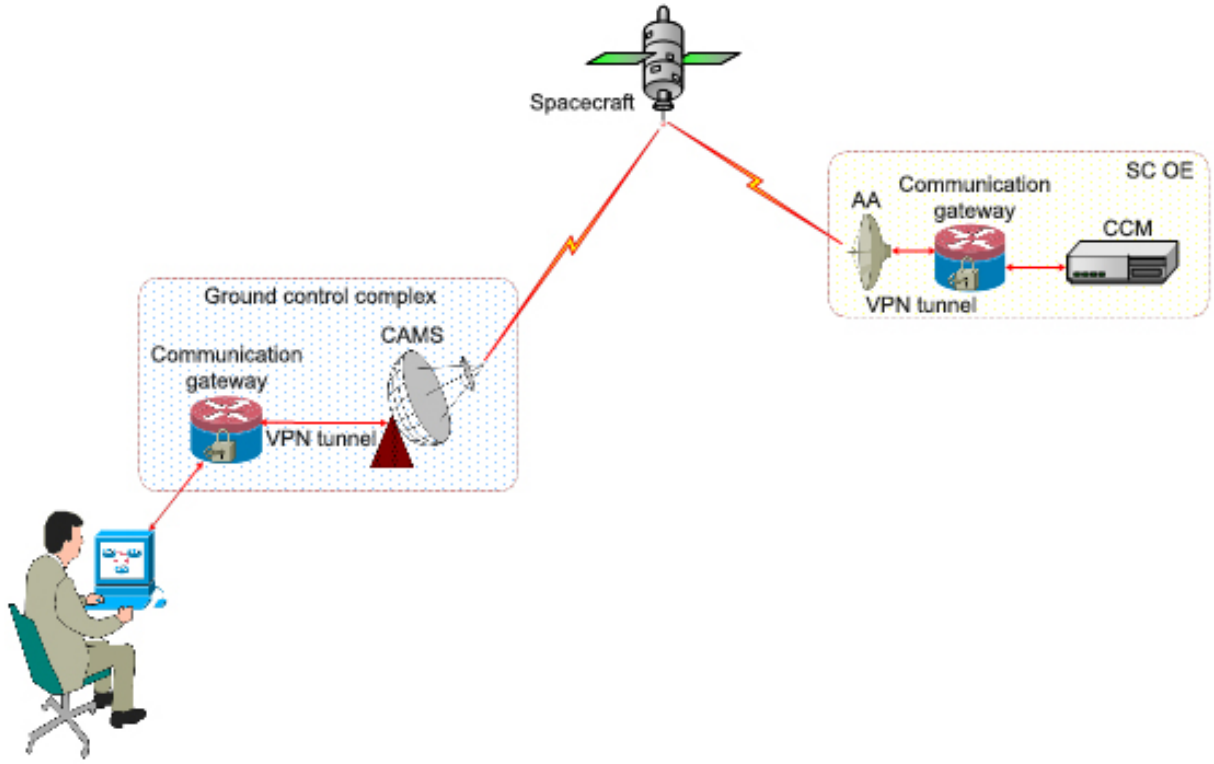

Fig. 6. Logical scheme of MCC operator access to the OE control system.

control system, improve its clearness, ergonomics and controllability along with reducing the decision-making time [1, 2]. The implementation of the TCP/IP protocol stack allows the transmission of flight control channel traffic and SC special purpose equipment data channel traffic through one radio link. For this purpose, the LCN is divided into two VLANs (Virtual Local Area Network): SC service-equipment-VLAN and SC special-purpose-equipment VLAN. With this in mind, the SC special-equipment VLAN is assigned the highest priority [7, 8, 9]. Transmitting overall SC traffic through a single radio link allows us to unify ground receiving stations (gateway stations) and CAMS.

The implementation of the TCP/IP protocol stack permits the usage of the following popular remote access protocols for SC onboard equipment control:

1) for text mode – tenet, SSH;
2) for graphics mode:

a) for WEB-interface access – HTTP protocols;

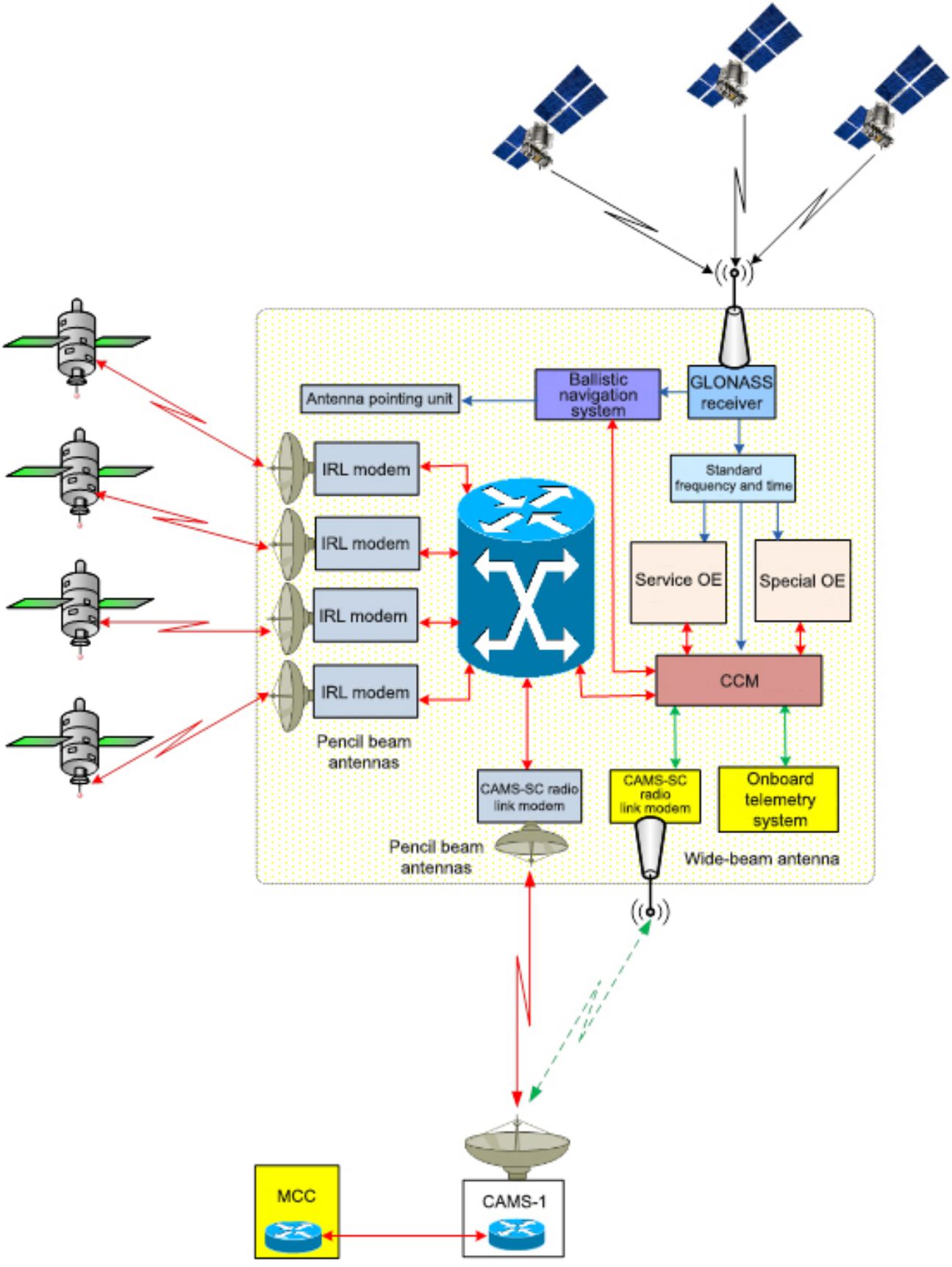

Fig.7. SC OE network architecture.

b) for desktop access – VNC (Virtual Network Computing) system (using the RFB (Remote Frame Buffer)protocol), RDP (Remote Desktop Protocol) – for example, Remmina Remote Desktop Client software;

c) for remote control – such computer network management protocols as SNMP (Simple Network Manager Protocol);

d) for remote control – SCADA (Supervisory Control And Data Acquisition) protocols, implemented for managing ground-based infrastructure elements of critical importance.

When remote access protocols are implemented, the MCC staff computer functions as a client, while the MCC or other SC onboard equipment that has controllers or management servers operates as a server.

The requirements for control data transmission rates through a link are set forth in Table 2.

Based on the information in Table 2, with an actual data transfer rate via ground-satellite uplink or IRL to pencil beam AA ranging from 300 Mbit/s, it is possible to control the entire OC using one or several CAMS.

The logical scheme of MCC operator access to the OE control system is given in Figure 6.

The network architecture of the spacecraft onboard equipment is shown in Figure 7.

2.2. Exploitation of traditional SC flight control technologies in the event of a contingency

The main problem of flight control through IRL is SC orientation accuracy during flight and pencil beam antenna array (AA) pointing accuracy. In the event of a single or multiple SC failure in the orbital constellation a way around them may be found by implementing dynamic routing protocols [7, 8, 9]. Yet, in this case, the issue of gaining access to the SC that lost its orientation arises. Consequently, there are at least two wide-beam AAs located along the spacecraft plus-Y and minus-Y axes of symmetry. They ensure a low-speed emergency radio link with a CAMS.

In the case of contingencies (for example, SC orientation loss), as well as during orbital insertion and disorbit, the CAMS is able to establish a connection with the SC via wide-beam AAs on the SC through the IRL or a ground-satellite uplink. However, the data link transfer rate will be low, ranging from 4.8 to 12 kbit/s. This is why it is necessary to switch to conventional SC flight control system mode – i.e., issuing control commands to the OE and receiving acknowledgement and telemetry data from the OE. Essentially, conventional SC flight control system mode will be a back-up mode for non-standard operating situations and it will help to ensure flight control system fault-tolerance.

Conclusion

The proposed control algorithm possesses the following advantages:

– control flexibility and agility

– flight control system high reliability

– provides a highly ergonomic and modern approach to solving the problems of SC flight control.

The implementation of TCP/IP protocols for computer networking will allow the usage of standard network equipment (custom-made) and standard software for building spacecraft OE along with setting up ground control complexes. This, in its turn, will significantly simplify the flight control system and architecture, and lower the production costs.

The flight control algorithms and architectural solutions for ground control and onboard control systems described in the paper make it possible to create a comprehensive and reliable, dynamic and effective communication and flight control system for SC in a single orbital constellation.

References

1. Panteleymonov I.N. Perspektivnye algoritmy upravleniya poletom kosmicheskogo apparata [Perspective Algorithms for Spacecraft Missions Control]. *Raketno-kosmicheskoe priborostroenie i informatsionnye sistemy* [Rocket-Space Device Engineering and Information Systems]. Moscow, FIZMATLIT, 2014, Vol. 1, No. 4, pp. 57–68. (in Russian)
2. Panteleymonov I. N. Kornienko V.I. Arkhitekturnye resheniya postroeniya bortovoy apparatury kosmicheskogo apparata i perspektivnaya metodika upravleniya poletom kosmiche-skogo apparata s primeneniem setevykh tekhnologiy [Architectural Solutions for Building the On-Board Equipment and Its Advanced Avenue for the Control of the Spacecraft Flight Using Network Technologies]. *Sbornik trudov VII Vserossiyskoy nauchno-tekhnicheskoy konferentsii*

"Aktual'nye problemy raketno-kosmicheskogo priborostroeniya i informatsionnykh tekhnologiy" [Proceedings of the VII All-Russian scientific and technical conference "Current problems of rocket and space device engineering and information technologies]. Moscow, AO "Rossiyskie kosmicheskie sistemy", June 2–4, 2015, 584 p. Ed. Romanov A.A. (in Russian)

3. Bulgakov N.N., Alybin V. G., Krivoshein A.A. Osobennosti postroeniya bortovoy apparatury komandno-izmeritel'noy sistemy kosmicheskogo apparata dlya upravleniya im kak v zone ego radiovidimosti s nazemnoy stantsii, tak i vne ee [Peculiarities of Building an On-Board Equipment of the Command and Measurement System of Spacecraft for Its Control Both in Its Radio Visibility Zone from the Ground Station and Beyond]. *24-ya Mezhdunarodnaya krymskaya konferentsiya "SVCh-tekhnika i telekommunikatsionnye tekhnologii"* [24th International Crimean Conference "Microwave Technology and Telecommunication Technologies]. September 7–13, 2014. Sevastopol, Veber, 2014, Vol. 1, pp. 6–9. (in Russian)
4. Bulgakov N.N., Alybin V. G., Krivoshein A.A. Osobennosti postroeniya dvukhkonturnoy bortovoy apparatury komandno-izmeritel'noy sistemy dlya upravleniya kosmicheskim apparatom na etape ego vyvoda na GSO [Peculiarity of On-Board Equipment of Command-Measuring System and Radio Link for Information Transmission for Spacecraft Intended for Detection of Heavenly Bodies Hazardous to Earth]. *Raketno-kosmicheskoe priborostroenie i informatsionnye sistemy* [Rocket-Space Device Engineering and Information Systems]. Moscow, FIZMATLIT, 2014, Vol. 1, No. 2, pp. 74–80. (in Russian)
5. Limanskaya T.V., Sergeev A.S. Odnopunktnoe upravlenie gruppirovkoy malorazmernykh kosmicheskikh apparatov [Single-station ground control complex for constellation of small-sized spacecraft]. *"Uspekhi sovremennoy radioelektroniki"* [Achievements of Modern Radioelectronics]. Moscow, Radiotekhnika, 2013, No. 1, pp. 78–82. (in Russian)
6. Gushchin V.N. *Osnovy ustroystva kosmicheskikh apparatov*. [Fundamentals of spacecraft design]. Moscow, Mashinostroenie, 2003, 272 p. (in Russian)
7. Wendell O. *Ofitsial'noe rukovodstvo po podgotovke k sertifitsirovannym ekzamenam CCNA ICND1* [Cisco CCNA Routing and Switching ICND2 200-101 Official Cert Guide]. 2nd edition. Moscow, OOO "I.D. Vil'yams", 2009, 672 p. (translated from English). (in Russian)
8. Wendell O. *Ofitsial'noe rukovodstvo po podgotovke k sertifitsirovannym ekzamenam CCNA ICND1* [Cisco CCNA Routing and Switching ICND2 200-101 Official Cert Guide]. 2nd edition. Moscow, OOO "I.D.Vil'yams", 2009, 736 p. (translated from English). (in Russian)
9. Olifer V.G., Olifer N.A. *Komp'yuternye seti. Printsipy, tekhnologii, protokoly* [Computer Networks: Principles, Technologies and Protocols for Network Design]. 3d edition. Saint Petersburg, Piter, 2006, 958 p. (in Russian)
10. Sultanov A.S., Panteleymonov I.N., Kornienko V.I. Otsenka perspektiv primeneniya K/Ka-diapazona v otechestvennykh sistemakh sputnikovoy svyazi [Assessment of the prospects of K/KA-band in domestic satellite communication systems*]. "Novyy universitet". "Tekhnicheskie nauki"* [NEW UNIVERSITY. Technical sciences]. Yoshkar-Ola, 2014, No. 1, pp.10–20. (in Russian).

ROCKET-SPACE DEVICE ENGINEERING AND INFORMATION SYSTEMS
Vol. 5, Iss. 2, 2018, pp. 79–83

Reconfiguration Control of the Ground Automatic Spacecraft Control Complex Based on Neural Network Technologies and AI Elements

D.A. Shevtsov, *postgraduate student, shevtsoff@inbox.ru*
Joint Stock Company "Russian Space Systems", Moscow, Russian Federation

Abstract. The article considers the problematic issues of control of direct reconfiguration of the ground automatic spacecraft control complexes.
It is shown that main properties affecting control of the reconfiguration are controllability and observability. The proposed solution to increase the controllability and observability on base of neural network technologies are given. The necessity of creating a neural network complex to control the reconfiguration of the ground automatic control complex of spacecraft comprising an input, output, and neural network layer with four neural subnetworks having two circuits: controllability and observability is proposed.
The major advantage of this approach is using the application of self-trained algorithms of the control configuration of the ground automatic control complex of spacecraft and a possibility to create a uniform information field of dynamic contours of the control of spacecraft and carrying out the measurements.

Keywords: ground automatic control complex, spacecraft, neural algorithm, artificial intelligence, controllability, observability

Introduction

The ground-based automated spacecraft control complex (GASCC) consists of 14 individual command and measurement complexes (ICMC) and individual measurement stations (IMS) distributed throughout the country and equipped with command, measuring and telemetry means, communications and data transmission equipment, and ground control means. The ground control complex (GCC), the measurement, data collection and processing complex (MDCPC) and the ground-based measurement complex (GMC) for the rocket boosters are formed from the GASCC facilities. That is, GASCC is an integrated structure, designed to produce of a single information and communication environment, which implements the processes of the spacecraft control and telemetry of launches of space technology (ST) products.

The planning of the use of GASCC facilities, as well as the provision of the technological cycle (TC) of spacecraft control and telemetry of the launch of ST products is carried out by the Main Test Space Center of the RF Ministry of Defense named after G.S. Titov (GIKTs).

The spacecraft is controlled in accordance with the technological control cycles (TCC), that determine the sequence, order and time intervals of the spacecraft control operations. Consequently, GASCC should have an architecture that allows the formation of various types of GASCC, and ensure the implementation of their TCC. In turn, the TCC are largely determined by the capabilities of the mission control center (MCC) to establish interaction with technical objects included in the GCC. Enhancing such capabilities is one of the development goals of the GASCC.

At the moment, the GASCC control about several dozen spacecraft, and there is the tendency to expand the orbital constellations, approximately by 3-4 spacecraft per year [1].

Information support for launches of the space technology products (launch vehicles (LV) and rocket boosters (RB)) consists in receiving telemetry information (TMI) by antenna systems (AS), registering it at receiving and recording complexes (RRC), preprocessing TMI and transmitting to centers of information processing and analysis, through closed and open communication channels. The interaction of technical facilities that are part of the MDCPC and GMC, as well as the ability to control their operation, is the determining task for the development of ground-based telemetry tools.

Today, GASCC provides measurements of about 20 launches of various types of space technology products.

Control of directed reconfiguration of GASCC

The functioning of GASCC is determined by a number of important factors:

1) The increasing role of spacecraft orbital constellations (OC) in military conflicts. The wars of the late twentieth and early 21st centuries (in Afghanistan, Iraq, Syria) showed the importance and practical benefit for parties of the conflict of using OC for space reconnaissance and communications, early warning of a rocket attack, and meteorological and navigational support.

In this connection, a targeted enemy air attack on the GASCC objects in order to reduce the effectiveness of the support of the Russian armed forces from space becomes likely [2].

2) Constant increase in the number of constellations and spacecraft in constellations.

3) Trends in the unification of ground-based controls and measurements, as well as an increase in the number of means of collective use.

4) Improvement of the onboard equipment of the spacecraft and launch vehicles.

As a consequence, the role of management and coordination processes by means of GASCC is increasing. It becomes important to consider the operation of the GASCC as a process of dynamic formation of an operative configuration of the SC control facilities (GCC) and measurement facilities (MDCPC and GMC) by conducting a directed systematic reconfiguration. For each configuration of GCC, MDCPC and GMC, its own set of mission control centers (MCC), command and measurement systems (CMS), data lines (satellite, radio relay, terrestrial fiber optic, etc.) and telemetry equipment is provided.

The GASCC performs about 1000 communication sessions with spacecraft per day during its normal operation. During emergency situations, and during direct combat operations, the requirement for the time of the GASCC reconfiguration (GMC, MDCPC and GCC) increases and reaches 5–10 minutes. In this connection, a significant increase in the level of observability and controllability of the GASCC is required.

GASCC becomes an integrated multi-functional ground-space structure with a single information space, and at this stage it is advisable to move away from the concept of a static control and measurement

loop and introduce the concept of dynamic control and measurement loop [3], and the GASCC will form such dynamic loops close to real time.

Controllability and observability of the GASCC facilities will become a defining characteristic, which will require expanding the capabilities of reconfiguration control using the GASCC and measurement facilities.

The task of increasing the observability of the GASCC consists in determination of the initial state of the system, namely:

- the state of technical means of the GASCC (maintenance, serviceability, currently engaged facilities);
- the presence of the necessary number of personnel to perform the tasks required to operate the GASCC;
- the state of data transmission systems (utilization of communication lines, maintenance, serviceability, currently engaged facilities).

The task of increasing the controllability of the GASCC lies is an increase in the capabilities of changing the operation states of the GASCC.

If the GASCC is maximally observable and controllable, then it is possible to create a control system that will allow to carry out a directed reconfiguration.

Thus, the directed reconfiguration of the GASCC becomes a multifactorial, intellectual task of controlling a complex technical object and requires an innovative approach to its solution.

The most promising information technology for solving multifactor tasks in complex technical systems is neural network programming and the use of artificial intelligence. The first studies of artificial intelligence were carried out with the advent of computers in the mid-twentieth century. The development of computing power, data transmission facilities, and communication lines over the past 10 years has resulted in a leap in the development of these technologies and in their application in engineering.

The use of a developed neural network complex will allow a number of improvements to be made in the methods of control of the directed reconfiguration of the GASCC. Its main difference from the ordinary software algorithms is that the task set will be solved not by direct programming, but by self-learning of a neural network component with feedback. This unique process allows minimizing the need for a direct human involvement in the formation of an operational configuration of the GASCC, and will also allow a solution to be developed based on the external data obtained by a neural network complex under rapidly changing conditions [4, 5].

The proposed neural network structure of the complex for reconfiguration of the GASCC and measurements is presented in Figure 1.

It is important to note that it is possible to distinguish two functional circuits in the structure of the neural network complex: the observability circuit and the controllability circuit. With the help of the neural network components introduced, these functional units directly solve the problem of increasing the level of observability and controllability.

The problem to be solved by the entire neural network complex is to find the optimal solution for the selection of the GASCC and measurements configuration by increasing the observability and controllability.

During the operation of GASCC, input data is formed as formalized information:

- on the technical condition of the GASCC and measurements (complex for monitoring the technical condition);
- on the analysis of the current situation (complex for situation assessment);
- on the analysis of tasks for spacecraft control and measurements (complex of analysis of tasks of spacecraft control and measurement).

The output data of the complex for monitoring of technical condition contains information about the integrity of the equipment and routine maintenance, spacecraft control and measurement operations; information about the number of personnel available to operate the GASCC equipment.

From the MCC and the ICMC command posts the complex for assessing the current situation receives information on the situation: maintaining daily activities, improving combat readiness or transition to a threatened period. This data is the output.

The task analysis complex derives data from the short-term, medium-term, long-term plans of the utilization of facilities, obtained from the mission control center and command posts.

Formed and formalized information is transmitted to the neural network component of the complex, which consists of four interconnected neural networks:

- technical means of the GASCC and measurements;
- synaptic weights and connections;
- conflict analysis;
- selection of means of the GASCC and measurements.

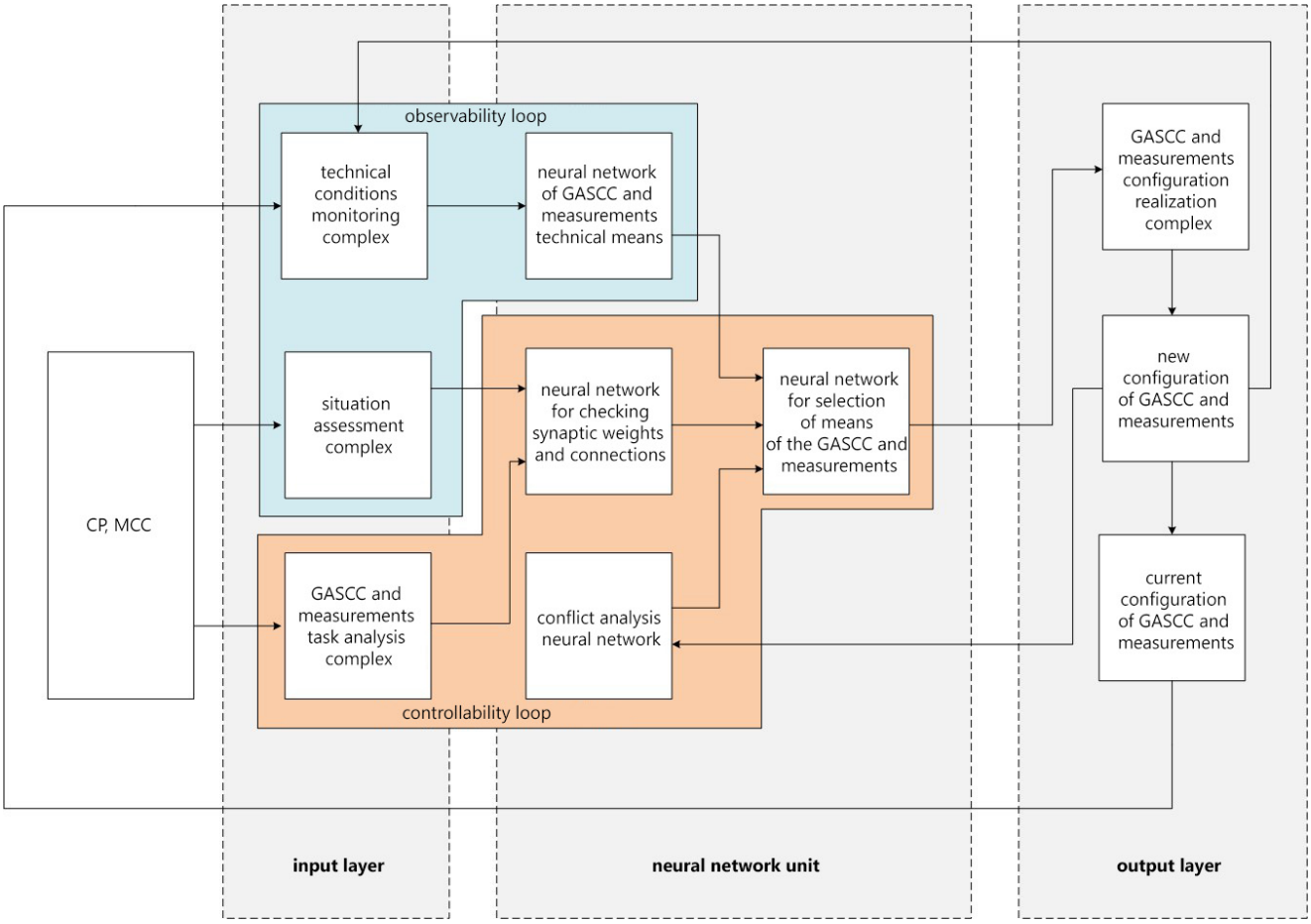

Fig. 1. Neural network structure of the control complex for reconfiguration of GASCC and measurements

The neural network monitoring the technical means of the GASCC and measurements receives information from the monitoring complex on the composition of the means ready for operation.

The neural network for synaptic weights and connections receives the assessment of the current situation from the complex and, depending on what period of the situation, the weight coefficients of connections (synapses) are determined.

The neural network of the conflict analysis is connected with the knowledge base of the output layer and checks the obtained results for conflictlessness in order to eliminate duplication of technical means of GASCC in various tasks of spacecraft control and measurements.

The data obtained as a result of the operation of the three networks mentioned above is transmitted to the neural network of means selection, where decision making takes place and in a formalized form is transmitted to the GASCC configuration and measurement implementation complex, which is the executive body of the neurocomplex output layer and directly controls the configuration of NACU KA hardware.

The output layer contains a new configuration of GASCC and measurements according to the problem being solved, the current situation and the state of technical facilities.

The structure of information obtained as a result of the work of the neural network is:

- the knowledge base of the neural network, which is used to provide feedback (recurrent structure), machine learning, creating templates and rules for further work;
- the visual component output to the display media.

Conclusion

Thus, the analysis of the current state of GASCC showed the need to manage the reconfiguration of GASCC in order to obtain a more flexible and dynamic structure in rapidly changing conditions.

As a result of the study, a variant was proposed for using the neural network complex for the task of controlling the reconfiguration of GASCC. This solution will provide a universal tool for creating dynamic spacecraft control loops and carrying out measurements close to real time, and also due to the recurrent structure of the neural network, will allow the system to learn and make decisions that are not obvious to humans based on the accumulated knowledge.

References

1. *Federal'naya kosmicheskaya programma 2016–2025* [Federal space program 2016–2025]. Moscow, Goskorporatsiya Roskosmos. (in Russian)
2. *Predlozheniya po obsecheniyu ustoychivosti upravleniya KA v osobykh usloviyakh. Nauchno-tekhnicheskiy otchet* [Offers for providing stability of spacecraft control in any conditions. Technological report]. Korolev, AO "VIKor". 2016, 50 **p**. (in Russian)
3. Okhtilev M.Yu., Sokolov B.V., Yusupov R.M. *Intellektual'nye tekhnologii monitoringa i upravleniya strukturnoy dinamikoy slozhnykh tekhnicheskikh ob"ektov* [Intellectual technologies of monitoring and control of a structured dynamics of complicated technical objects]. Moscow, Nauka, 2006, 410 **p**. (in Russian)
4. Callan R. *Neyronnye seti: kratkiy spravochnik* [The Essence of Neural Networks]. Moscow, Izdatel'skiy dom "Vil'yams". 2017, 279 p. (in Russian) (translated from English)
5. Haykin S. *Neyronnye seti. Polnyy kurs* [Neural networks. A Comprehensive Foundation]. Second edition, edited. Moscow, Izdatel'skiy dom "Vil'yams". 2006, 1104 p. (in Russian) (translated from English)

ROCKET-SPACE DEVICE ENGINEERING AND INFORMATION SYSTEMS
Vol. 5, Iss. 2, 2018, pp. 84–92

SOLID-STATE ELECTRONICS, RADIO ELECTRONIC COMPONENTS, MICRO- AND NANOELECTRONICS, QUANTUM EFFECT DEVICES

Video Telemetric Control of Industrial Products

D.I. Klimov, *contact@spacecorp.ru*
Joint Stock Company "Russian Space Systems", Moscow, Russian Federation

Abstract. The principles of creating a system of contactless measurement of the physical quantities and parameters characterizing impact of external factors on industrial products are considered. Introduced are the concepts and definitions concerning remote contactless measurement of parameters. The article describes a variant of the system with a temperature measurement unit, a contactless method of temperature measurement by means of video cameras based on pyrometric methods and the theory of thermal radiation taking into account the integral coefficient of thermal radiation of a gray body. The temperature dependences of the integral coefficient of thermal radiation for some metals are given. After processing video information by the spectral method, the calculation of the integral value of temperature in the controlled zones under examination by a color spectrum or brightness is carried out. Provided is the analysis of the existing algorithms of compression of video information. Application requirements and the principles of creating a system with a wide-range temperature measurement unit and its distinctive features are formulated.

Keywords: video telemetry, thermo-video telemetry, telemetry, power-loaded areas, temperature, external influencing factors, measurement, video image

Definitions and concepts

Telemetry (telemeasurement) — a set of technologies for carrying out remote contactless measurements and collecting information to be later passed on to the operator or users; a constituent part of telemechanics. The term comes from the Greek roots *tele* — "remote" and *metron* —"measurement". Even though the term, in most cases, is used in reference to methods of remote data transmission (for example, via radio or infrared radiation), it also characterizes the process of transmitting data with the help of other means of mass communication, such as telephone and computer networks, fiber-optic or other wired communications [1].

Either telemetry sensors with a special embedded communication module or a remote terminal unit (telemetry system) to which ordinary sensors are connected are generally used for gathering information. Yet, for industrial products there are areas or objects the average temperature in standard operating mode of which exceeds 1200-1500 K, as well as areas with increased radiation, humidity and mechanical loading. Such areas are referred to as "power-loaded areas".

Power-loaded areas in industrial products – areas (determined by an a priori estimate) with a heightened probability of damage (product component failure) caused by radiation and/or thermal radiation.

A contact method of temperature measurement by using temperature sensors is not applicable due to the substantial radiation and thermal radiation emissions and to the impact of mechanical overloads (large energy release in an enclosed space as a whole). The aforementioned power-loaded areas are prone to contingencies and emergencies.

For this reason, a remote contactless method using video cameras for measuring the impact of external factors on industrial products – video telemetry– is proposed.

Video telemetry – a remote contactless method of measuring parameter values (levels of external factor impact on industrial products) with the help of video cameras that consists in converging video images into measurement signals with the subsequent imaging of value information for the parameters of interest.

Design concept of video telemetry systems

Let us consider the video telemetry system functional diagram. Parameters subject to telemetry are measured by processing video images of the object and by measuring the physical quantities that characterize the impact of external factors on industrial products. Figure 1 gives the generalized functional diagram of the video telemetry system inclusive of measurement and display equipment.

The video image in the form of electric signals or digital stream (video stream) from video cameras is sent to the video information processing unit where parameters being telemetered are calculated (only variant (a)); further processing and compression of information as well as preparation for targeted information transmission (in this case, video stream) through a radio link is carried out. The signal is transmitted through the link to the receiver station and afterwards – to the video information display equipment, where physical quantities that characterize factors affecting industrial products (only variant (b)) are also calculated.

The received information flow is demodulated and processed in the video information reception unit. Processed information is transferred to the parameter calculation and display unit with a polling rate of approximately 1…3 fps.

The video control system design is suggested to be as shown in Figure 1. The component functions are set forth in Table 1.

Video telemetry system for temperature measurement

Temperature is the principal external influencing factor that affects the parameters of the constructional material. **Temperature** is a scalar physical quantity that approximately characterizes the average kinetic energy of particles of a macroscopic system in the state of thermodynamic equilibrium per one degree of freedom [2].

Thermo-video telemetry – a method of measuring the temperature of industrial products with the help of video cameras and subsequent information processing.

The essence of the method is in obtaining information about temperature and its distribution over the surface of the object in question from video cameras equipped with photorecorders, which are used to convert the video image into a digital signal [3]. After video information is processed (in the range from infrared to ultraviolet

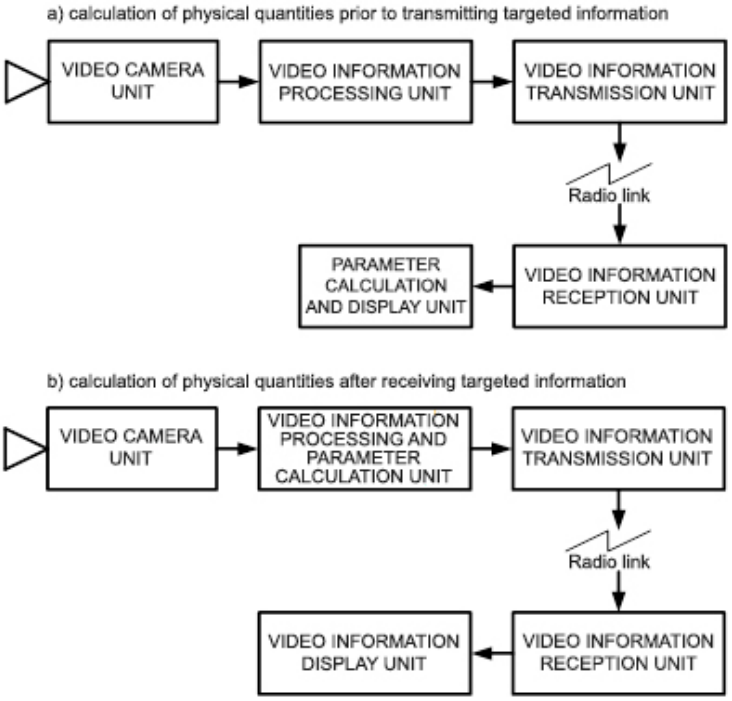

Fig. 1. Generalized functional diagram of a video telemetry system

radiation), pyrometric methods are implemented to calculate the integral value of temperature[1] in the controlled zones under examination by a color spectrum [4] or brightness[2] — a method based on Planck's law and the principles of spectral and brightness pyrometry [5 - 7].

In accordance with (6.10) with account for (6.11), we shall graph ε(T) for the most common types of metals (Figure 2), prior to this we shall tabulate coefficients a and ρ_0 (Table 2) [5].

Thus, adequate surface temperature measurement using pyrometers is conditioned by the correct choice of a temperature measurement range and spectral range in which it is possible to measure the temperature of this type of objects. The emissive ability of every material in accordance with (6.10) depends on the temperature and concurrently, taking (1.3) into account, it can change for the same material in different areas of the spectrum [9].

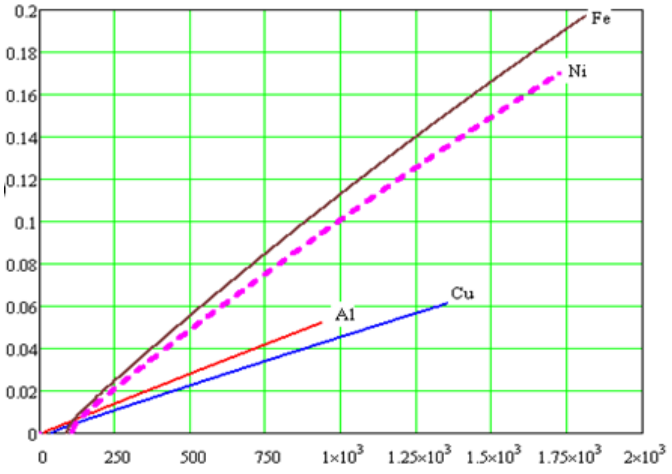

Fig. 2. ε(T) graphs for different types of metals

[1] When calculating temperature parameters, it is necessary to take into account the full radiation power of a black body at temperature T (**radiation temperature T_r of a body** – the temperature of an absolutely black body at which its radiant exitance R is equal to the radiant exitance R_m of the given body in a wide range of wavelengths) over the whole range from $\lambda = 0$ *to* $\lambda = \infty$, determined by the Stefan–Boltzmann law [8]:

$$R_0(T)=\sigma_0 T^4 \quad (1.1)$$

where $\sigma_0 = 5.6696 \times 10^{-8} \frac{W}{m^2 K^4}$ is a given constant.

Seeing that the physical law expressed by equation (1.1) concerns measuring the temperature of an absolutely black body, the measured energy of a real gray body is determined by equation (1.1) with an accuracy of ε, known as the **integral (or full) coefficient of thermal radiation**:

$$\varepsilon = \frac{R_0(T)}{\sigma_0 T_a^4} \quad (1.2)$$

This quantity is the ratio of the radiation energy emitted by the material at temperature T to the radiation energy emitted by a black body at the same temperature T, whence it follows that:

$$T_a = {}^{T}/_{\sqrt[4]{\varepsilon}} \quad (1.3)$$

[2] **Brightness temperature T_b of a body** – the temperature of an absolutely black body at which its spectral exitance f(λ,T) for a particular wavelength is equal to the spectral exitance r(λ,T) of the given body for the same wavelength.

Table 1. Functionality of video telemetry system components

Component	Functions
Video camera unit	- video shooting of observed object, - conversion of video image to electric signal, - conversion of video signal to digital stream,* - information stream compression* - video stream transmission through a unified interface.*
Video information processing unit	- video stream reception through a unified interface,** - temporary video stream storage, - software-based physical quantity calculation using already developed methodologies in accordance with calibration results,*** - application of anti-jamming coding to information stream (encoding), - acquisition of telemetry information regarding the functional state (system constituent performance capability), - preparation for transmission of targeted data via radio link.
Video information transmission unit	- targeted information stream modulation, - amplification of modulated information stream, - transfer of information stream to the required frequency range, - information transmission through a high-frequency link to antenna-feeder device.
Video information reception unit	- target information reception via a radio link, - information stream demodulation.
Parameter calculation and display unit	- target information decoding, - acquisition of raw data (video images or information about physical quantities),**** - numeric representation of the measured parameters using required units of measurement (e.g., SI system), - visual or graphical display of measured parameters.
* - function realization is possible in the video information processing unit ** - in the event of video signal digitization in the video camera unit *** - function realization is allowed in the parameter calculation and display unit **** - reverse operation of preparation for targeted data transmission via radio link	

Table 2. Thermal properties of some metals

Metal	Resistivity of metal at 20°C (ρ_0, ohm-cm)	Coefficient of thermal variation of resistivity (α)	Melting temperature, (K)
Aluminum	2.82×10^{-6}	3.6×10^{-3}	933
Copper	1.72×10^{-6}	4.0×10^{-3}	1356
Iron	9.80×10^{-6}	5.0×10^{-3}	1808
Nickel	7.24×10^{-6}	5.4×10^{-3}	1726

For defining the gray body temperature it is sufficient to measure the power Y(λ,T) emitted by the unit surface area of the body in a fairly narrow spectral interval (proportional r(λ,T)) for two different waves [5]. The ratio of Y(λ,T) for two wavelengths is equal to the ratio of the dependences f(λ,T) for these waves, expressed by the ratio:

$$\frac{Y(\lambda_1,T)}{Y(\lambda_2,T)} = \frac{r(\lambda_1,T)}{r(\lambda_2,T)} = \frac{f(\lambda_1,T)}{f(\lambda_2,T)} \quad (1)$$

The temperature T can be derived mathematically from the given equality. The temperature thus obtained is referred to as "color temperature". The color temperature of a body, determined by formula (1), will be equal to the actual temperature, assuming that the monochromatic absorption coefficient does not strongly depend on the wavelength. Otherwise, the concept of color temperature loses its meaning. According to [2, 4], "the color temperature of a gray body coincides with the actual temperature, and can also be calculated from Wien›s displacement law".

The more widely used pyrometers for controlling industrial product surface temperatures work in the spectral sensitivity range of 7 to 14 (up to 18) μm. Nonetheless, pyrometers are mostly based on the principle of measuring total radiation [10].

The estimation accuracy of the measured object surface temperature with the application of total-radiation pyrometers depends on the correct definition of ε.

In this case, temperature measurement in controlled areas is carried according to color spectrum[3] [4] or brightness, based on Planck's law and the principles of spectral and brightness pyrometry.

Thermo-video systems based on the pyrometric method[4] of temperature measurement are applicable for object thermal control. With their help, it is possible to control deterioration of thermal protection and mechanical damage to the structure.

Hot bodies with temperatures exceeding 250–300°C are of particular interest within the framework of the present paper. Temperature values [4, 11] given in Table 3 call for special attention from the operator during temperature monitoring after video information processing because breakage of various materials occurs in the vicinity of the given temperatures.

With the purpose of expanding the temperature range for temperature monitoring in the chosen image field, cameras should be installed in twos pointing at one field-of-view in a protective heat-insulated enclosure [12]. One camera will be equipped with a virtual phase charge-coupled device and the other – with an infrared charge-coupled device. Both cameras should be set to the same field-of-view and should simultaneously send the received information streams to the information display equipment. Since photorecorders have differing resolutions, equal fields-of-view for two cameras can be provided by installing lenses with different pupil diameters of objective lenses and different focal lengths.

Considering the use of a wide spectral band, the video camera should be equipped with special lenses and photorecorder devices for data reception in the infrared, visible and ultraviolet bands. Such lenses are: a "sapphire window" (for the wide range 0.2 -6.0 μm), quartz glass (for near ultraviolet band, visible and near infrared bands 0.2-2.2 μm), optical silicon (for near and middle infrared band 1.2-6.0 μm), germanium (for middle infrared band 1.2-15.0 μm) [10]. As for photo recorders, for the 0.2-1.0 μm band virtual phase charge-coupled devices should be used; for the 1.2-5.3 μm band – infrared charge-coupled devices with thermoelectric coolers (Peltier) [15], for the 8-14 μm band – microbolometer modules [10].

Table 3. Melting and deformation temperatures of some types of metals

Material	Melting point, K	Temperature of irreversible changes in the crystal lattice, K
Aluminum	933	723
Titanium	1933±20	1156
Iron	1812	1042
Tungsten	3695	1473
Steel (mean values)	1720…1795	1258
Nickel	1726	956

[3] According to [4], **spectral exitance r(l,**T)=dW/dl is the amount of energy emitted by the body's surface unit per unit of time at one unit wavelength (near the wavelength of interest l). In other words, the quantity is numerically equal to the ratio of energy dW emitted by a surface unit per unit of time in a narrow wavelength interval from l to l+dl, to the width of the interval. It depends on the body temperature, wavelength, as well as on the nature and state of the surface of the emitting body. The SI system r(l, T) base unit is [W/m^3].

Radiant exitance R(T) is related to the spectral exitance r(l, T) the following way:

$$R(T) = \int_0^\infty r(\lambda, T)\, d\lambda, \text{ [W/m}^2\text{]}, \quad (3.4)$$

According to [5], **the color temperature T_c of a body** is the temperature of an absolutely black body at which the relative distributions of spectral exitance of a black body and of the body in question are as close as possible in the visible region of the spectrum.

The color temperature is the radiation temperature of separate chemical elements; it is displayed on the spectrograph in the form of individual spectral lines emitting at a particular frequency (wavelength).

The method of spectral (color) pyrometry is based on the Planck distribution in the wavelength range, namely [3]:

$$Y = \frac{2\pi hc^2}{\lambda^5} * \frac{1}{e^{\frac{hc}{kT\lambda}} - 1} * \varepsilon_\lambda, \quad (3.5)$$

where k = 1.8×10^{-23} J/K is Boltzmann's constant, h = 6.63×10^{-34} Js is Planck's constant, c = 3×10^8 m/s is the speed of light, T is temperature (K), λ is wavelength (m), ε_λ is the integral coefficient of thermal radiation.

[4] The spectral pyrometer is calibrated against the radiation of an absolutely black body (on the same wavelength) in degrees of brightness temperature T_{ij}, related to the thermodynamic scale by the ratio [13].

$$\frac{1}{T_{aij}} - \frac{1}{T_{ij}} = \frac{\lambda_{ij}}{1.438} \ln \varepsilon_{\lambda ij}, \quad (4.6)$$

where T_{a_ij} is the actual (calibrated) average temperature in the controlled zone of the image field,

$$T_{a\_ij} = \frac{1.438 T_{ij}}{1.438 + \lambda_{ij} T_{ij} \ln \varepsilon_{\lambda ij}} \quad (4.7)$$

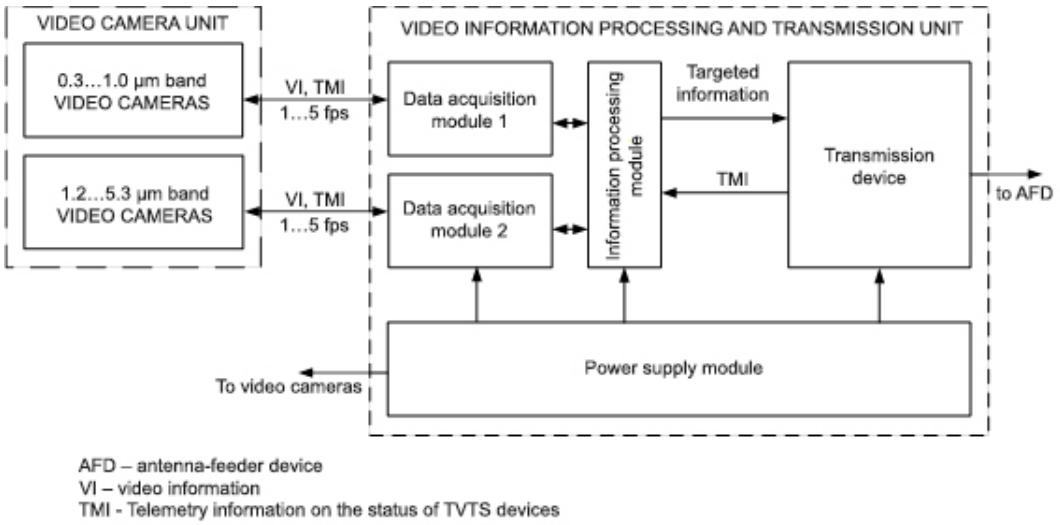

Fig.3. Temperature measuring video telemetry system functional diagram

For measuring temperatures of power-loaded areas of industrial products the 500…3000 K [4, 9] temperature range should be chosen. However, in areas with high radiation under the influence of ionizing flux, the spectral components of the thermal radiation of materials can radiate both in the visible and, even, in the ultraviolet region. Various materials (for example, metals), depending on the chemical properties and atom structure, have their own radiation spectrum and it can be located in different parts of the bands in question. In addition to this, as the temperature rises the spectral density of radiation shifts from the infrared band towards the ultraviolet band. For this reason, to ensure higher accuracy and thermal control efficiency, the maximum measured temperature should be increased up to 9500 K and, in doing that, the 0.3–5.3 μm band will be used.

Figure 3 depicts a functional diagram of the transmitting part of the temperature measuring telemetry system. It includes two types of video cameras that differ in spectral bands, photorecorder resolution and lens materials. Data acquisition modules receive information streams (or video signals), carry out their digitalization (if needed) and provide temporary video information storage.

Before transmitting information through a wireless channel, it is necessary to ensure anti-jamming coding and compression that are carried out by the video information processing module. Figure 4 gives an overview of the video information compression algorithms [7, 14].

Moving on to the receiving part of the video telemetry system for temperature measurement — the functional diagram of the temperature measurement unit is given in Figure 4. Video information in the information display equipment is sent to a packet decoding device with a frequency of 1...3 fps and in output we receive the brightness value. The image field in question is divided into zones. The total amount of dots in an image field defined by the resolution of the photorecorder is divided into zones with an area ranging between 5×5 pixels and 20×20 pixels. The choice of the required zone for temperature monitoring is made either by the operator or in automatic mode upon introduction of a threshold temperature when programming the processor of the video telemetry system. The information about the brightness or chromaticity of the object (usually gray)[5])

[5] All bodies in nature partially reflect the radiation falling on their surface; therefore, they do not belong to absolutely black bodies.

If the monochromatic absorption coefficient of a body is the same for all wavelengths and is less than one (α(λ,T) = αT = const < 1), then such a body is referred to as gray. According to [4], "to determine the absorption capacity of bodies relative to electromagnetic waves of a certain wavelength the concept of the monochromatic absorption coefficient is introduced – the ratio of the monochromatic wave energy absorbed by the body surface to the energy magnitude of the incident monochromatic wave:

$$\alpha(\lambda,T) = \frac{W_{abs}(\lambda,T)}{W_{inc}(\lambda,T)} \quad (5.8)$$

The quantity α(λ,T) can take on values from 0 to1. Kirchhoff demonstrated that for all bodies, regardless of their nature, the ratio of spectral exitance to the monochromatic absorption coefficient is the same universal function of wavelength and temperature f(λ,T) as the spectral exitance of an absolutely black body:

$$\frac{r(\lambda,T)}{\alpha(\lambda,T)} = f(\lambda,T) \quad (5.9)$$

Table 4. Comparative analysis of video information compression algorithms

Parameter	MPEG-2	JPEG2000	H.264
Transform	Discreet cosine transform	Discreet wavelet transform	Hadamard transform and integral discreet cosine transform
Video processing	Intraframe statistical, interframe encoding and the use of the motion vector for prediction	Intraframe statistical	Intraframe statistical, interframe encoding and the use of the motion vector for prediction
Recommended field of application	Video image encoding	Static image encoding	Dynamic image of rectangular format encoding
Possibility of lossless compression	Yes	Yes	Yes
Typical compression ratio range	15-50	20-150	40-200
Compression ratio with noticeable resolution loss	Higher than 1:50	Higher than 1:150	Higher than 1:200
Computational complexity	Medium	Medium	High
Disadvantages	Low compression efficiency	Irreversible information loss at high compression ratios	Complex algorithms, resource-intensive encoding and decoding

in the given zone and the results of its comparison with the radiation energy matrix in the decision making device, with account of wavelength, the value of brightness (spectral temperature) in the zone in question, is calculated [3].

The thermodynamic temperature of the controlled area of the measured object image field is determined by comparing the received values with the data of spectral pyrometry calibration ratios [11].

Conclusion

Thus, a thermo-video telemetry system (TVTS) is a system of video telemetry for contactless temperature (radiation of physical bodies[6] – objects) measurement in a wide temperature range via optical method application by the integral coefficient of radiation[7] of power-loaded industrial products.

The distinctive features of the observed object thermo-video telemetry are the following:

- contactless temperature measurement
- wide range of measured temperature for object points
- video rendering of temperature distribution across observed object surface
- a visual representation of the temperature dynamics of the object surface as a whole
- prompt detection of anomalous temperature zones.

Temperature measuring video telemetry systems will allow for a substantial decrease in the quantity of temperature sensors and cables with a simultaneous increase in the quantity and improvement in the quality of the information received about the temperature of

[6] The integral coefficient of radiation is temperature-dependent. In the case of dielectric materials ε(T) it usually decreases with the increase of temperature. This has to do with the fact that the refractive index of materials increases with the temperature. Yet, the electrical conductivity of metals decreases as the temperature rises due to the thermal excitation of the molecular lattice, which causes the increase of ε(T). It should be noted that ε does not change for water and is approximately equal to 1 (one), for graphite ε ≈ 0.95…0.98. The approximate expression is known for the temperature-dependent integral coefficient of radiation for metals [5]:

$$\varepsilon(\mathrm{T}) \approx 0.5737\sqrt{\rho(T)\mathrm{T}} - 0.769\rho(T)\mathrm{T} \quad (6.10)$$

$$\rho(T) = \rho_0(1 + \alpha(T - 293)) \quad (6.11)$$

where ρ(T) is the temperature-dependent resistivity of the metal, ρ_0 – resistivity of the metal at 20°C (293 K), α – coefficient of thermal variation of resistivity.

[7] The spectral pyrometer is calibrated against the radiation of an absolutely black body (on the same wavelength) in degrees of brightness temperature T_{ij}, related to the thermodynamic scale by the ratio [4]

$$\frac{1}{T_{aij}} - \frac{1}{T_{ij}} = \frac{\lambda_{ij}}{1.438} \ln \varepsilon_{\lambda ij} \quad (7.12)$$

where T_{a_ij} is the actual (calibrated) average temperature in the controlled zone of the image field,

$$T_{a\_ij} = \frac{1.438T_{ij}}{1.438 + \lambda_{ij}T_{ij} \ln \varepsilon_{\lambda ij}} \quad (7.13)$$

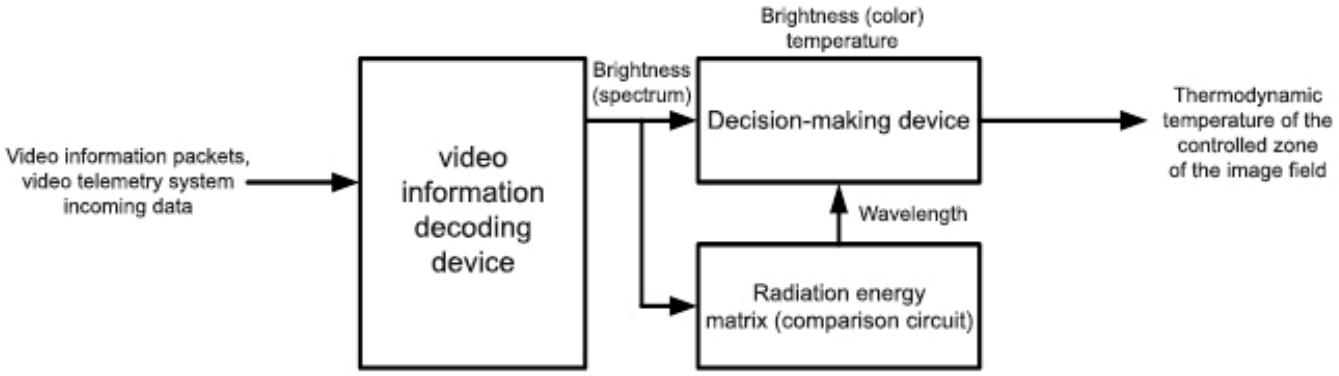

Fig. 4. Functional diagram of temperature measuring unit

power-loaded elements of the object or product by carrying out both point and zone monitoring to track temperature parameters.

The implementation of thermo-video telemetry will permit to increase the controlled area of the surface of the controlled object of the industrial product and, at the same time, it will widen the range of the measured temperature and reduce the temperature information flow. Thermo-video telemetry will promptly analyze standard, contingency and emergency situations by monitoring anomalous temperature zones in power-loaded areas via video images of the surface of the observed object.

The paper proposes a method for measuring the temperature of observed object power-loaded areas with use of a thermo-video system along with:

– introducing definitions concerning video telemetry control of industrial products

– developing a generalized functional diagram of a video telemetry system

– developing a functional diagram of the transmitting segment of the temperature measuring video telemetry system

– formulating the requirements to the spectral range of the thermo-video telemetry system for measuring temperature in the power-loaded areas of industrial products

– developing a functional diagram of the temperature measurement unit of the video telemetry system

– carrying out a comparative analysis of the existing video information compression algorithms

– formulating the requirements to the implementation of a video telemetry system and its distinctive features.

References

1. Nazarov, A.V., G. I. Kozyrev, I. V. Shitov et al. *Sovremennaya telemetriya v teorii i na praktike. Uchebnyy kurs*. [Modern telemetry in theory and practice. A training course]. Nauka i tekhnika, 2007, 672 p. (in Russian)
2. Savel'ev, I.V. *Kurs obshchey fiziki* [Course of General Physics] Nauka, 1979, Vol. 3, 537 p. (in Russian)
3. Klimov, D.I. *Ispol'zovanie infrakrasnogo i ul'trafioletovogo diapazonov dlya otslezhivaniya temperaturnykh parametrov KA i RN* [Use of infrared and ultraviolet ranges to monitor temperature parameters of spacecraft and launch vehicles] Radiotekhnika, 2012, No. 12. pp. 22-26. (in Russian)
4. *Tablitsy fizicheskikh velichin* [Tables of physical quantities]. Ed. by I.K. Kikoin. Atomizdat, 1976, 1009 p. (in Russian)
5. Gossorg, Zh. *Infrakrasnaya termografiya. Osnovy, tekhnika, primenenie* [Infrared thermography. Fundamentals, technique, application]. Mir, 1988, 416 p. (in Russian)
6. *Metodicheskie ukazaniya k vypolneniyu laboratornykh rabot po kursu "Teoreticheskie osnovy teplotekhniki". Laboratornaya rabota №7 "Izmerenie temperatury beskontaktnymi metodami"* [Methodical instructions for the performance of laboratory works on the course "Theoretical Foundations of Heat Engineering". Laboratory work №7 "Temperature measurement by non-contact methods"]. Mordovian State University, 10 p. (in Russian)
7. Richardson, Ya. *Videokodirovanie. H.264 i MPEG-4 - standarty novogo pokoleniya* [Video coding. H.264 and MPEG-4 – the standards of the new generation]. Tekhnosfera, 2005, 368 p. (in Russian)

8. *Protokol №62/03 "Otsenki metodicheskikh polozheniy izmereniya temperatury poverkhnosti nagretykh ob"ektov s termoizoliruyushchim pokrytiem THERMAL COAT"* [Protocol No.62/03 "Estimations of methodological positions for measuring the surface temperature of heated objects with thermal insulation coating THERMAL COAT"]. Department of Building Physics and Resource Saving Institute of Building Constructions. Kiev, 2003, 9 p. (in Russian)
9. Poskachey, A.A. *Optiko-elektronnye sistemy izmereniya temperatury* [Optoelectronic temperature measuring systems]. Energoatomizdat, 1988, 248 p. (in Russian)
10. Korotaev, V.V. *Osnovy teplovideniya* [Fundamentals of thermal imaging]. St. Petersburg National Research University of Information Technologies, Mechanics and Optics, 2012, 123 p. (in Russian)
11. Koshkin, N.I. *Spravochnik po elementarnoy fizike* [Handbook of elementary physics]. 3rd ed., revised and enlarged. Nauka, 1965, 248 p. (in Russian)
12. D.I. Klimov, V.A. Blagodyrev. Termovideosistema dlya ustanovki na kosmicheskie apparaty i rakety-nositeli [Thermo-Video-System with Radiation and Heat Shielding of Objective Lenses and Charge-Coupled Devices for Installation on Spacecraft]. *Raketno-kosmicheskoe priborostroenie i informatsionnye sistemy* [Rocket-Space Device Engineering and Information Systems]. 2016, Vol. 3, No. 3., pp. 76-83. (in Russian)
13. Klimov D.I., Blagodyrev V.A. *Otsenka vozmozhnosti ispol'zovaniya sushchestvuyushchikh ob"ektivov dlya proetsirovaniya videoizobrazheniya na fotoregistriruyushchie pribory* [Evaluation of the possibility of using existing lenses for projecting video images to photographic recorders]. Radiotekhnika, 2015, Vol. 16, No. 8, pp. 63-71.
14. Jan Ozer, J. *H.264 Royalties: what you need to know*. Streaming Learning Center, 2009, P. 1.
15. Vishnevskiy, G.I. Otechestvennye UF i IK FPZS i tsifrovye kamery na ikh osnove [Russian UV and IR FPZS and digital cameras based on them]. *Elektronika: nauka, tekhnologiya, biznes* [Electronics: Science, Technology, Business], 2003, No. 8, pp. 18-24. (in Russian)